2018

Modelling Of Corona Ignition System

Akshay Ravi
University of Windsor

MODELLING OF CORONA IGNITION SYSTEM

By

Akshay Ravi

A Thesis
Submitted to the Faculty of Graduate Studies
through the Department of Electrical and Computer Engineering
in Partial Fulfillment of the Requirements for
the Degree of Master of Applied Science
at the University of Windsor

Windsor, Ontario, Canada

2018

MODELLING OF CORONA IGNITION SYSTEM

by

Akshay Ravi

APPROVED BY:

_____

D. Ting

Department of Mechanical, Automotive and Materials Engineering

_____

M. Abdelkhalek
Department of Electrical and Computer Engineering

_____

X. Chen, Advisor
Department of Electrical and Computer Engineering

_____

M. Zheng, Co-Advisor
Department of Mechanical, Automotive and Materials Engineering

2 February, 2018

DECLARATION OF ORIGINALITY

I hereby certify that I am the sole author of this thesis and that no part of this thesis has been published or submitted for publication.

I certify that, to the best of my knowledge, my thesis does not infringe upon anyone's copyright nor violate any proprietary rights and that any ideas, techniques, quotations, or any other material from the work of other people included in my thesis, published or otherwise, are fully acknowledged in accordance with the standard referencing practices. Furthermore, to the extent that I have included copyrighted material that surpasses the bounds of fair dealing within the meaning of the Canada Copyright Act, I certify that I have obtained a written permission from the copyright owner(s) to include such material(s) in my thesis and have included copies of such copyright clearances to my appendix.

I declare that this is a true copy of my thesis, including any final revisions, as approved by my thesis committee and the Graduate Studies office, and that this thesis has not been submitted for a higher degree to any other University or Institution.

ABSTRACT

Modern emission regulations demand the reduction of nitrogen-oxide emissions significantly and this trend is likely to continue. Emission reduction and fuel efficiency improvement have become the prime objectives of the automobile industry today. One of the ways in which these objectives can be met is by using an ignition method that can enable the engine to run under highly lean conditions and high exhaust gas recirculation (EGR) rates. Corona ignition is a method of ignition which has demonstrated potential to achieve high fuel efficiency by enabling engine to operate under highly lean conditions and high exhaust gas recirculation (EGR) rates to reduce emissions. To achieve optimum performance of corona ignition system there is a need to describe system dynamics through modelling which can help in studying its electrical behavior. The primary objective of this work is to put forward a model of corona ignition system based on first principles. Tests were performed to study the behavior of the system with and without corona discharge. The various electrical parameters of the system were measured using an impedance analyzer. The effect of variation of electrical parameters affecting system behavior was also studied which can help in circuit design. The measured electrical parameters were then used in the physics based model of corona ignition system to simulate system behavior without corona discharge. The results obtained from the model and measurement were compared for model verification. It was observed that the model captured the trend of magnitude behavior of the system.

DEDICATION

I dedicate this thesis to my parents, Ravi V.C. and Shanthi Seetharaman. Without both of them life doesn't have a meaning, but with their guidance and support the whole world can be conquered. I also thank my friends Jeba Kibeon, Anuj Kumar, Swagatika Patasahani, Bharat N.C., Siva Prasanth, Ganapathy Raja and Siddharth Patel who have constantly encouraged me on all my endeavours.

ACKNOWLEDGEMENTS

I feel gifted to be a part of the Clean Combustion Research group. I would like to take this opportunity to thank my supervisors Dr. Xiang Chen and Dr. Ming Zheng whose guidance and support helped me complete my research work. I feel that working under them is a privilege.

I would also like to thank my committee members Dr. David Ting, Dr. Maher Abdelkhalek and the Chair of Defence for giving me constructive criticism and helping me to improve my thesis.

I would also like to convey my heartiest thanks to Dr. Shui Yu and Qingyuan Tan for their help in conducting tests during the course of my research. I want to especially thank Hua Zhu for her help in the impedance analyzer measurements and during running tests of the corona ignition system. I would also like to take this opportunity to thank all members of the Clean Combustion Research group, Dr. Meiping Wang, Dr. Xiao Yu, Dr. Tadanori Yanai, Prasad Divekar, Marko Jeftic, Tongyang Gao, Shouvik Dev, Zhenyi Yang, Kelvin Xie, Gaz Bryden, Mark Ives, Chris Aversa, Divyanshu Purohit and Navjot Singh Sandhu for all their help during day to day lab activities. I would also like to convey my special thanks to all the funding agencies for their support.

TABLE OF CONTENTS

LIST OF TABLES

LIST OF FIGURES

NOMENCLATURE

Abbreviations

AC	Alternating Current	[-]
ACIS	Advanced Corona Ignition System	[-]
CARB	California Air Resources Board	[-]
CAFE	Corporate Average Fuel Economy	[mpg]
CI	Compression Ignition	[-]
DC	Direct Current	[-]
ECU	Electronic Control Unit	[-]
EGR	Exhaust Gas Recirculation	[-]
EPA	Environmental Protection Agency	[-]
IC	Internal Combustion	[-]
KVL	Kirchoff's Voltage Law	[-]
MHz	Mega Hertz	[-]
MOSFET	Metal Oxide Semiconductor Field Effect Transistor	[-]
mpg	miles per gallon	[mpg]
NHTSA	National Highway Traffic Safety Administration	[-]
NO_X	Nitrogen Oxide(s)	[ppm]
ppm	Parts per Million	[-]
RF	Radio Frequency	[-]
SI	Spark Ignition	[-]

US	United States	[-]
USD	United States Dollar	[-]
VF	Velocity Factor	[-]

Symbols

ϕ	Phase Difference between Voltage and Current	[Degrees]
λ	Air Excess Ratio	[-]
π	pi	[-]
Δt	Time Delay	[ns]
C	Capacitance determined from Impedance Analyzer	[pF]
C	Capacitance of Igniter	[pF]
F	Resonant Frequency determined from Impedance Analyzer	[MHz]
f	Oscillating Frequency of Voltage and Current Signals	[Hz]
f_r	Resonant Frequency	[Hz]
i_c	Current Flowing through the Capacitor	[Amps]
i_p	Primary Current	[Amps]
i_s	Secondary Current	[Amps]
k	Coefficient of Coupling	[-]
L	Inductance of Igniter	[µH]
L	Inductance determined from Impedance Analyzer	[µH or mH]
L_P	Primary Inductance	[µH]
L_S	Secondary Inductance	[µH]
M	Mutual Inductance	[µH]
n	Turns Ratio	[-]
Q	Quality Factor	[-]

r	Length of Coaxial Cable	[metres]
R	Resistance determined from Impedance Analyzer	[Ω]
R	Resistance of Igniter	[Ω]
t	Time	[Seconds]
v_{dc}	Input DC Voltage given to Half-Bridge Inverter	[Volts]
v_{load}	Voltage across the load of Half-Bridge Inverter	[Volts]
v_p	Primary Voltage of Transformer	[Volts]
v_s	Secondary Voltage of Transformer	[Volts]
ω	Angular Frequency	[radians/second]
|Z|	Magnitude of Impedance	[Ω]

CHAPTER 1: INTRODUCTION

1.1 Motivations

In-order to improve air quality and prevent harmful effects of climate change, governmental agencies such as the US Environmental Protection Agency (EPA) and California Air Resources Board (CARB) have been enforcing strict emission regulations. These regulations dictate the maximum amount of emissions which can be emitted from automobiles [1-2]. The National Highway Traffic Safety Administration (NHTSA), an agency under the US Department of Transportation, has also enforced regulations such as Corporate Average Fuel Economy (CAFE) due to increasing concern on fossil fuel depletion and to tackle the fluctuations in price of fuels such as diesel and gasoline. Stringent emission regulations and the demand for fuel efficient vehicles have motivated automotive manufacturers to develop technologies which enable vehicles to run fuel efficiently and reduce emissions [3-5].

The emission regulations enforced by the EPA for cars and light duty trucks fueled by gasoline have been shown in Figure 1.1 which indicates that there has been substantial reduction in the nitrogen-oxide emissions over the past decade [1]. Hence, it is likely that the regulations will be further tightened in the coming years.

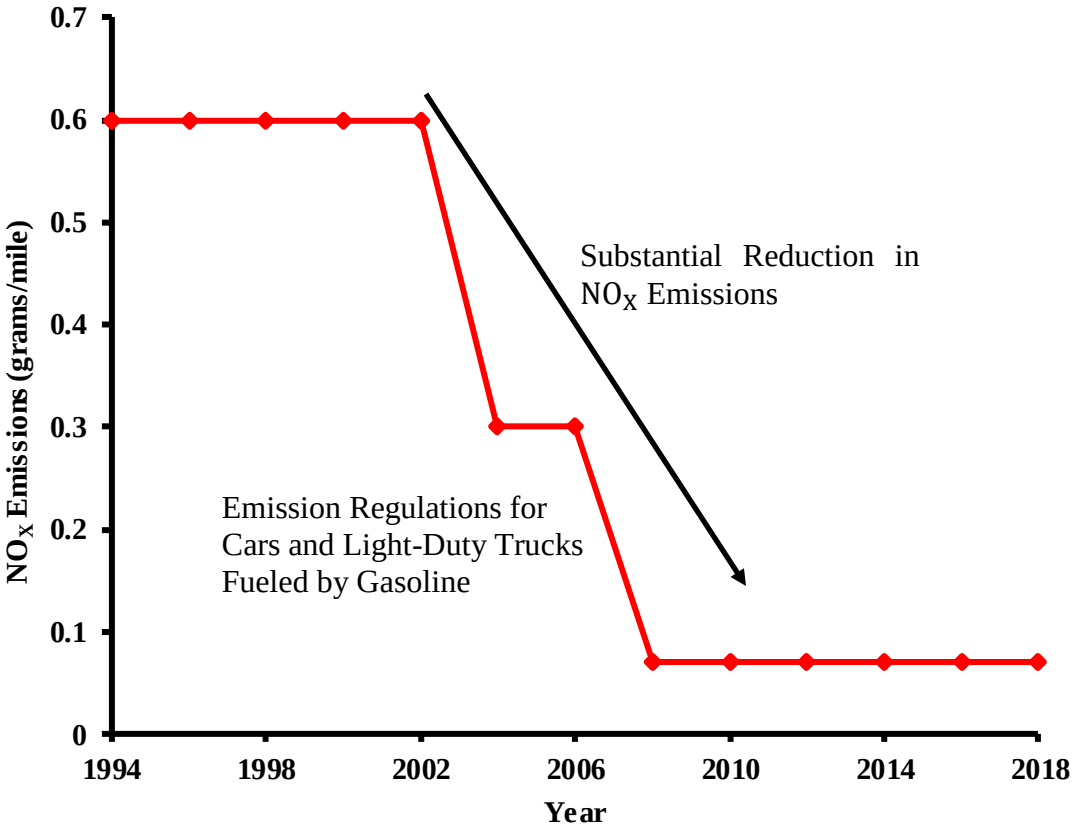

Figure 1.1: Emission Regulations Introduced by US EPA

The fluctuation in oil prices, for example the oil shocks of 1973-74, and need to reduce U.S. dependence on foreign oil prompted the U.S. Congress to enact laws that improve fuel economy of vehicles sold in the U.S. [6]. Figure 1.2 indicates the fluctuations in the price of retail gasoline per gallon sold in the U.S. [7]. Figure 1.3 indicates the CAFE (Corporate average fuel economy) standard enacted by the U.S. congress to improve the average fuel economy of light vehicles sold in the U.S. The fuel economy standards are expressed in miles per gallon (mpg) which is defined as the average mileage traveled by an automobile per gallon of gasoline or equivalent amount of other fuel. The fuel economy requirements were increased till year 1985 and stood unchanged till peak oil prices in 2011. This again

resulted in further increase in the CAFE fuel economy requirements. The trend shown in Figure 1.3 indicates that there is a substantial increase in the fuel economy requirements from the year 1978 to 2011 [2]. The projected fuel economy requirements for the future owing to fears of price rise due to fossil fuel depletion are also high as shown in Figure 1.3.

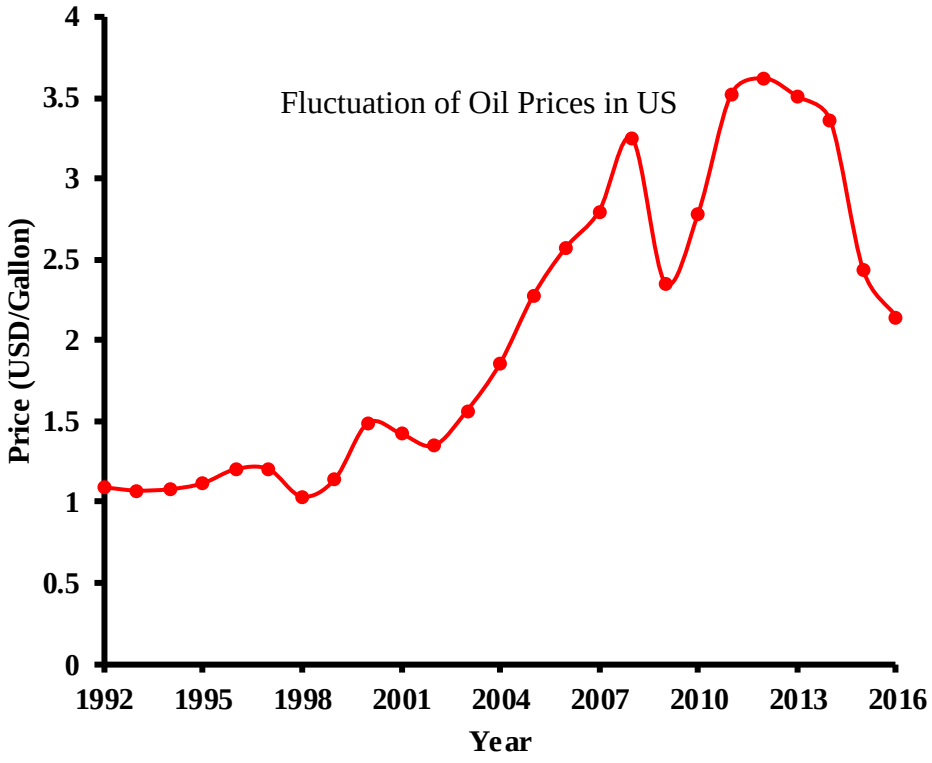

Figure 1.2: Graph Showing the Fluctuations in Price of Retail Gasoline in United States

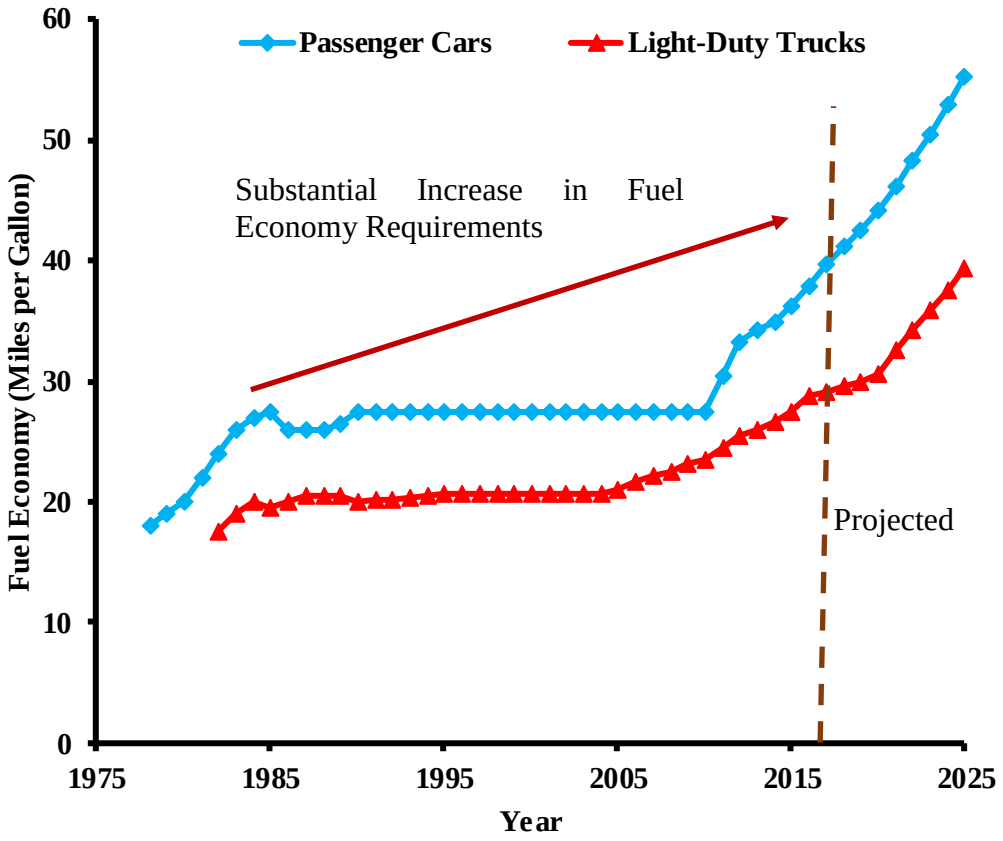

Figure 1.3: Fuel Economy Requirements Introduced by CAFE Standard

This research focuses on one of the methods of ignition which can potentially help in achieving the emission and fuel economy regulations of the future.

1.2 Background

1.2.1 Ignition Strategies in Spark Ignition Engines

IC engines are classified as SI (spark ignition) and CI (compression ignition) engines. SI engines involve the ignition of air-fuel mixture in the combustion chamber by an external ignition source like a spark plug whereas in CI engines the fuel is injected into the cylinder just before the end of the compression stroke and auto-ignition occurs because of the high

temperature generated due to high compression ratios. The reliable ignition of fuel in an IC engine is one of the most important factors which directly impact emissions, fuel economy and performance [8, 9-10].

The ignition strategies which produce multiple ignition spots have been successful in igniting highly lean mixtures which can potentially lead to reduced emissions and higher fuel economy [8].

1.2.2 Radio-Frequency Corona Ignition

Radio-frequency corona ignition is one of the methods of ignition which works on the concept of streamer theory of discharge [11]. When high voltage is applied to an electrode, the electrons are accelerated at high speeds. These electrons overcome the ionization potential of the neutral air molecules to produce free electrons and positive ions. This process is known as ionization. Now these free electrons knock off other electrons from neutral air molecules to further produce free electrons and positive ions. This process is called secondary ionization. Hence, an avalanche of electrons and positive ions are produced which are drifting towards oppositely charged electrodes which leads to the formation of corona discharge. The free electrons produce ionization as long as they have the kinetic energy to overcome the ionization potential of the neutral air molecules they are colliding with. The electrons possess high kinetic energy because of the repulsive force from the electric field of cathode. Hence, this process of ionization occurs in a confined region. This is called corona discharge [11]. During corona discharge, no conducting path is formed between the electrons and the positive ions. The process of corona formation is shown in Figure 1.4.

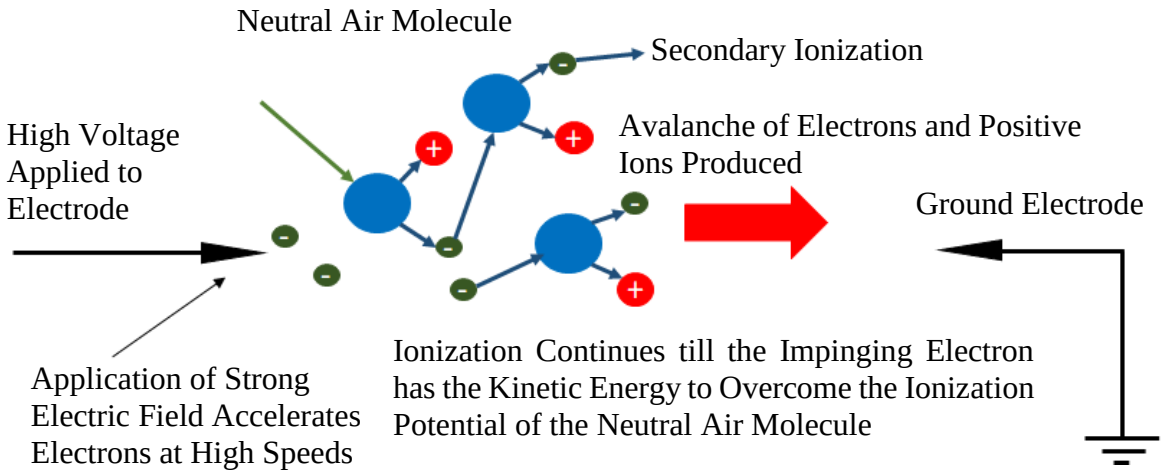

Figure 1.4: Formation of Corona Discharge

RF Corona ignition involves application of high voltage and high frequency which produces multiple streamers with multiple ignition spots that can potentially cover a larger volume of combustion chamber due to which the ignitable volume is increased. This enables the engine to be run under highly lean conditions and high EGR rates which could have the benefit of reduced emissions and higher fuel economy [10,12, 13-14]. The study of the dynamic electrical behavior of the corona ignition system can help in improving its performance [15].

1.3 Literature Review

In literature substantial studies have been conducted which highlight the importance of corona ignition in enabling lean operation of the engine to improve fuel efficiency and reduce especially in-cylinder NO_X emissions.

Cimarello et al studied the effect of corona ignition on a single cylinder optical engine fueled by gasoline with specific focus on stable, near-limit and unstable conditions [16]. The study encompassed effects on emissions, lean operation and flame development using high speed camera. The Federal Moghul Advanced Corona Ignition System (ACIS) family prototype corona igniter was used in this study. A high frequency amplifier was used to provide the desired energy to the igniter assembly. The ignition timing signal was received from the Electronic Control Unit (ECU). The igniter assembly inserted into the combustion chamber produced corona discharge when excited to the resonant frequency. The igniter assembly was electrically represented as a series RLC circuit and consisted of an inductor to raise the voltage to the desired high value and the firing tip of the igniter had four sharp tips. The duration of corona was kept at 300μs. The voltage at the firing end could reach a maximum of 70 kV. It was observed that corona ignition allowed the extension of lean limits from λ=1.4 (spark ignition) to λ =1.65 (corona ignition) during low-load, low-speed engine operation. Almost 88% reduction in NO_X emissions was observed. The initial flame growth speed for corona ignition was four times faster than spark ignition.

Yu et al studied the relationship between spark discharge characteristics and inductive spark ignition circuit parameters with the help of a simplified circuit model. The proposed simplified circuit model to simulate the spark discharge process made use of equations representing the underlying physics in the system and electrical parameters. The measured

electrical parameters such as coupling coefficient, primary and secondary inductance used for transformer action, and leakage inductance of primary winding were used in the model each of which parameters had their own physical meaning. It was observed that the proposed model followed the principle behavior of the spark discharge process [17].

1.4 Research Objectives

Primary objective of this research was to put forward a model of corona ignition system without corona discharge based on first principle laws. First principles based model enabled an understanding of the physics behind the system and made use of measured physical parameters [18, 19]. Firstly, the dynamic measurements from the corona ignition system were carried out which represented its behavior with and without corona discharge. Then the values of various electrical components of corona ignition system were measured each of which had a physical meaning [17]. The measured parameters were used in the physics based model of the corona ignition system for simulating the electrical behavior and describe its dynamics. The results from the model were then compared with the experimental data for model verification. The electrical parameters which affected the system behavior during corona discharge and the circuit used to drive the corona ignition system were also studied.

1.5 Thesis Outline

Chapter 1 presents the primary objective and outline of the thesis.

Chapter 2 deals with the experimental set-up used for performing the tests with and without corona discharge, impedance analyzer used for measuring values of different electrical

parameters of the system. The method by which the measurements are performed is also described. The principle of operation of each component of the corona ignition system is mentioned in detail.

Chapter 3 deals with the test results with and without corona discharge. The time domain and frequency domain analyses are conducted to study and understand system behavior and conclusions drawn from the results are presented.

Chapter 4 presents the measurements performed to determine the electrical component values of corona ignition system. Measurements are also performed to study the effect of variation of different electrical parameters influencing system behavior.

Chapter 5 explains the physics based model of corona ignition system without corona discharge and model verification is performed by comparing with experimental measurement.

Chapter 6 provides recommendations to carry this research forward and future scope of work.

CHAPTER 2: EXPERIMENTAL SETUP

This chapter outlines the experimental setups used for conducting the study in this thesis. The corona setup used for performing the tests with and without corona discharge, and the impedance analyzer setup used for measuring the electrical component values of the corona ignition system are described. The method by which data acquisition is performed, and the sensors and analyzers used for acquiring the experimental data are presented as well.

2.1 Structure of Corona Ignition System

The structure of the corona ignition system consists of a half-bridge inverter, step-up transformer and corona igniter as shown in Figure 2.1. The schematic of the system indicating energy flow is also shown in Figure 2.2. The simplified circuit representation of the corona ignition system is shown in Figure 2.3. The system consists of input AC supply from mains that can be adjusted by a variac transformer, and is converted into DC by a full wave rectifier and is fed to the half-bridge inverter which provides the primary source of power to the corona igniter. The gating signal to the MOSFETs of the half-bridge is provided by the function generator for both of the tests with and without corona discharge. The output voltage of the half-bridge inverter is stepped-up by the step-up transformer and is fed to the corona igniter. The corona igniter is electrically represented as a series RLC circuit [10, 16, 20]. The high voltage required for producing corona discharge is obtained by voltage magnification which occurs during resonance represented by the voltage

magnification factor Q. The Q factor depends on the values of resistance, inductance and capacitance of the series RLC circuit of the igniter [16].

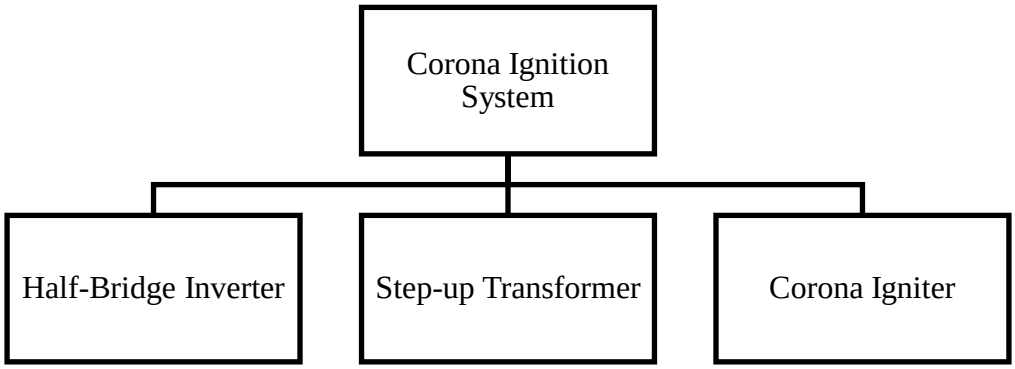

Figure 2.1: Structure of Corona Ignition System

Two sets of tests were performed. One with corona discharge and the other without corona discharge. Figure 2.2 illustrates the schematic representation of test setup for the case with corona discharge, while the equivalent circuit representation is shown in Figure 2.3. The setups shown in Figures 2.2 and 2.4 were designed by postdoctoral scholar Dr. Shui Yu at the Clean Combustion Engine Laboratory. Figure 2.4 illustrates the schematic representation of the setup for the test performed without corona discharge. The equivalent circuit representation of the schematic is shown in Figure 2.5. The point of measurement of voltage and current signals are also shown in the circuit diagrams. The attenuation of the voltage and current measurement probes are 2000:1 and 10:1 respectively [21-22].

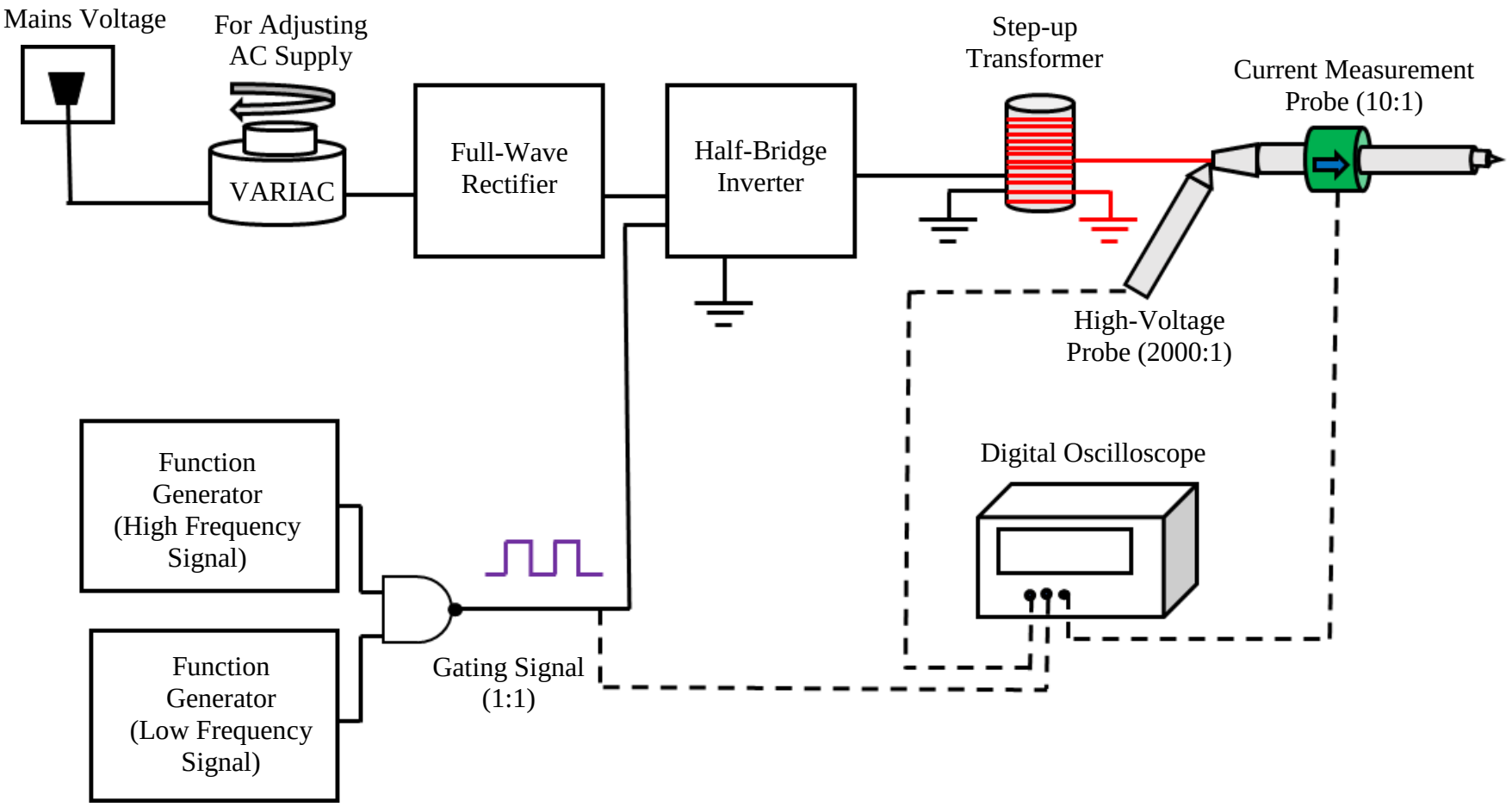

Figure 2.2: Schematic Representation of Corona Ignition System for Test with Corona Discharge

[The Test Setup shown was designed by Dr. Shui Yu]

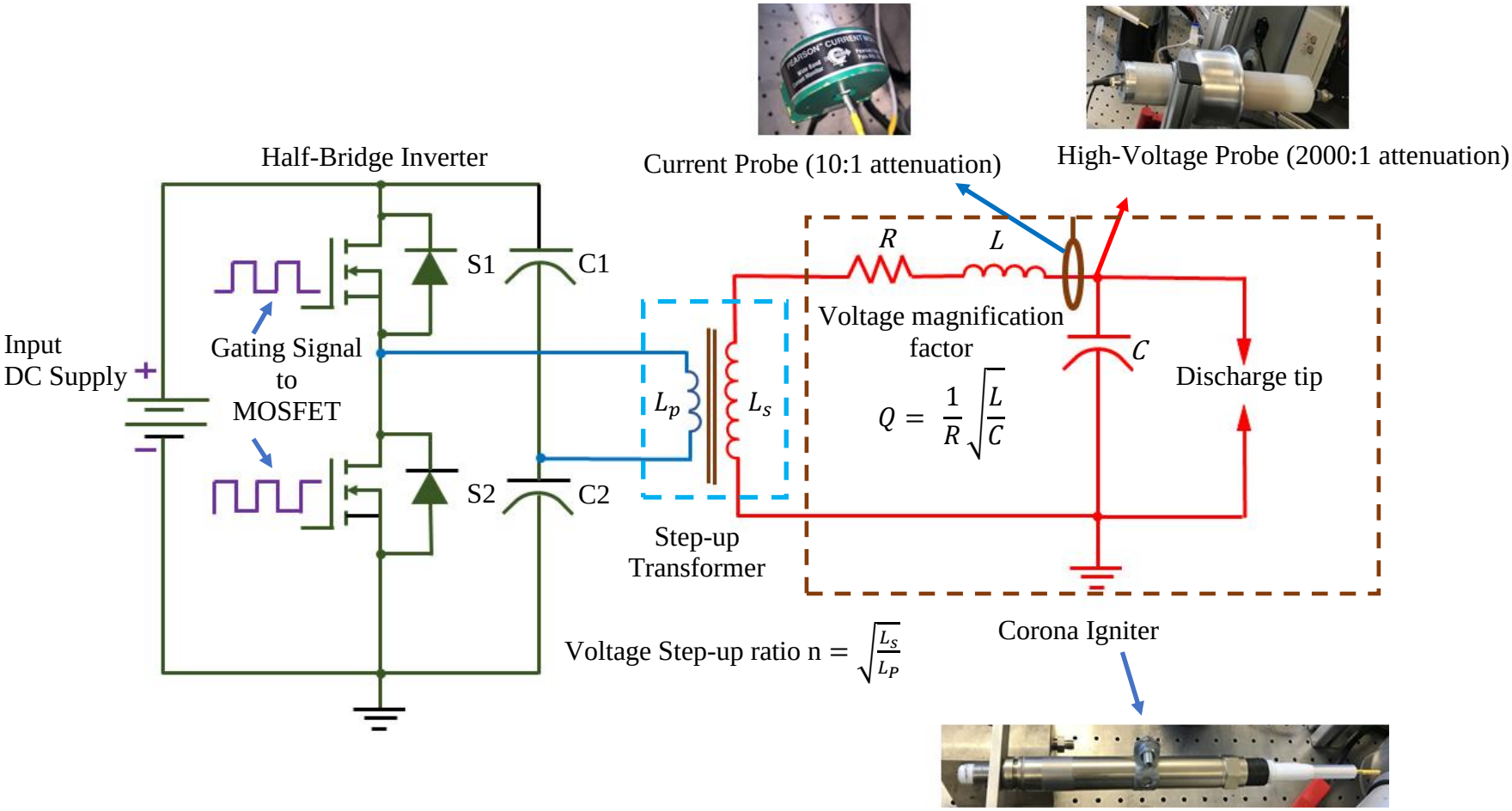

Figure 2.3: Circuit Representation of Corona Ignition System for Test with Corona Discharge

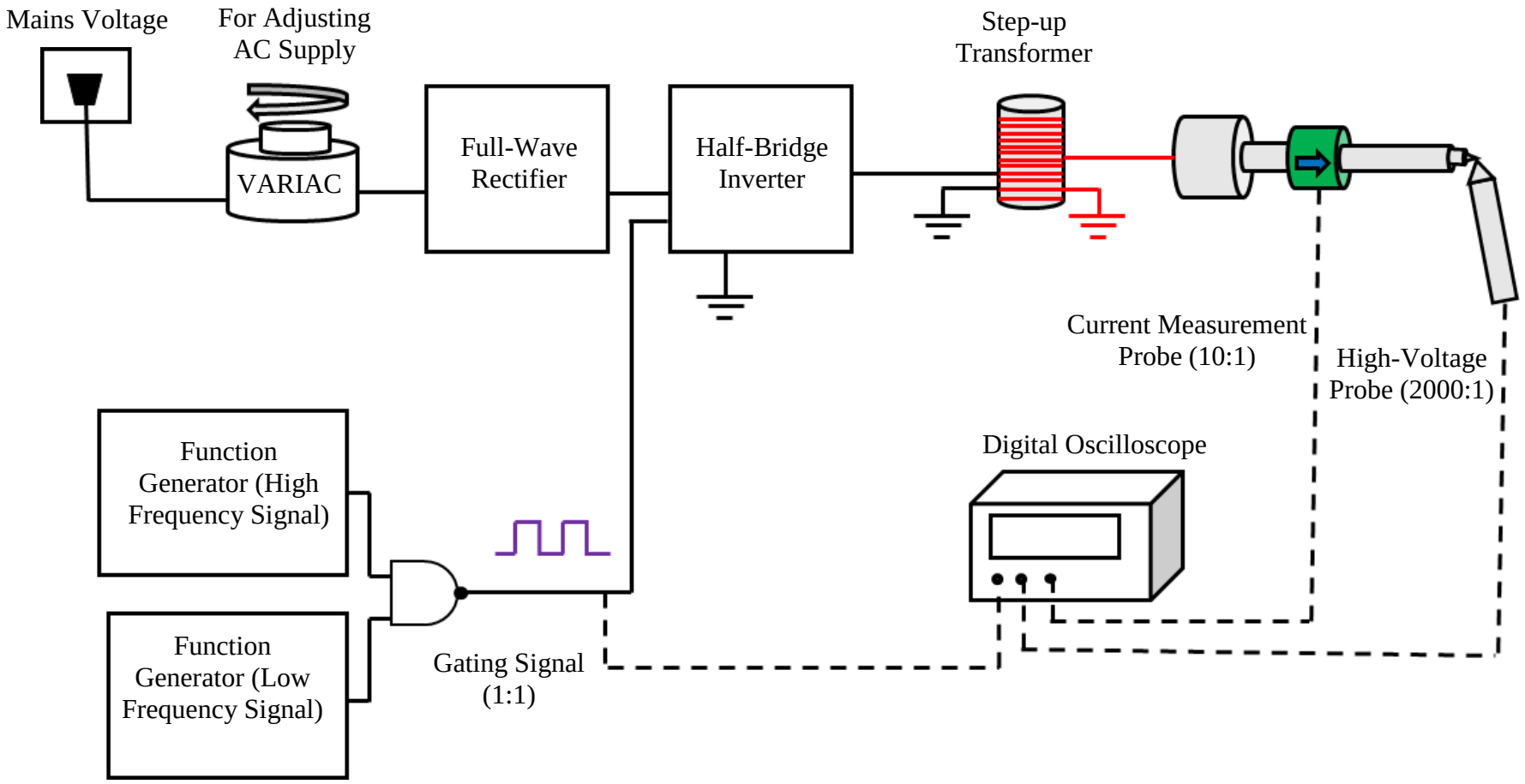

Figure 2.4: Schematic Representation of Corona Ignition System for Test without Corona Discharge

[The Test Setup shown was designed by Dr. Shui Yu]

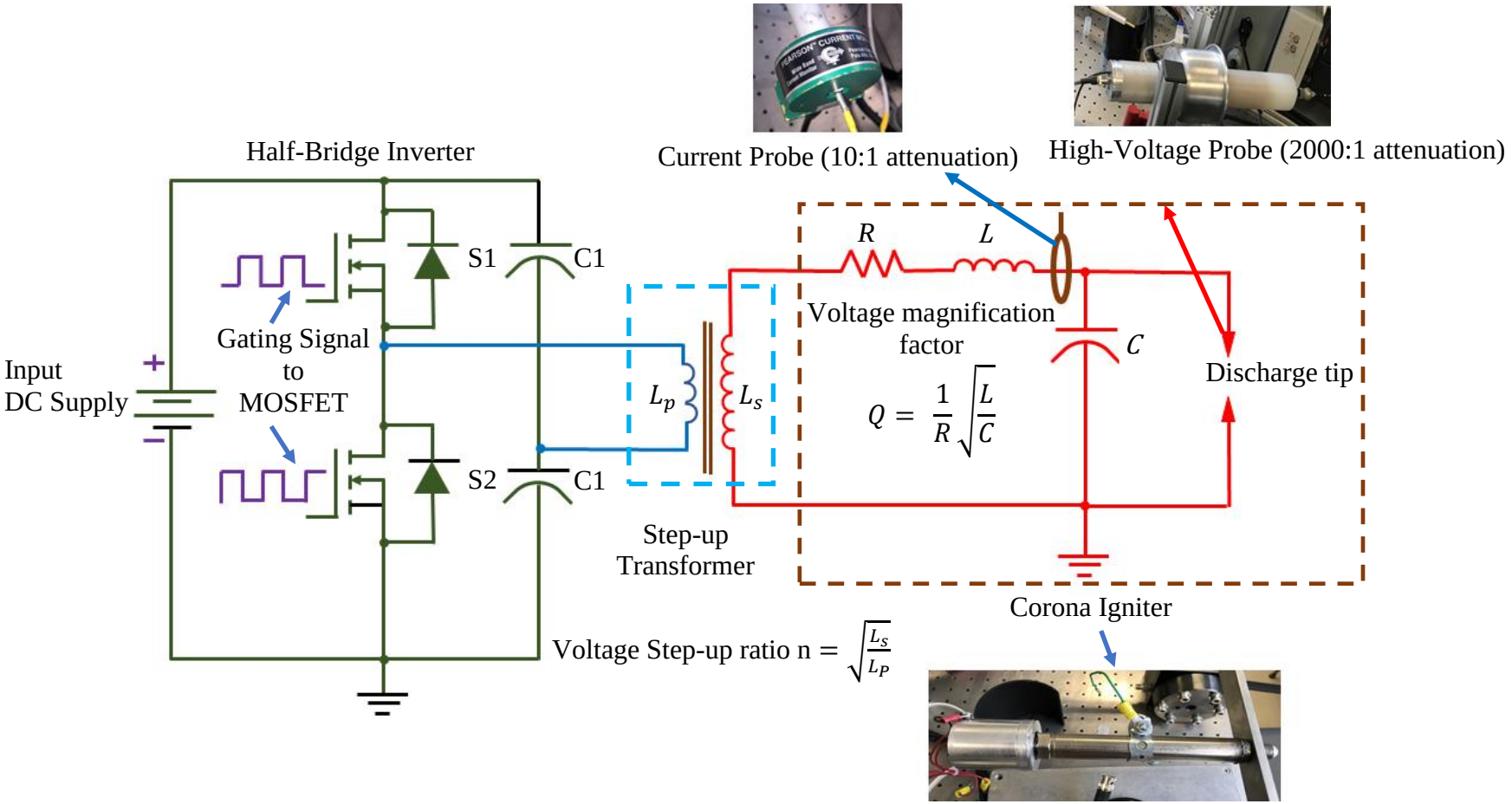

Figure 2.5: Circuit Representation of Corona Ignition System for Test without Corona Discharge

2.2 Corona Igniter

2.2.1 Structures of Corona Igniter

The corona ignition system consists of two igniter structures which are electrically represented as a series RLC circuit [10, 16, 20, 23]. The two igniter structures shown in Figures 2.6 and 2.7 are designed and patented by Zheng et. al. and developed at the Clean Combustion Engine Laboratory. The igniter used for the test with corona discharge as shown in Figure 2.6 does not have a coil inside it for resonation and the resonating inductance is provided by the leakage inductance of the secondary winding of the step-up transformer. The L shown in the circuit representation in Figure 2.6 refers to the leakage inductance of the secondary winding of the transformer. For the test without corona discharge, an igniter similar to the structure shown in Figure 2.7 is used that has a coil inside it for resonation and a separate step-up transformer is used for stepping up the output voltage from the half-bridge inverter. The capacitance C of both the igniter structures is contributed by the gap between the conducting wire inside the igniter and the walls of the metal enclosure of the igniter [23]. The resistance R in Figures 2.6 and 2.7 represents the combined resistance when the secondary winding of the transformer is connected to the igniter.

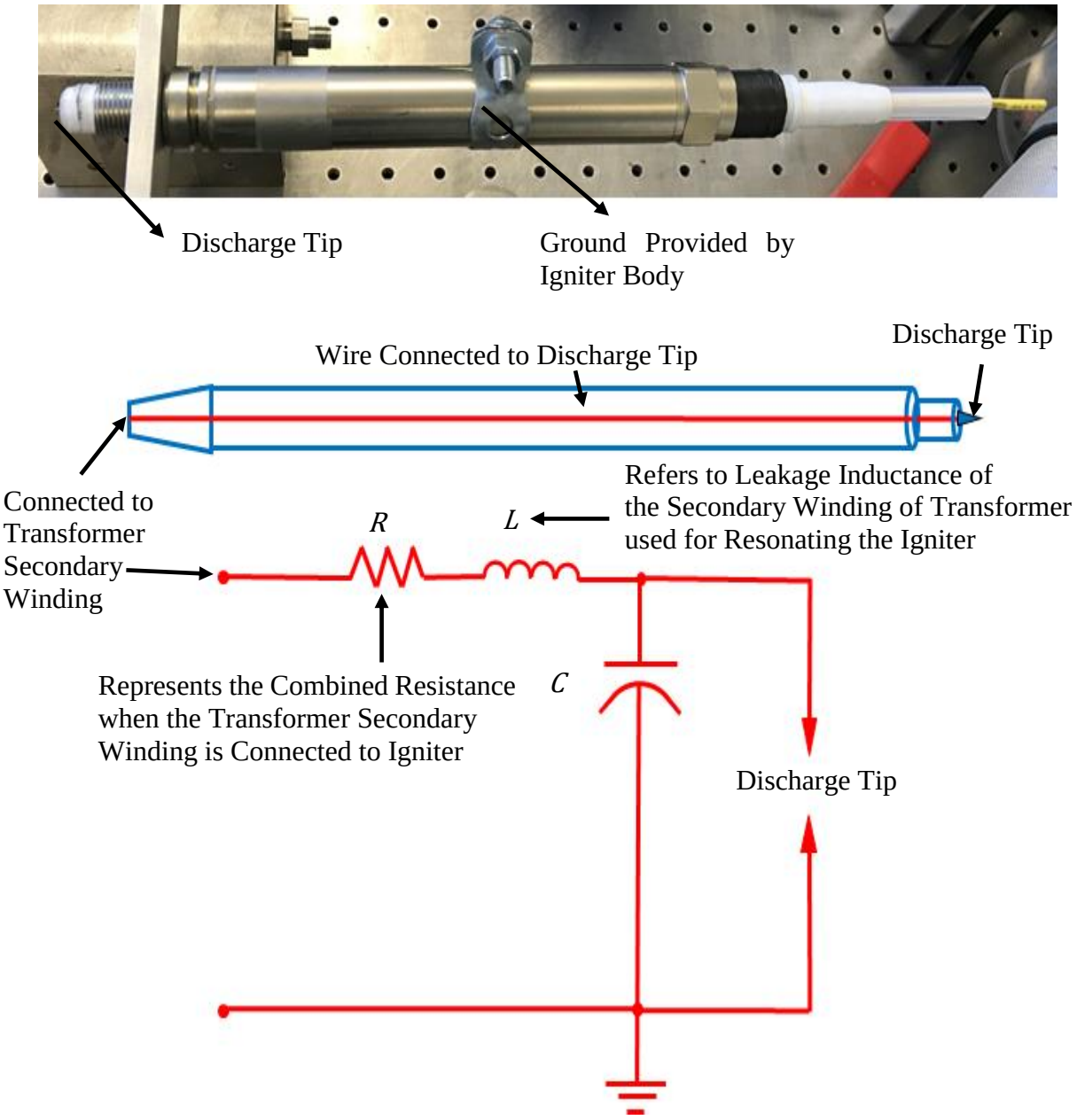

Figure 2.6: Structure of Corona Igniter used with Corona Discharge

[Igniter Structure Designed and Built by Dr. Shui Yu]

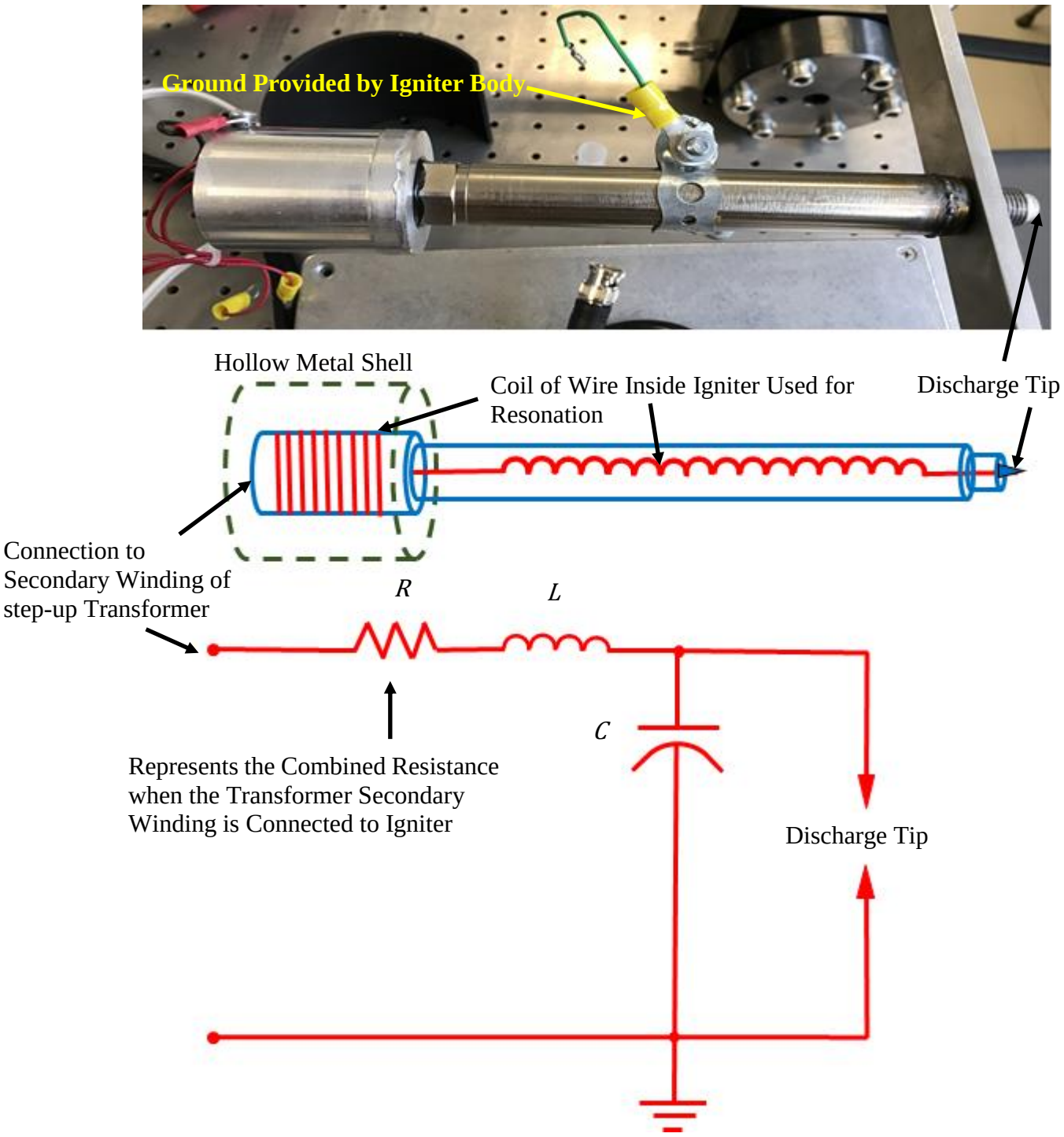

Figure 2.7: Structure of Corona Igniter used without Corona Discharge

[Igniter Structure Designed and Built by Dr. Shui Yu]

2.2.2 Working Principle of Corona Igniter

The corona igniter works on the principle of RLC resonance. The secondary voltage from the transformer is amplified by a quality factor (Q) or voltage magnification factor of the RLC circuit [20]. The voltage magnification factor is given by Equation 2.1.

$$Q = \frac{1}{R}\sqrt{\frac{L}{C}} \tag{2.1}$$

Where R, L and C are the combined resistance when transformer secondary is connected to igniter, inductance used for resonating igniter, and the capacitance of the igniter respectively. The higher the value of Q, greater is the voltage magnification [20, 24]. The voltage magnification in the RLC circuit leads to the production of corona discharge which involves streamers emanating from the igniter's discharge tip.

The resonant frequency of the RLC circuit of the corona igniter is determined by the expression,

$$f_r = \frac{1}{2\pi\sqrt{LC}} \tag{2.2}$$

Where f_r is the resonant frequency, L is the inductance of the igniter, C is the capacitance of the igniter. At the resonant frequency, the capacitive and the inductive reactance cancel each other. The resultant impedance is a pure resistance. Hence, maximum value of current and voltage is obtained at the resonant frequency [20, 24]. At frequencies other than the resonant frequency, there is a resultant impedance which has a reactive part. Thus, the voltage and current at frequencies other than the resonant frequency are lower in magnitude. The magnitude of the impedance, and the phase difference between the voltage

and the current signals are influenced by the values of R, L and C of the igniter. The equations describing the relationship between the magnitude of impedance and the phase difference between the voltage and current signals are given below:

$$|\mathrm{Z}| = \sqrt{R^2 + \left(2\pi fL - \frac{1}{2\pi fC}\right)} \tag{2.3}$$

$$\phi = tan^{-1}\left(\frac{2\pi fL - \frac{1}{2\pi fC}}{R}\right) \tag{2.4}$$

Where ϕ is the phase difference between voltage and current signals and f is oscillating frequency of the voltage and current signals, |Z| represents the magnitude of the overall impedance of the RLC circuit [24].

2.3 Step-up Transformer

The step-up transformer consists of primary and secondary coils wound on a core. The primary winding has an inductance equivalent to L_P. The secondary winding has an inductance equivalent to L_S. A portion of the secondary inductance of the transformer is used for stepping up the voltage, and the leakage portion of the inductance is used for performing voltage magnification to produce corona discharge [25].

The step-up transformer is used here for increasing the amplitude of voltage supplied to the igniter. The voltage is stepped-up by a factor of n, which represents the turns ratio of the transformer. Ideally, the secondary current is reduced by a factor of n when it is transformed from the primary to the secondary winding. The circuit representation of the mutual inductor is shown in Figure 2.8.

$$\text{Turns ratio} = \sqrt{\frac{\text{Secondary inductance}}{\text{Primary inductance}}} \tag{2.5}$$

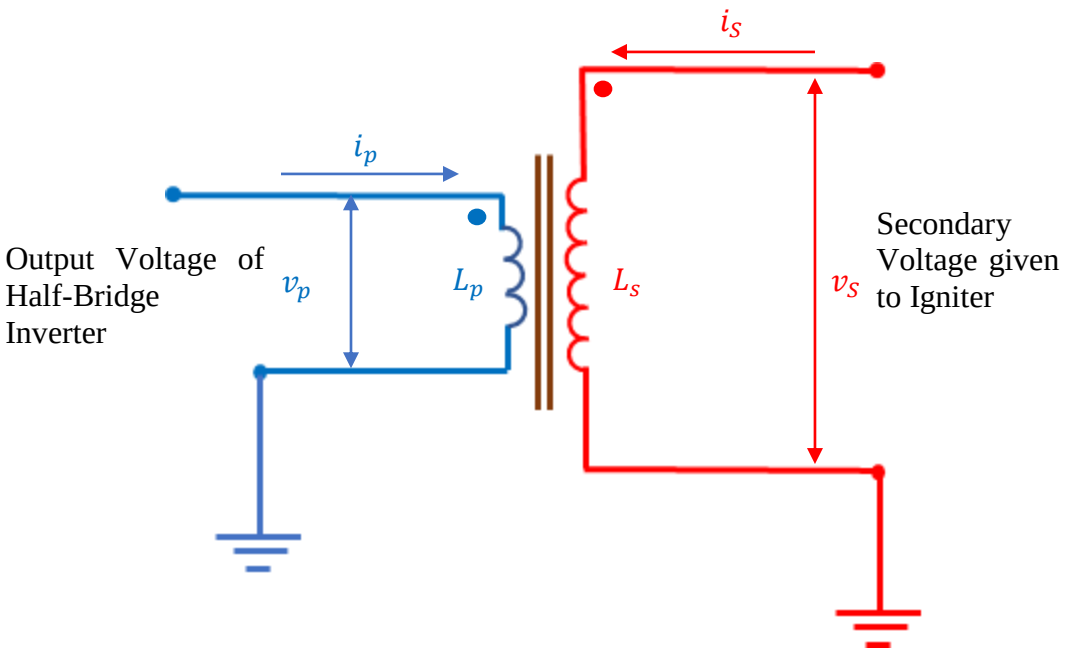

Figure 2.8: Step-up Transformer Circuit Representation

The coefficient of coupling is another factor that affects the amplitude of the secondary voltage. The higher the coefficient of coupling, the greater the amplitude of the secondary voltage of the transformer because it indicates that all the magnetic flux generated by the primary winding is interacting with the secondary winding thereby inducing a large voltage in the secondary winding. Since the transformer is a mutual inductor, the current in one winding affects the voltage in the other winding. The formulae for primary and secondary voltages of a mutual inductor are given as follows.

$$v_{\mathrm{p}} = L_p \frac{di_p}{dt} + M \frac{di_s}{dt} \tag{2.6}$$

$$v_s = L_s \frac{di_s}{dt} + M \frac{di_p}{dt} \tag{2.7}$$

$$M = k\sqrt{L_p L_s} \tag{2.8}$$

Where v_p, v_s, i_p, $i_{s,}$ L_p, L_s are the primary and secondary voltages, currents and inductances respectively. M is known as the mutual inductance of the two coils which is influenced by the value of the coupling coefficient k.

Under practical conditions, some power is lost while transforming the voltage from primary to secondary due to factors such as leakage of flux [26]. In-order to determine the primary and secondary inductances of the transformer, the impedance analyzer is used. The method of performing the measurements is discussed in later sections of this chapter.

2.4 Half-Bridge Inverter

The half-bridge inverter is the driver circuit used for driving the corona ignition system at high frequencies. The circuit of the half-bridge inverter connected to a load is shown in Figure 2.9. The half-bridge inverter converts the input DC voltage into AC voltage which has a fundamental component equal to the switching frequency of the two MOSFET switches. The AC voltage waveform produced by the half-bridge inverter consists of odd harmonics which are multiples of the fundamental switching frequency.

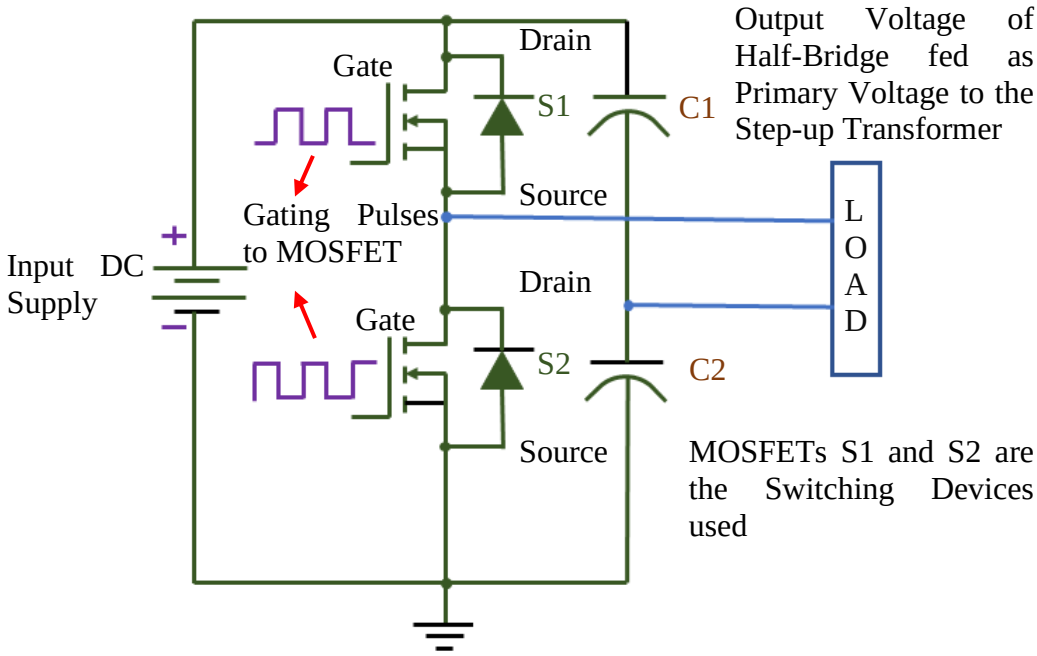

Figure 2.9: Circuit of Half-Bridge Inverter

2.4.1 Structure of Half-Bridge Inverter

The half-bridge circuit consists of two switches which are MOSFETs S1 and S2 as shown in Figure 2.9. Two capacitors C1 and C2 are connected in parallel to the switches. The load terminals are connected at the middle of switches S1 and S2, and capacitors C1 and C2. The gating pulses to the MOSFETs are supplied from the function generator.

2.4.2 Working of Half-Bridge Inverter

The MOSFETs S1 and S2 are switched complementary to one another at equal switching frequency to avoid potential short-circuit. Input bias is provided by a D.C supply. The positive terminal of the D.C bias is connected to the drain of MOSFET S1 and one end of capacitor C1. The negative terminal of the DC supply, source of MOSFET S2 and one end of capacitor C2 are grounded.

- **When Switch S1 is ON:** When switch S1 is ON and S2 is OFF, the voltage available at the upper terminal of the load is v_{dc}. The voltage at the bottom terminal of load is $\frac{v_{dc}}{2}$. Hence, the resultant voltage across the load is

$$v_{load} = v_{dc} - \frac{v_{dc}}{2} = \frac{v_{dc}}{2} \tag{2.9}$$

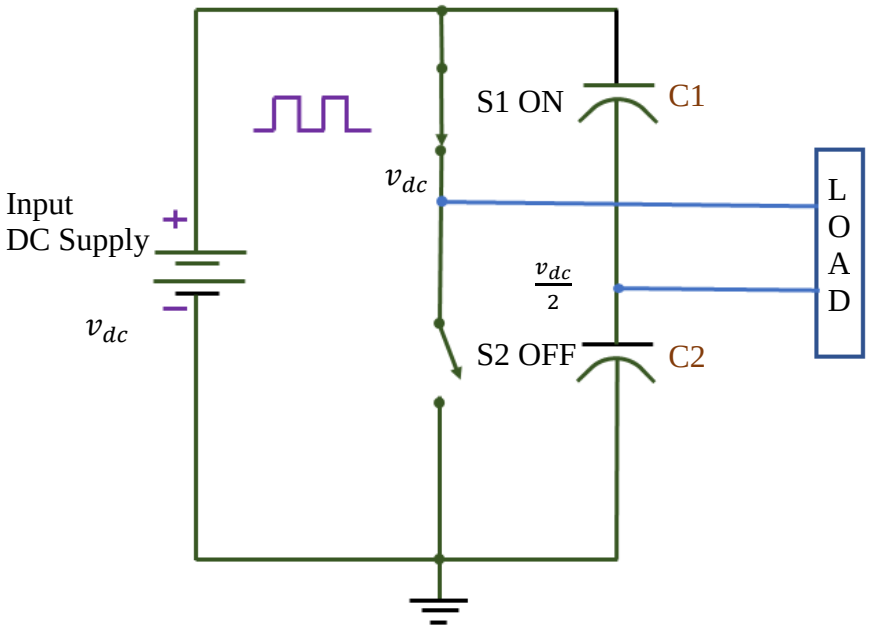

Figure 2.10: S1 ON and S2 OFF State

- **When Switch S2 is ON:** When the switch S1 is OFF and S2 is ON, the upper terminal of the load is at ground potential and the other end of load is connected to the mid-point between the two capacitors. Hence, we have

$$v_{load} = 0 - \frac{v_{dc}}{2} = -\frac{v_{dc}}{2} \tag{2.10}$$

Hence, the alternating voltage with value of $\frac{v_{dc}}{2}$ and $\frac{-v_{dc}}{2}$ is available across the primary winding of the transformer during positive and negative half-cycles respectively [27-28].

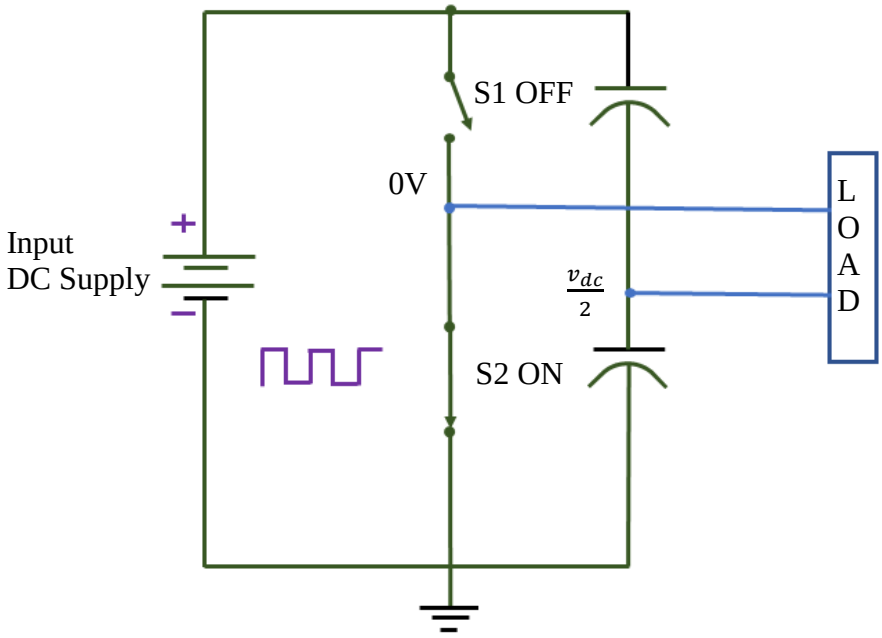

Figure 2.11: S2 ON and S1 OFF State

The output voltage of the half-bridge inverter has odd harmonic components which are multiples of the fundamental frequency. The equation representing the output voltage of the half-bridge inverter is shown below.

$$\text{Output Voltage} = \frac{v_{dc}}{2}\left(sin3\omega t + \frac{sin3\omega t}{3} + \frac{sin5\omega t}{5} + \ ...\right) \qquad (2.11)$$

Where v_{dc} is the input D.C voltage to the half-bridge inverter, ω is the angular frequency and t is the time. The angular frequency is given by the expression,

$$\omega = 2\pi f \tag{2.12}$$

Where f represents the fundamental frequency of the gating signal of the MOSFETs. The simulation results of half bridge inverter are discussed in Appendix A.

2.5 Data Acquisition from Corona Ignition System

The data acquired from corona ignition system includes the high voltage measurement from the igniter and the current flowing through the igniter. A high voltage probe was used for voltage measurement and a current probe was used for current measurement. The structure of the voltage and current measurement probes, and the factors influencing the measurement are described below.

2.5.1 Voltage Measurement Probe

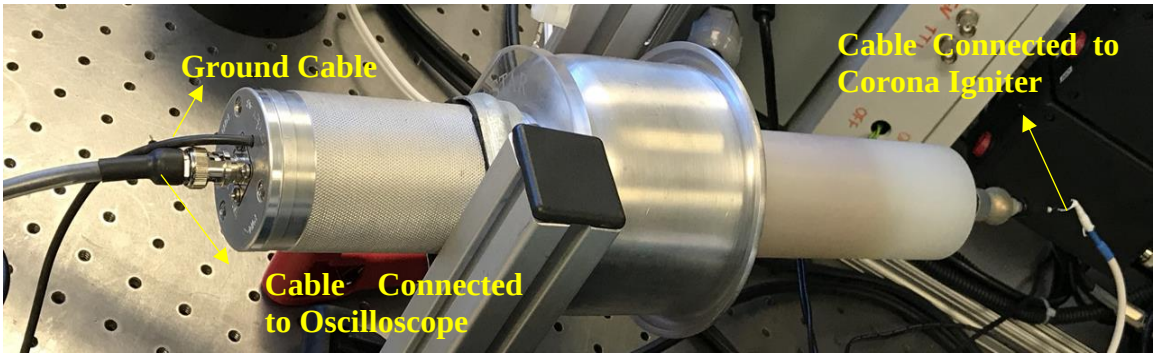

Figure 2.12: High Voltage Measurement Probe

The Northstar PVM6 high voltage probe shown in Figure 2.12 is used for measuring the high voltage signals from the corona igniter. The measurements are obtained by connecting the voltage probe at different locations as described in Figures 2.2 and 2.4 for tests with

and without corona discharge. Since the voltage at the igniter has a high magnitude, the probe attenuates the measured signals by a factor of 2000:1 so that they can be recorded by the digital oscilloscope. A 4.572m (15ft) coaxial cable with a solid polyethylene dielectric insulator is used for displaying the measured voltage signals in the oscilloscope. The high voltage probe as shown in Figure 2.12 consists of three connections. One measurement pin is connected to the igniter at the desired point of high voltage measurement as described in Figures 2.2 and 2.4. The second connection is the coaxial cable for transmitting the attenuated voltage signal to the digital oscilloscope. The third connection provides the ground. The high voltage probe adds an impedance to the system which has been described in Chapter 5 under measurement of electrical component values [21]. The high voltage probe also produces a propagation delay for the voltage signal being displayed in the oscilloscope and subsequent measurement. The voltage and current signals measured are typically assumed to be travelling at the speed of light. But in practice, there is a certain amount of loss introduced by the dielectric material of the coaxial cable. The factor which accounts for the loss in velocity of the voltage and current signals because of the dielectric material is known as the velocity factor [29]. The propagation delay produced by the 15ft coaxial cable used to display high voltage signals in the oscilloscope is calculated as shown below:

The velocity factor (V.F.) for a solid polyethylene dielectric lossless transmission line is 0.66 [29].

$$\text{Speed of light} = 3\text{x}10^{8}\ \text{m/s} \qquad (2.13)$$

Length of coaxial cable = 15ft = 4.572 m (2.14)

Velocity factor = (Velocity of propagation of signal) / (Velocity of light in vaccum) (2.15)

Velocity of propagation of signal = velocity of light x %VF (2.16)

Velocity of propagation of signal = $0.66 \times 3 \times 10^8 = 1.98 \times 10^8$ m/s (2.17)

Time delay, Δt = (Length of the cable) / (Velocity of propagation of the signal) (2.18)

Time delay, $\Delta t = (4.572)/(1.98 \times 10^8) = 23.09$ ns (2.19)

From the time delay calculated above, we can determine the phase delay of a voltage signal of fixed frequency.

2.5.2 Current Measurement Probe

The 411 Pearson wideband current measurement probe shown in Figure 2.13 was used for the current measurement from the system. A 5ft coaxial cable with polyethylene dielectric material was used for recording the measured current signals through the oscilloscope. The measured current signals were attenuated by a factor of 10:1 [22].

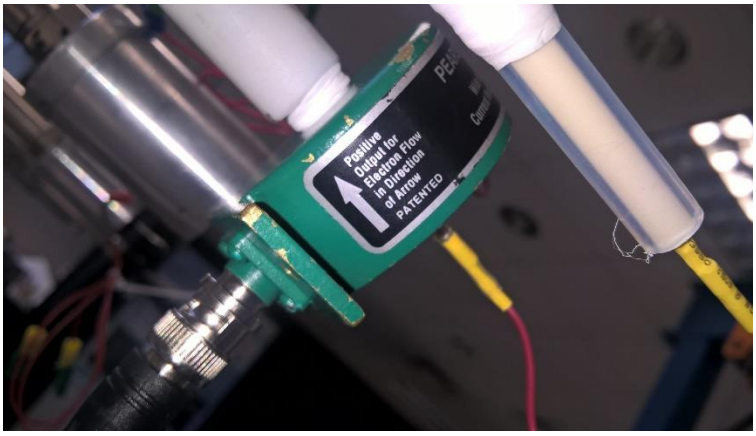

Figure 2.13: Current Measurement Probe

This coaxial cable used in the current measurement probe also introduced a time delay in the signal. The length of the coaxial cable used for the current measurement was 5ft (1.524m) and Equations 2.13 to 2.18 were used to calculate the time delay involved in the signal, which was found to be 7.69 ns.

2.6 Impedance Analyzer Setup

2.6.1 Impedance Analyzer used for Measurement

Measurements were carried out using the impedance analyzer to measure the electrical parameters of the corona ignition system such as the inductance of the primary and the secondary windings of the transformer, coupling coefficient k of transformer, value of resistance R, inductance L, and capacitance C of the igniter. The resistance, capacitance and inductance added by the high voltage measurement probe to the system were measured [21]. The system parameters obtained from the measurement of electrical component values were used in the physics based model of corona ignition system to simulate the system behavior.

A Keysight technologies E4990A impedance analyzer is used for measuring the electrical component values of corona ignition system. The frequency range of measurement for this impedance analyzer is in the range 20 Hz to 120MHz [17, 30]. The measurement gives us the resistance, inductance, and capacitance of the component or device being measured. The impedance analyzer used in measurement of the electrical component values is shown in Figure 2.14.

Figure 2.14: Impedance Analyzer (Keysight Technologies E4990A)

2.6.2 Choosing the Equivalent Circuit Model

During the measurement of the transformer or the igniter using the impedance analyzer, a model or equivalent circuit of the impedance being measured had to be chosen for the impedance analyzer to display the values of resistance, inductance and capacitance. A series RLC circuit model as shown in Figure 2.16 was chosen for determining the values of resistance R, inductance L, and capacitance C of the impedance being measured. During

the measurement of electrical component values of the corona ignition system, the sweeping range was chosen from 20KHz to 2MHz.

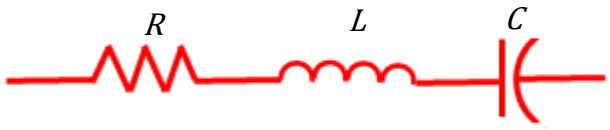

Figure 2.15: Series RLC Circuit Model for Determining the Parameters of Igniter and Transformer

2.6.3 Determination of Transformer Parameters

The inductance of the primary winding was measured using the impedance analyzer by choosing the series RLC circuit model. The inductance of the primary winding was calculated by performing two measurements - measuring the primary inductance with the secondary winding open-circuited and short-circuited.

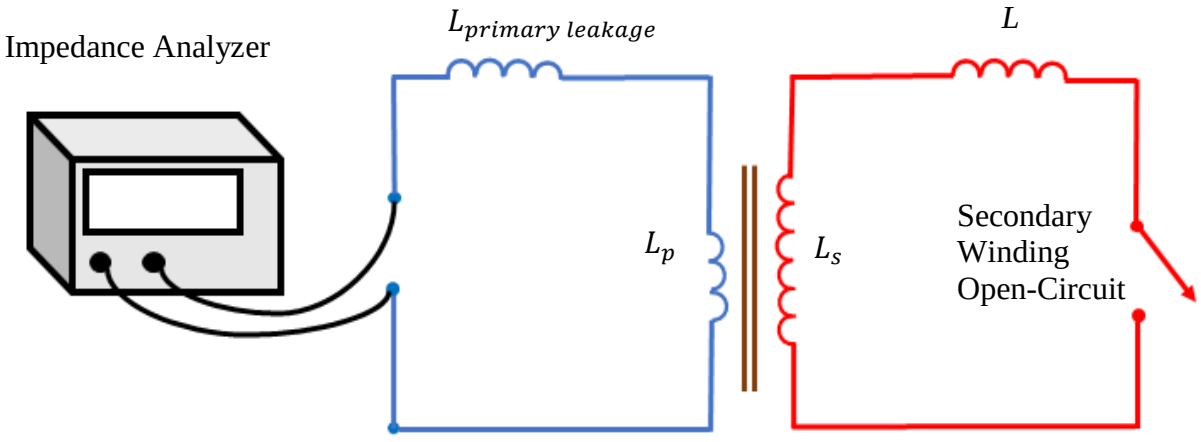

Figure 2.16: Determination of Coupled and Leakage Inductance of Primary Winding

There is always a certain portion of the inductance of a winding which is not perfectly coupled with the other winding of the transformer. This inductance of a winding which is not coupled with the other is called leakage inductance. The leakage inductance of a winding in a transformer does not take part in transformer action [31].

The inductance value obtained with the secondary winding open-circuited represents the coupled portion of primary inductance plus the leakage part as shown in Figure 2.17, whereas the leakage portion of primary inductance which does not participate in transformer action is obtained by short-circuiting the secondary winding. The primary winding taking part in transformer action is determined by subtracting the inductance values obtained from open circuiting and short circuiting the secondary winding [17, 31]. In Figure 2.17, L_P and L_s represent the primary and secondary inductances of the transformer taking part in transformer action respectively, whereas $L_{Primary\ leakage}$ and L represent the leakage inductances of primary winding and secondary winding connected to the igniter.

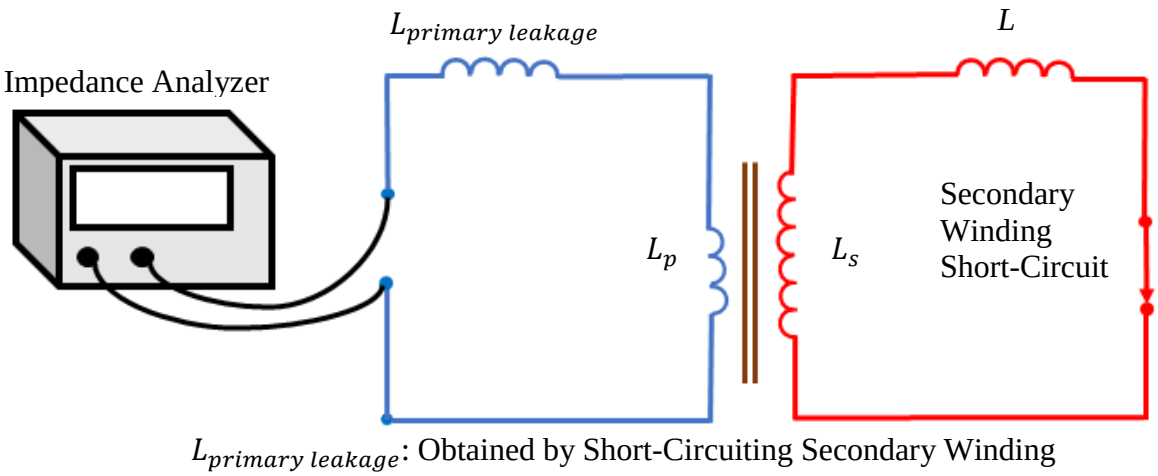

Figure 2.17: Determination of Leakage Inductance of Primary Winding

Equation 2.20 shows the determination of the transformer coupling coefficient k for the primary winding [17, 31-32].

$$k = \sqrt{1 - \frac{L_{primary\ leakage}}{L_{primary\ leakage} + L_p}} \tag{2.20}$$

2.6.4 Determination of Electrical Parameters of Igniter connected to Transformer

The secondary winding of the transformer is connected to the igniter which represents a combined inductance. Hence, we need to know which portion of this inductance is used for transformer action and which portion of inductance is used for resonating the corona igniter. The corona igniter is connected to the secondary winding of the transformer for performing the measurement. The primary winding of the transformer is open-circuited and the combined impedance of the secondary winding connected to the igniter is determined. This measurement gives the inductance of the secondary winding plus the leakage inductance used for resonating the corona igniter. The resistance and capacitance are also determined from this measurement [17, 31].

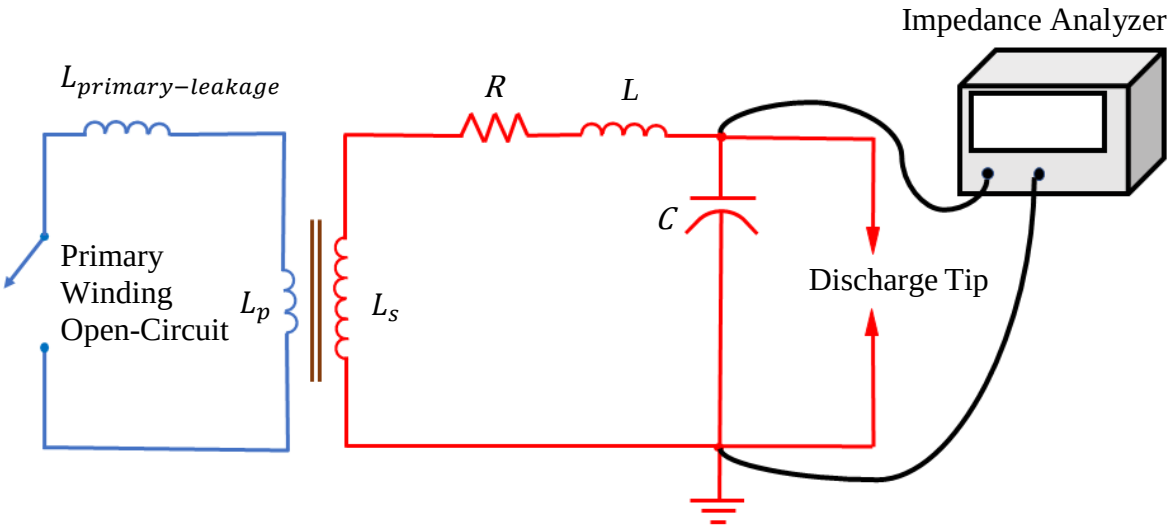

Figure 2.18: Determination of Igniter Parameters by Open-circuiting Primary Winding

In the second measurement, the primary winding is short circuited with the igniter connected to the transformer secondary winding as shown in Figure 2.20. This measurement gives the portion of inductance which is not perfectly coupled with the primary winding and is used in resonating the igniter. The resistance and capacitance are also determined from this measurement. The inductance of the secondary winding used in transformer action is determined by subtracting the inductance values obtained by open-circuiting and short-circuiting the primary winding. The coupling coefficient of the secondary winding is determined from these measurements. The formula used for determining the coupling coefficient of the secondary winding is similar to the one for primary winding [17, 31-32].

$$k = \sqrt{1 - \frac{L}{L + L_s}} \tag{2.21}$$

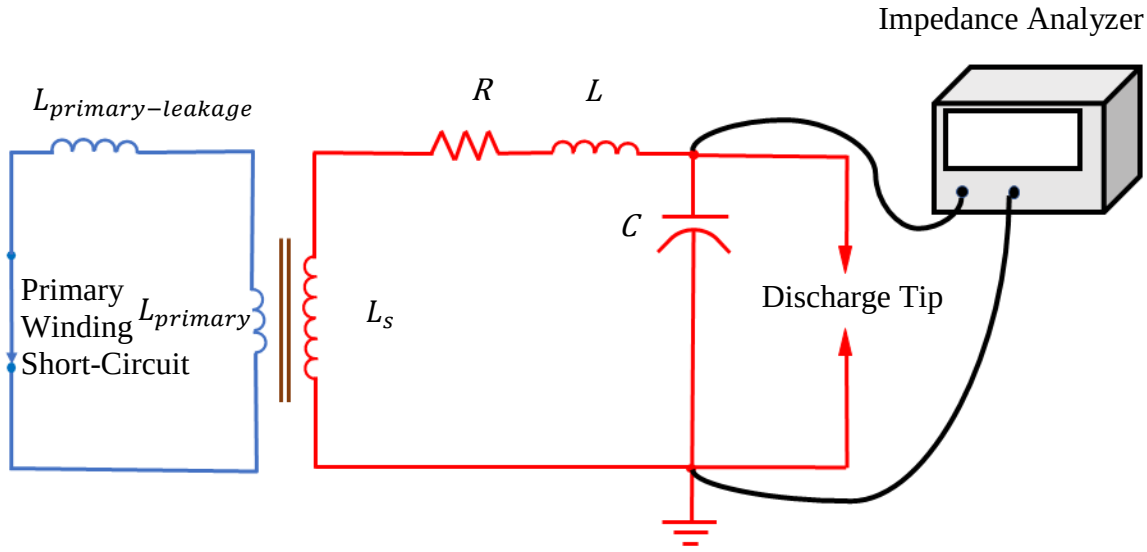

L: Obtained by Short-Circuiting Primary Winding

Figure 2.19: Determination of Igniter Parameters by Short-circuiting Primary Winding

The resistance and capacitance obtained by short-circuiting the primary winding are hypothesized to be representing the resistance and capacitance of the igniter when the transformer's secondary winding is connected to it.

2.6.5 Determination of Electrical Parameters of High Voltage Probe

The electrical parameters of the high voltage probe used in the system are determined using the impedance analyzer. The measurement involves cable of the probe used for measuring high voltage and the cable used for displaying high voltage signals in the digital oscilloscope connected to the impedance analyzer. The ground cable is not included in the

measurement. This measurement gives the resistance, inductance and capacitance of the high voltage probe.

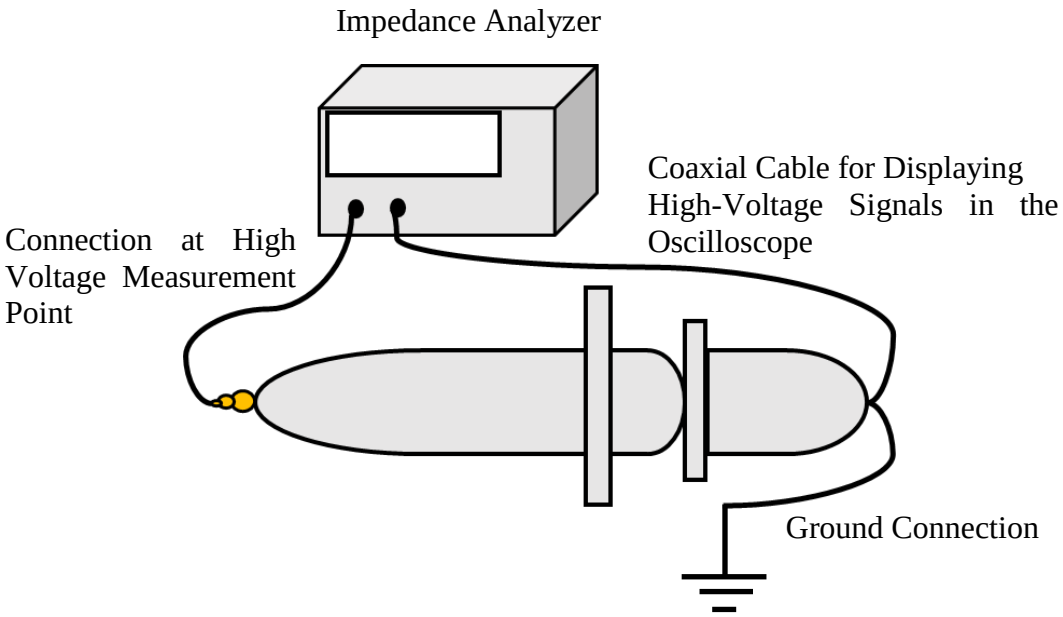

Figure 2.20: Determination of Impedance of Voltage Probe

2.6.6 Investigation of Effect on Electrical Parameters of Transformer and Igniter

Measurements were performed to determine the electrical parameters of the transformer and igniter such as quality factor, resonating inductance and secondary inductance with change in position of primary coil inside the hollow metal shell of corona igniter. Figure 2.22 illustrates the measurement performed. Measurement was done using the procedure as described in section 2.6.4 for transformer connected to the igniter by placing the primary coil over a range of distances from the surface of hollow metal shell. The electrical parameters of the transformer and igniter were measured at each position of the primary coil. Measurement of the distance at which the coil was placed inside the metal shell from

the metal shell surface was done using a Vernier Calliper. The igniter shown in Figure 2.7 was used in the measurement of electrical parameters with change in the position of the primary coil. The results of the measurement are discussed in Chapter 5.

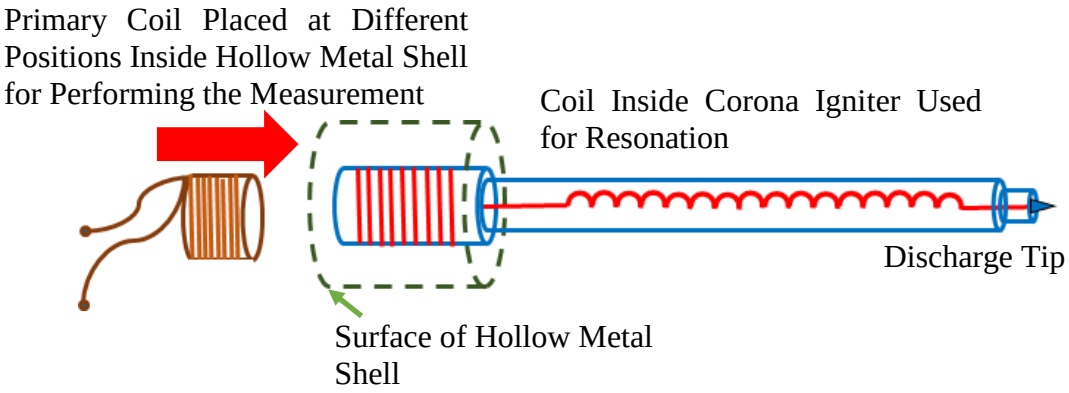

Figure 2.21: Corona Igniter with Hollow Metal Shell

CHAPTER 3: TESTS WITH AND WITHOUT CORONA DISCHARGE

This chapter pertains to tests performed to study the electrical behavior of corona ignition system with and without corona discharge in ambient air. The different electrical parameters that were analyzed were the voltage and current signals, instantaneous power and the phase difference between voltage and current signals. The frequency domain analysis was also conducted to understand the system behavior.

3.1 Investigation of System Behavior with Corona Discharge

Table 3.1: Test Conditions for case with Corona Discharge

Parameter	Value
Gating Signal Duration	0.5ms or 500µs
Input DC supply	77.6V
Frequency of Gating Signal	Varied
Duty cycle	50%
Sampling Frequency of Measured Voltage and Current Signals	62.5MHz

The circuit described in Figures 2.2 and 2.3 is used in this test. The frequency at which the peak values of voltage, current and power are obtained is known as the resonant frequency of corona ignition system [33-34]. The frequency sweep is performed to first identify the resonant frequency of the corona ignition system during corona discharge.

3.1.1 Investigation of Frequency Domain Behavior

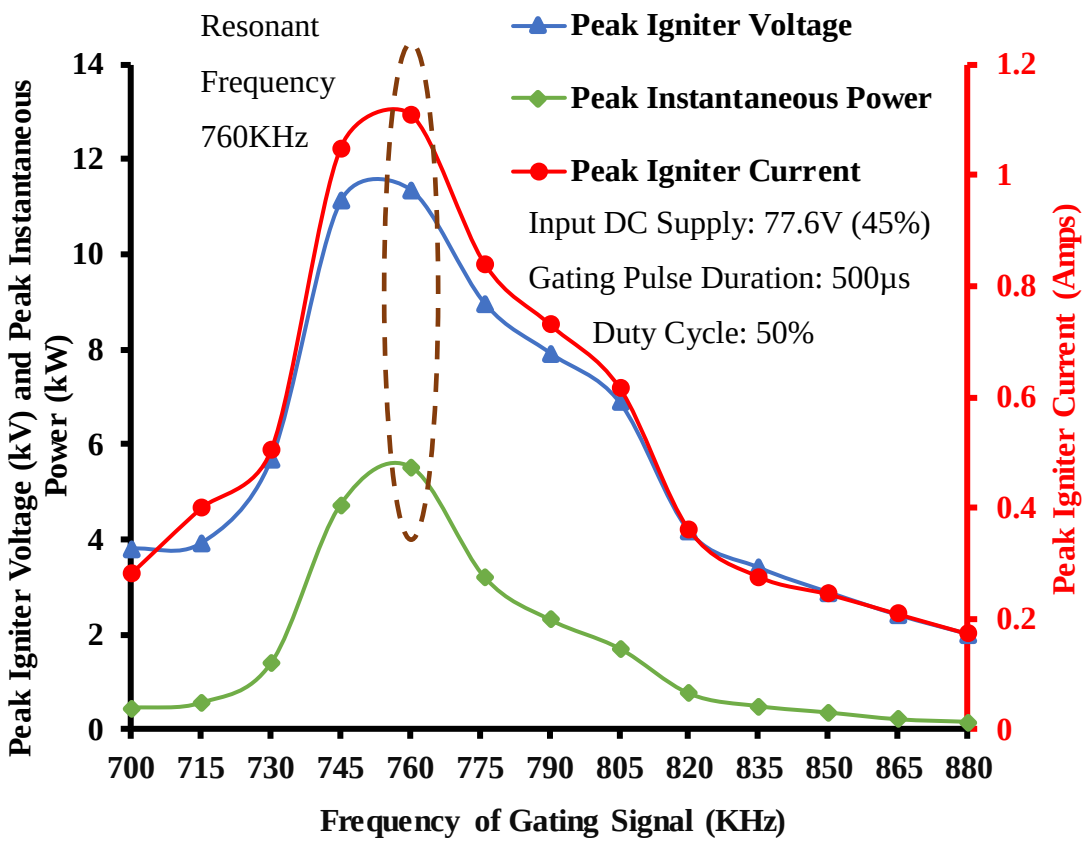

Figure 3.1: Resonant Frequency During Corona Discharge

The frequency sweep was performed for 13 frequencies from 700KHz to 880KHz at equal intervals of 15KHz. As shown in Figure 3.1, the peak voltage, current and instantaneous power occurred at a frequency of 760KHz. Hence, 760KHz was regarded as the resonant frequency of the corona ignition system during corona discharge.

Frequency domain analysis was performed for the measured voltage and current signals for the case where the frequency of gating signal was 760KHz to observe if the voltage and

current signals have the same frequency as the frequency of gating signal applied at the input [35-36].

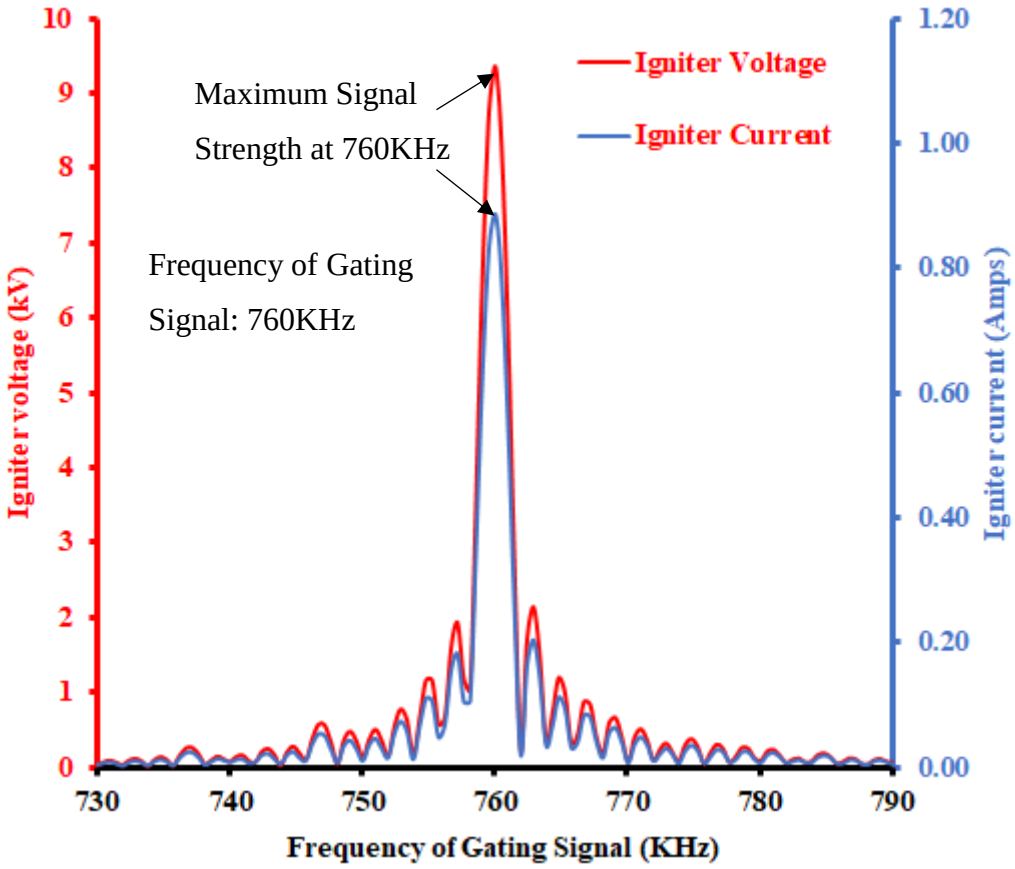

Figure 3.2: Igniter Voltage and Current vs Frequency

It was observed that the igniter voltage and the current signals had maximum signal strength at the frequency of 760KHz which was same as the frequency of input gating signal. There were certain other harmonic components present in the signals as seen from the above graph which had much lower signal strength.

The same procedure of determining the frequency of the igniter voltage and current signals was performed for the frequency sweep of the gating signal of the output voltage and

current signals had the same frequency as the gating signal applied at the input. The relationship between the frequency of measured voltage and current signals with change in frequency of gating signal applied at the input is illustrated in Figure 3.3.

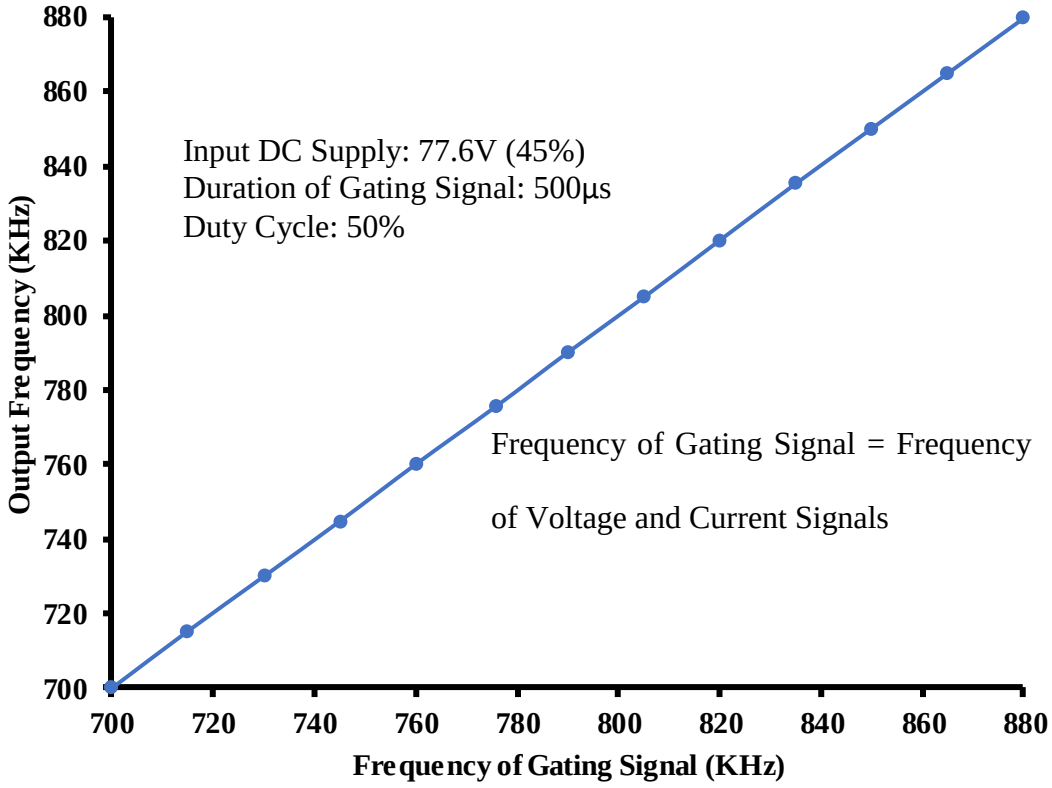

Figure 3.3: Output Frequency vs. Input Frequency with Corona Discharge

3.1.2 Investigation of Time-Domain Behavior

The behavior of the system in the time domain was studied. The measured igniter voltage and current at a frequency of 760KHz were considered in the analysis. The behaviors of the system in the time domain is shown in Figure 3.4 and Figure 3.5 for the voltage and current signals respectively.

The gating signal was applied for a duration of 500µs and at a frequency of 760KHz. Hence, the igniter voltage and current signals appeared for a duration of 500µs. It was also observed that there were variations in the amplitude of voltage and current signals during corona discharge. This could be attributed to the fact that during corona discharge, there was variation in the impedance of the system.

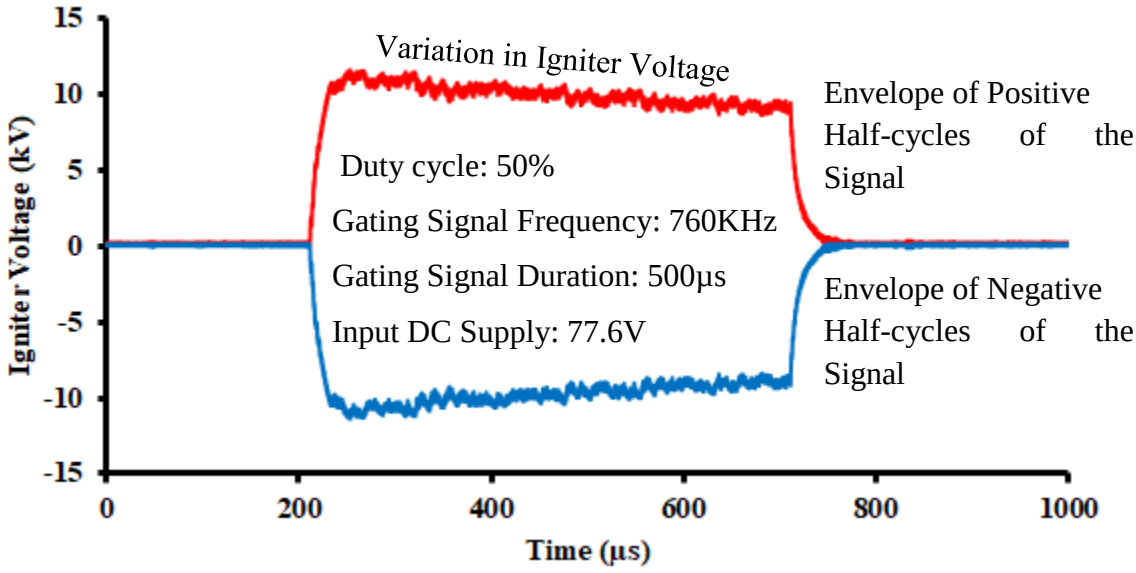

Figure 3.4: Envelope of Igniter Voltage vs Time

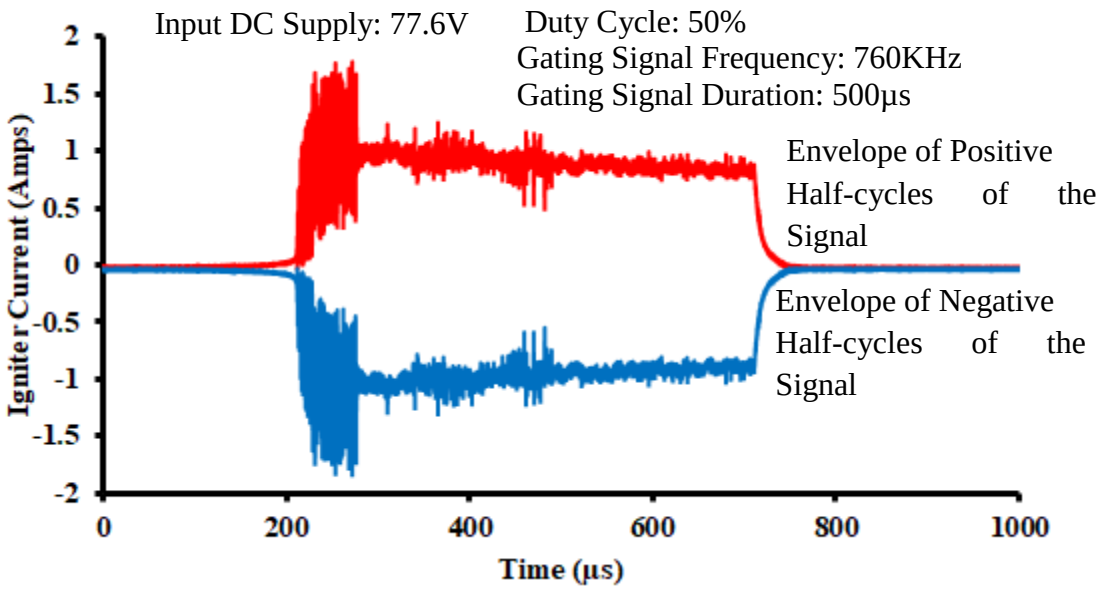

Figure 3.5: Envelope of Igniter Current vs Time

It was observed that initially when the trigger was applied, the voltage signal did not appear immediately (Figure 3.6). There existed a delay for the voltage signal to appear. As time progressed, it was observed that the phase of the voltage changed and it began to lead the trigger signal as represented in Figure 3.7. This could be attributed to the non-linearities present in the phase behavior of the system.

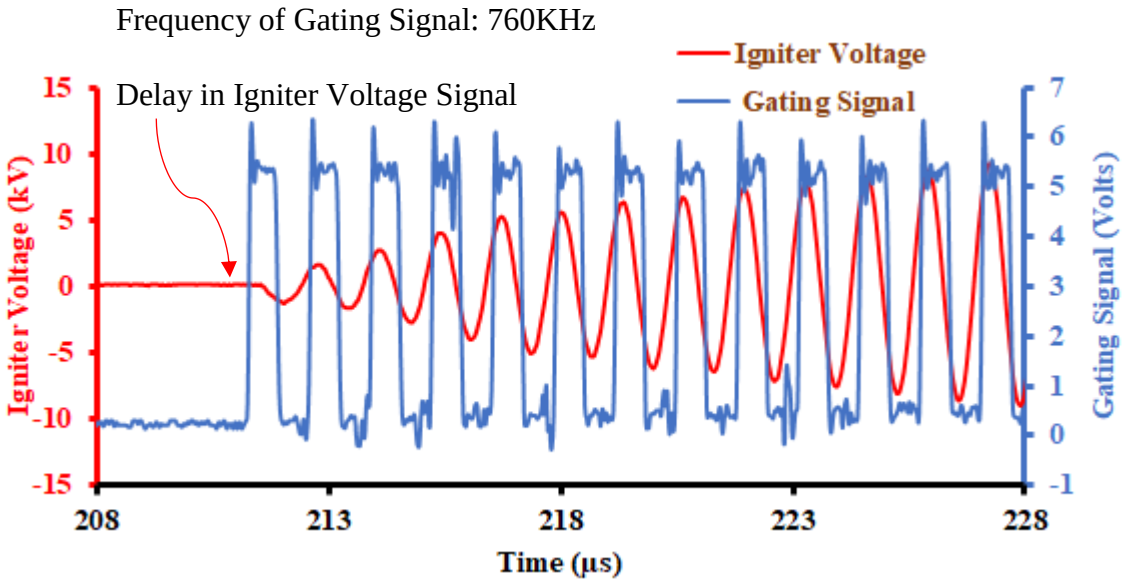

Figure 3.6: Igniter Voltage upon Application of Gating Signal

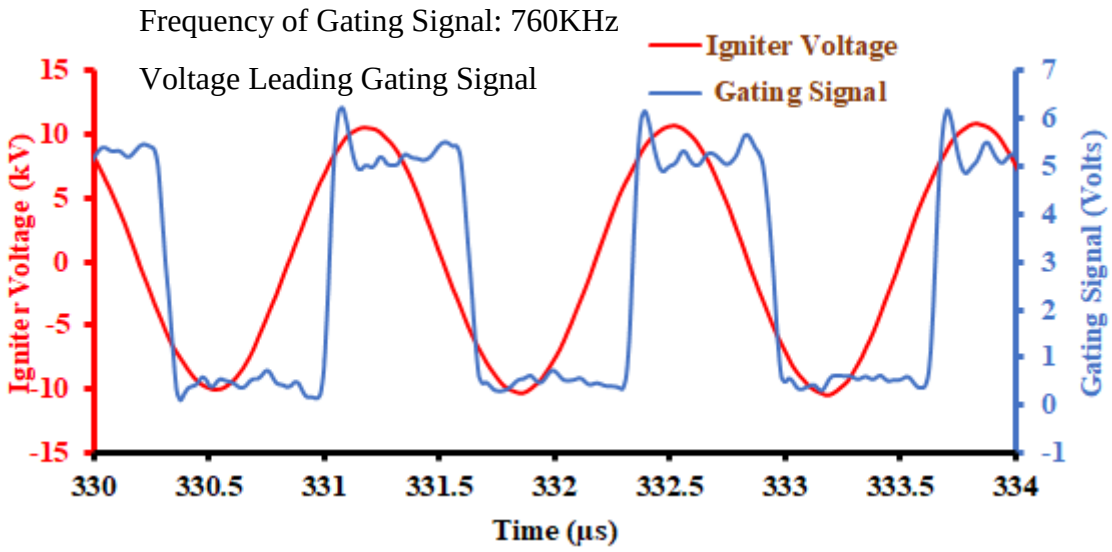

Figure 3.7: Igniter Voltage and Gating Signal vs. Time

To further understand the behavior of the system during corona discharge, the phase difference between the measured igniter voltage and current signals in the time domain was investigated when the frequency of the gating signal was 760KHz. Two particular ranges in time are shown in Figures 3.8 and 3.9.

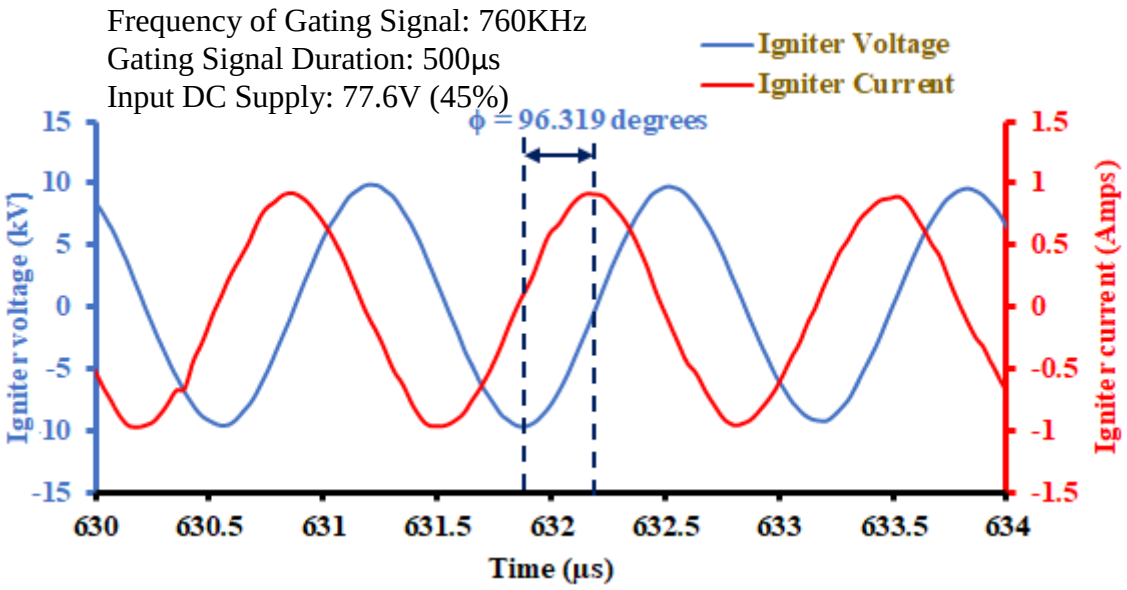

Figure 3.8: Variation of Phase Difference vs Time

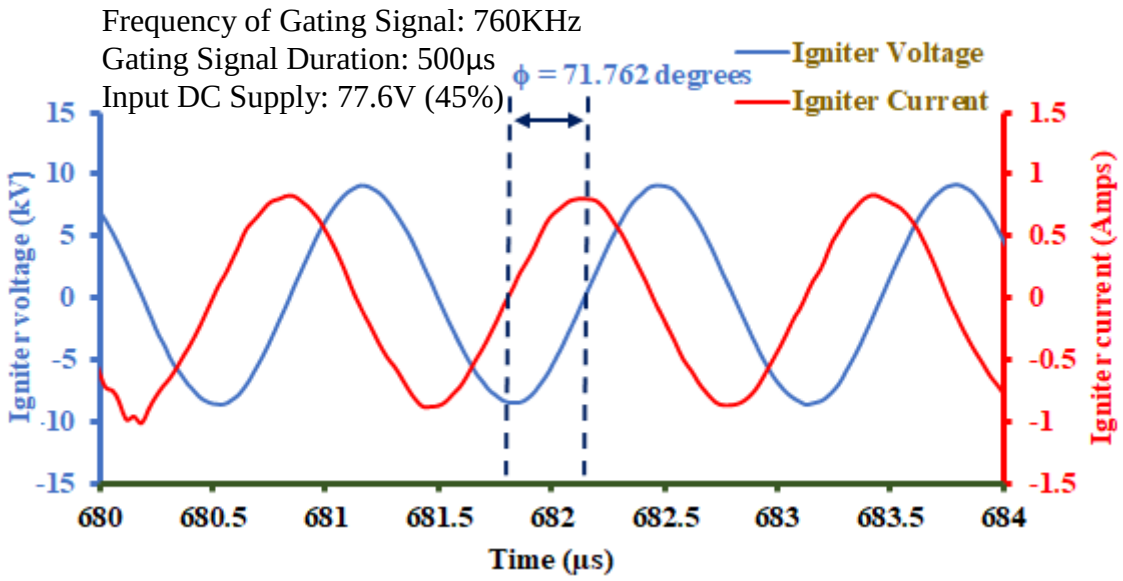

Figure 3.9: Variation of Phase Difference with Progression of Time

It was observed that the phase difference was not constant. Previously (Figure 3.2) it had been observed that the frequency of the igniter voltage and current signals was identical to the frequency of input gating signal at 760KHz. Hence, from Equations 2.3 and 2.4 it was concluded that the change in phase difference between voltage and current signals was probably because of the change in the impedance of the corona ignition system during corona discharge.

From the time domain and frequency domain results during corona discharge, it was understood that the system exhibited capacitive behavior, and there was variation in impedance of the system [37]. This impedance variation during corona discharge caused the phase difference between the voltage and current signals to decrease from 96.319 degrees at 632µs to 71.762 degrees at 682µs [38].

3.2 Investigation of System Behavior without Corona Discharge

The electrical behavior of the corona ignition system without corona discharge was investigated. The circuit diagram of the experimental setup and the point of measurement of voltage and current signals are shown in Figure 2.5. The test was performed in ambient air similar to the case with corona discharge. The test conditions are given in Table 3.2.

Table 3.2: Test Conditions for case without Corona Discharge

Parameter	Value
Gating Signal Duration	0.5ms or 500µs
Input DC supply	20.5 Volts
Input Frequency	Varied
Duty cycle	50%
Sampling Frequency of Measured Voltage and Current Signals	62.5MHz

The time domain and the frequency domain behavior of the signals were investigated similar to section 3.1. The frequency sweep was conducted for six frequencies namely 889.8KHz, 900.3KHz, 909.8KHz, 940.3KHz, 980.4KHz, 1MHz. The D.C supply to the half-bridge inverter was 20.5V. The duty cycle and duration of gating signal were kept at 50% and 500µs respectively. The time domain and frequency domain analyses were performed on the measured voltage and current signals to understand their behavior without corona discharge.

3.2.1 Investigation of Frequency Domain Behavior

Figure 3.10 shows the peak values of igniter voltage, current and instantaneous power vs frequency of the gating signal. The peak values were observed at a frequency of 889.8KHz. The corona ignition system without corona discharge was hypothesized to be a series RLC circuit connected to a transformer. No impedance change was expected due to absence of corona discharge.

The frequency domain behavior was investigated by observing the variation of frequency of gating signal with frequency of measured voltage and current signals [35-36]. The result representing the variation of gating signal frequency with frequency of measured voltage and current signals is presented in Figure 3.11.

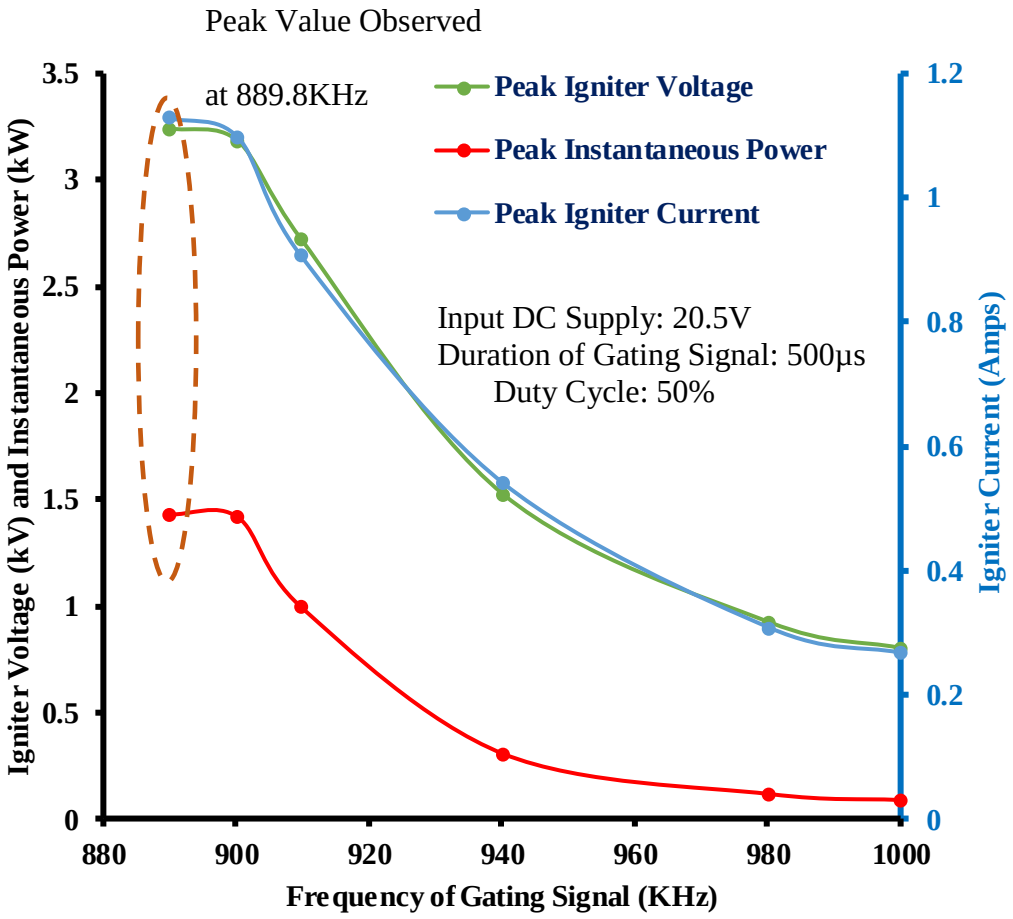

Figure 3.10: Peak Igniter Voltage, Current and Instantaneous Power vs. Frequency of Gating Signal

As shown in Figure 3.11, it was observed that the frequency of the measured voltage and current signals was equal to the frequency of the input gating signal. This was similar to the behavior of the system with corona discharge. Hence, irrespective of whether there was corona discharge or not, the frequency of measured voltage and current signals remained same as the frequency of the input gating signal given to switch the MOSFETs of the half-bridge inverter.

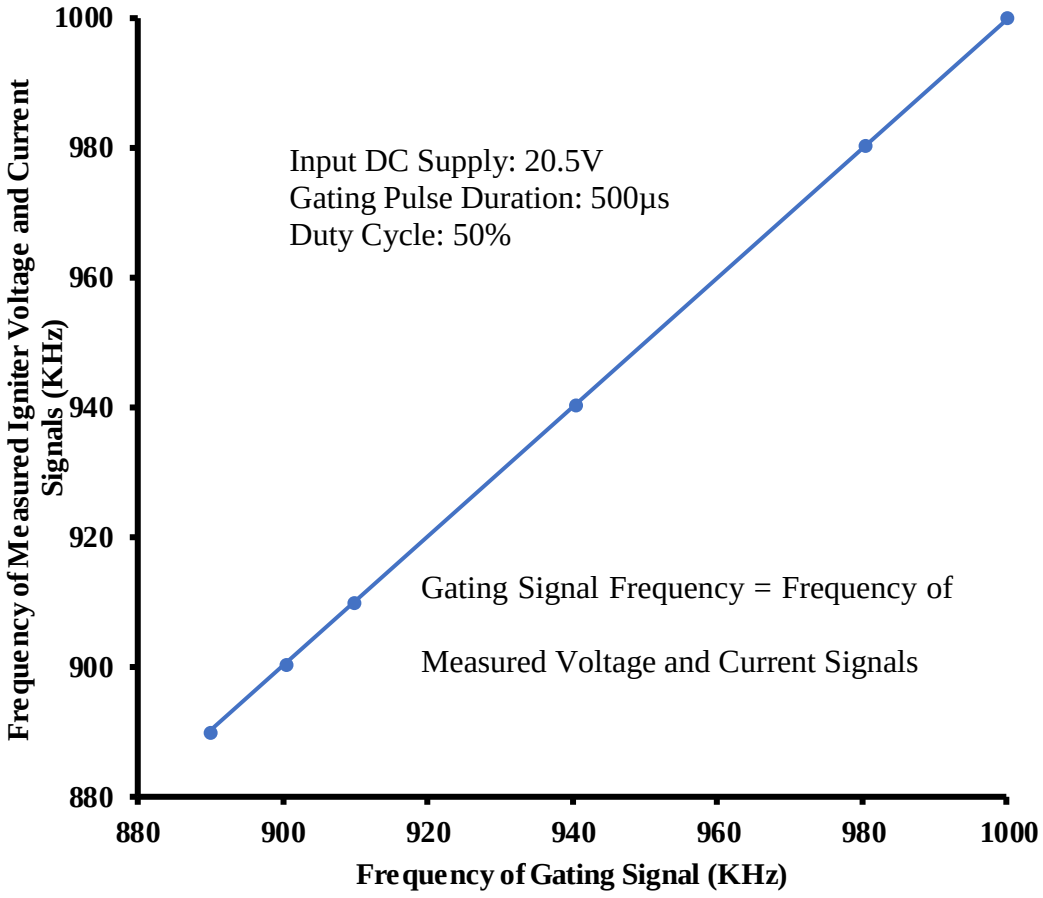

Figure 3.11: Input Frequency vs. Output Frequency without Corona Discharge

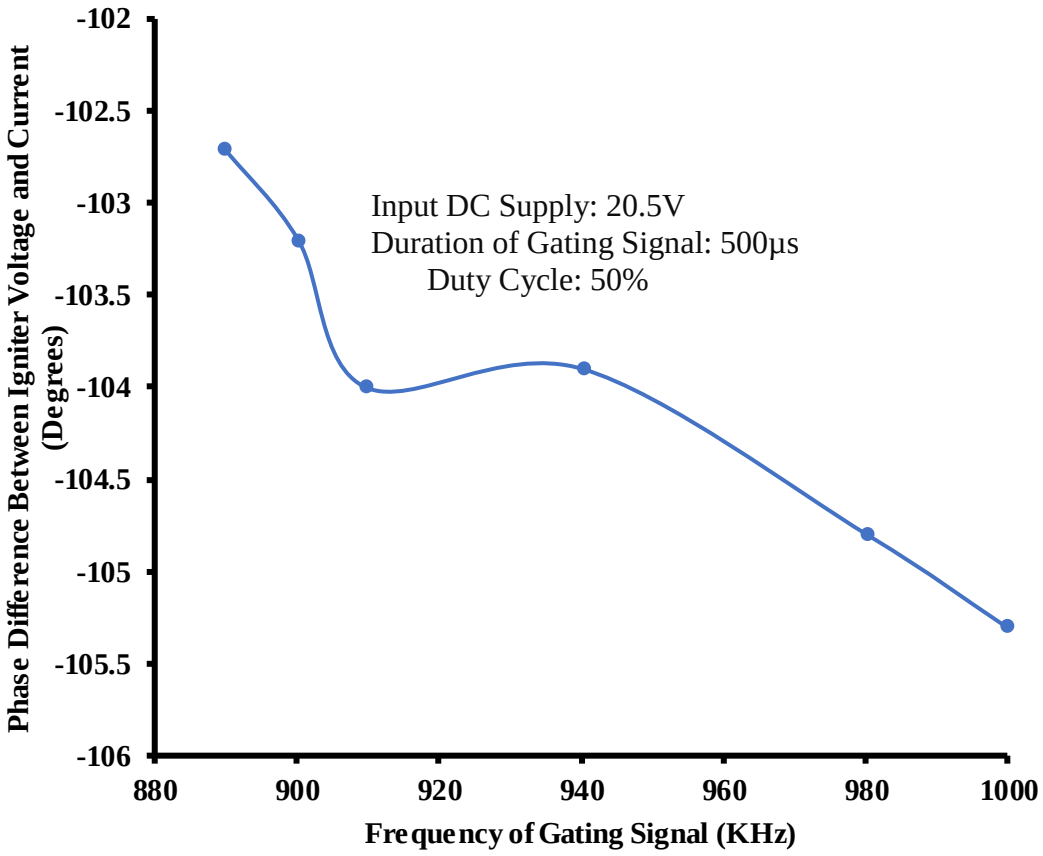

Figure 3.12: Phase Difference Between Igniter Voltage and Current Signals vs. Frequency of Gating Signal

The phase difference between voltage and current signals varied with frequency (Figure 3.12). A decreasing trend in the phase difference was observed except at a frequency of 940.3KHz. From the negative value of phase difference between voltage and current signals, we could observe capacitive behavior at all swept frequencies for the case, without corona discharge, with current leading the voltage.

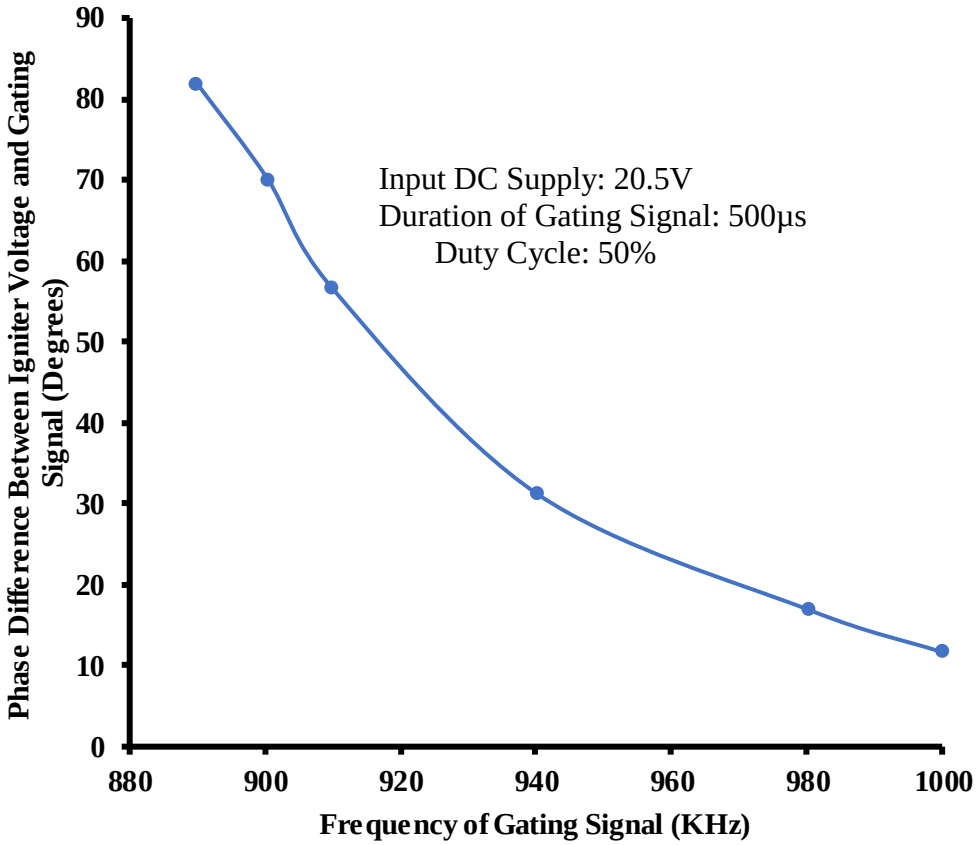

Figure 3.13: Phase Difference between Igniter Voltage and Gating Signal

As shown in Figure 3.13, there existed a phase difference between applied gating signal and the igniter voltage signal which reduced with increase in frequency. The igniter voltage signal lead the gating signal since the phase difference between them was positive.

3.2.2 Investigation of Time Domain Behavior

The time domain behavior of the measured voltage and current signals was investigated. The results of the time domain behavior of voltage and current signals are represented in the Figures 3.14, 3.15 and 3.16.

The transient and steady states of measured igniter voltage for the case without corona discharge are represented in Figure 3.14. It is observed that without corona discharge, the signals do not fluctuate because the impedance of the system remains constant. The envelope of the measured current signal is shown in Figure 3.15 which is similar to the voltage signal. There is no fluctuation in amplitude due to the absence of corona discharge.

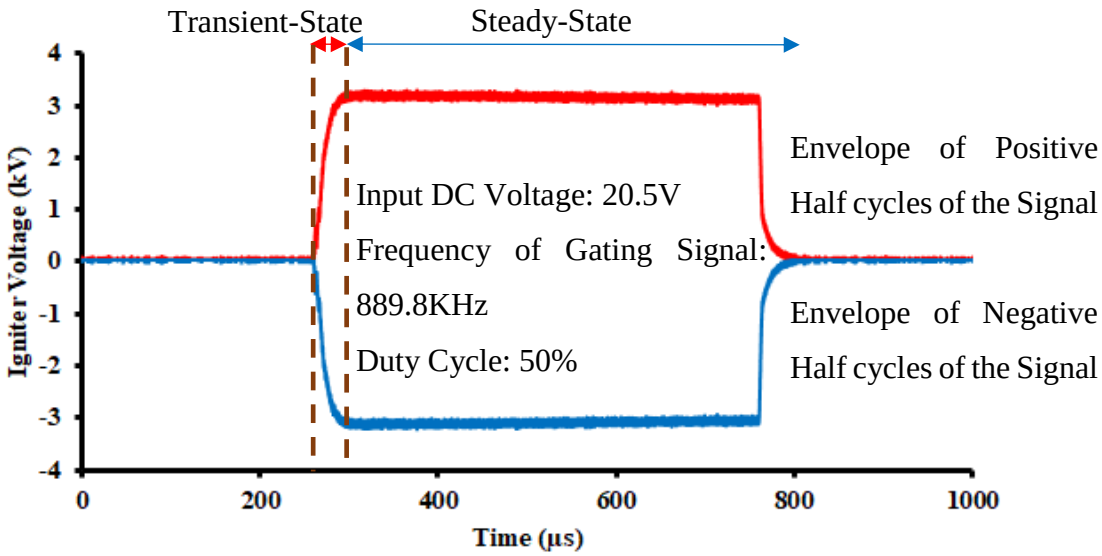

Figure 3.14: Envelope of Igniter Voltage vs Time without Corona Discharge

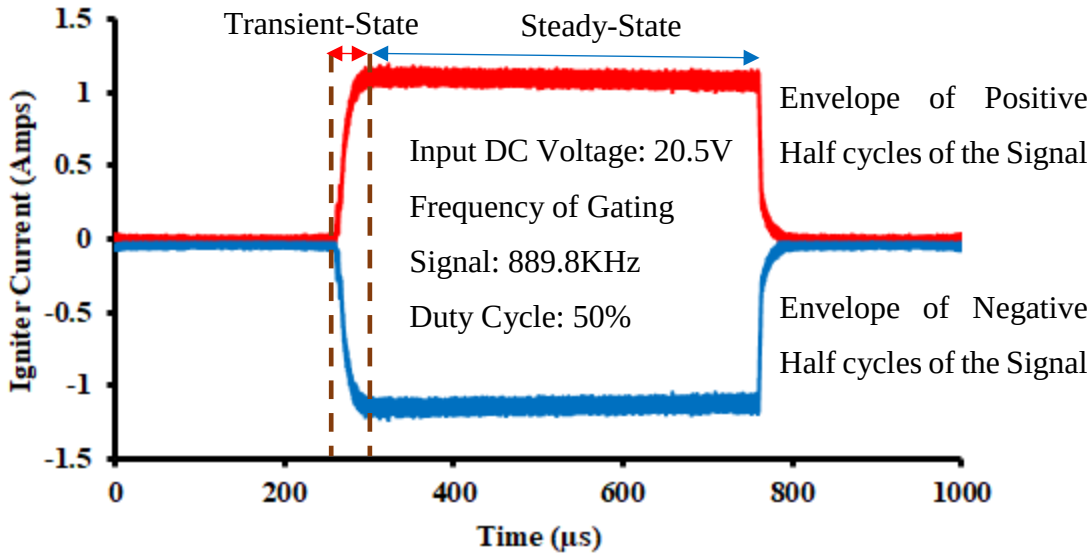

Figure 3.15: Envelope of Igniter Current vs Time without Corona Discharge

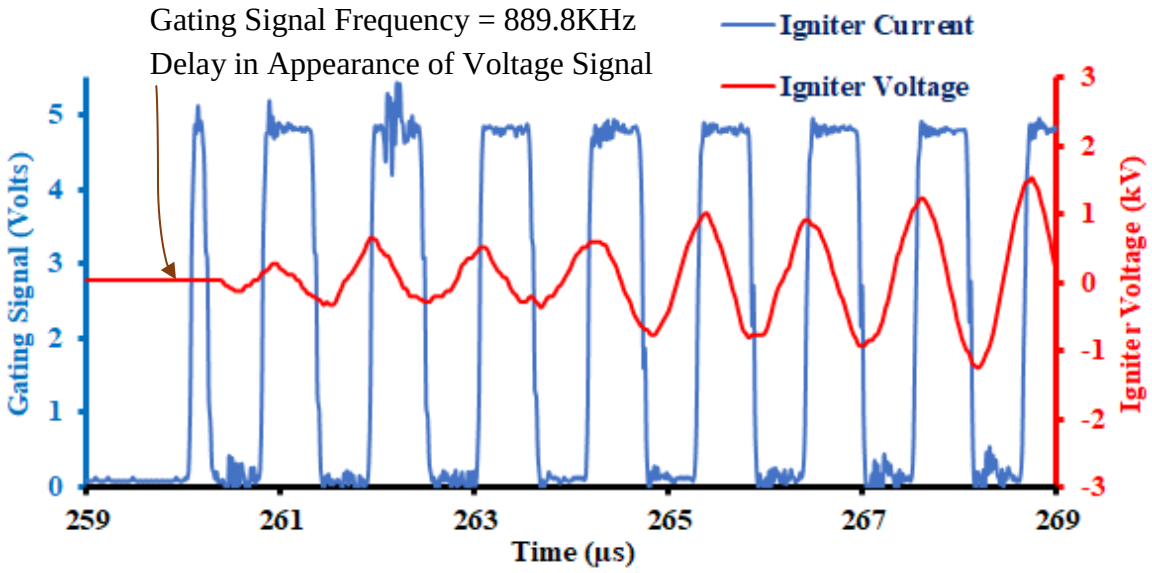

Figure 3.16: Variation of Igniter Voltage and Gating Signal vs Time

Initially during the application of the gating signal, the voltage signal did not appear immediately. The voltage signal appeared after a certain time delay similar to Figure 3.6, whereas after it reached the steady state, the igniter voltage began to lead the gating signal

as shown in Figure 3.17 due to the change in phase of the voltage signal. However, for the case without corona discharge, it was observed that once the voltage signal reached steady-state, the phase of the signal remained constant. The igniter voltage and current signals in the time domain are represented in Figure 3.18.

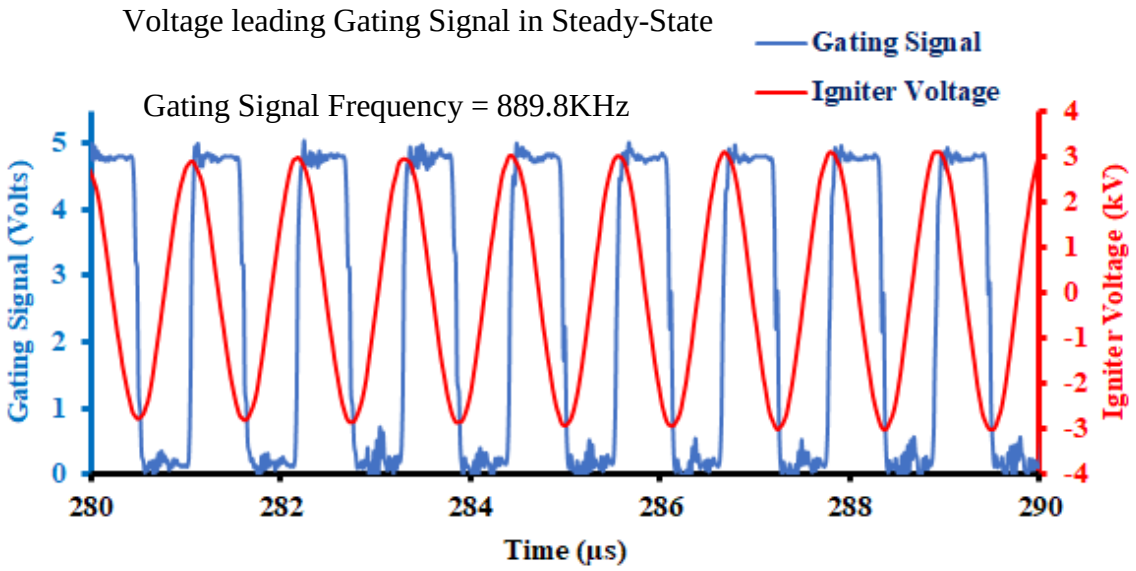

Figure 3.17: Variation of Igniter Voltage and Gating Signal with Progression of Time

The capacitive behavior exhibited by the measured igniter voltage and current signals without corona discharge was similar to the case with corona discharge. With corona discharge, the major difference was the change in impedance of the system. This impedance change caused the phase difference between measured voltage and current signals to vary, even though the frequency of the measured voltage and current signals were same as the frequency of the gating signal applied at the input.

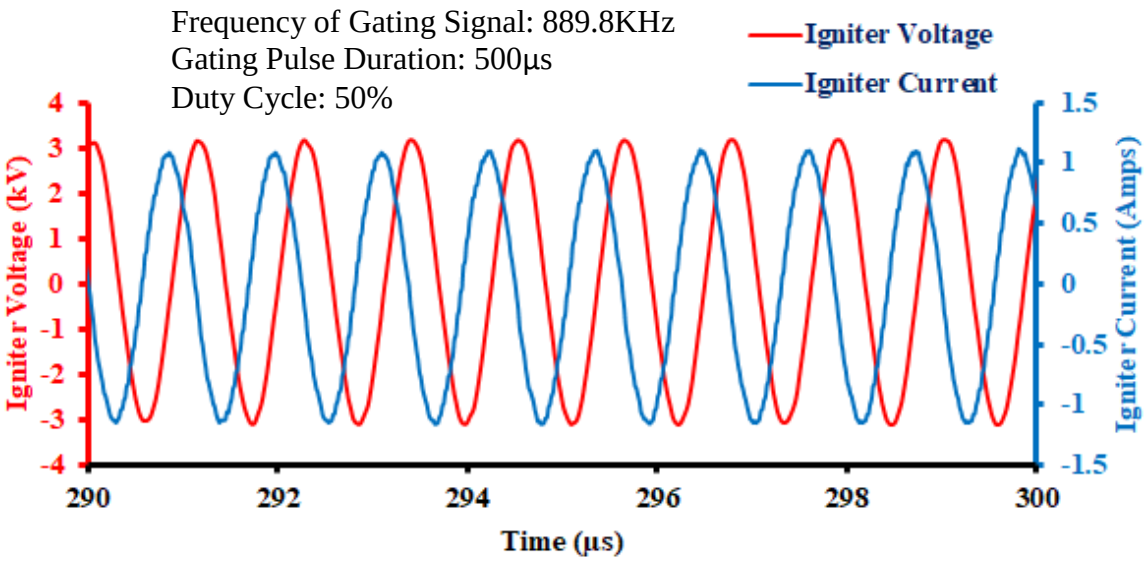

Figure 3.18: Igniter Voltage and Igniter Current vs Time

CHAPTER 4: MEASUREMENT OF ELECTRICAL COMPONENT VALUES

4.1 Introduction

This chapter outlines the results of measurement of the electrical component values of corona ignition system. The electrical parameters were determined for the transformer and igniter used in the tests with and without corona discharge as described in Chapter 2. The resonant frequency could be determined from the measured values of inductance and capacitance of the corona igniter, and compared with the experimentally obtained resonant frequency during corona discharge. The inductances of the primary and secondary windings of transformer, and the resistance, inductance and capacitance of the series RLC circuit of corona igniter used in the test without corona discharge were determined as well. The obtained measurements were then used in the first principles model of corona ignition system discussed in Chapter 5. Measurements were also performed to study the effect on parameters such as quality factor, resonating inductance and secondary inductance of the transformer with change in position of primary coil inside the cylindrical metal shell of corona igniter.

4.2 Measurement of Inductance of Transformer

The inductance of the transformer was measured using the impedance analyzer. The series RLC circuit model was used for determining the values of inductance. For a transformer, either the primary or the secondary winding had a portion of inductance that was coupled with the other winding which was used in the transformer action. The portion of inductance which was not perfectly coupled with the other winding was known as the leakage

inductance of that winding. In the case of corona ignition system, the leakage inductance associated with the secondary winding connected to the igniter was used for resonation. The inductances of the primary and secondary windings of the transformer used in the test without corona discharge were determined as described in Chapter 2.

In Table 4.1, the inductance obtained by short-circuiting the secondary winding is the leakage inductance of the primary winding. The inductance obtained by open-circuiting the secondary winding represents the sum of the primary inductance used in transformer action and the leakage inductance of the primary winding of the transformer. The coupling coefficient of the transformer used in the test without corona discharge is determined from Equation 2.20 described in Chapter 2 [17, 31-32].

Table 4.1: Measurement of Inductance of Primary Winding for Case without Corona Discharge

Secondary Open-Circuit	Secondary Short-Circuit	k Calculated
$L_p + L_{primary-leakage}$ (µH)	$L_{primary-leakage}$ (µH)	
1.10	1.09	0.095

4.3 Measurement of Electrical Parameters of Igniter

The corona igniter was connected to the secondary winding of the transformer to measure the combined electrical parameters using the impedance analyzer. The combined electrical parameters of the corona igniter and transformer were measured, because they influenced the overall system impedance during its operation. The series RLC circuit model was used

for the impedance analyzer to display values of resistance, inductance and capacitance of the igniter.

Tables 4.2 and 4.3 represent the measured electrical parameters with igniter and transformer secondary connected together with and without corona discharge respectively. The inductance obtained by short-circuiting the primary winding represents the leakage inductance used for resonating the igniter. The inductance obtained by open-circuiting the primary winding represents the sum of leakage inductance and the coupled portion involved in transformer action when transformer secondary is connected to the corona igniter [17, 31-32]. It is also observed from Tables 4.2 and 4.3 that the resistance and capacitance obtained by open circuiting and short-circuiting the primary winding does not differ by a huge value. The resistance and capacitance values obtained with primary short-circuited as shown in Table 4.3 are used in the Physics based model of corona ignition system and the determination of resonant frequency. The coupling coefficient of the secondary winding of the transformer is determined to be 0.2797 using Equation 2.21 for the case without corona discharge. Since the coupling coefficients determined from the primary and secondary windings of transformer for the case without corona discharge are different, the higher value of 0.2797 from the two measurements is used in the model described in Chapter 5.

Table 4.2: Measurement of Electrical Parameters of Igniter Connected to Secondary Winding of Transformer for the case with Corona Discharge

Primary Open-Circuit			Primary Short-Circuit		
R (Ω)	**L (mH)**	**C (pF)**	**R (Ω)**	**L (mH)**	**C (pF)**
254.49	1.40	17.6	271	1.33	17.5

Table 4.3: Measurement of Electrical Parameters of Igniter Connected to Secondary Winding of Transformer for the Case without Corona Discharge

Primary Open-Circuit			Primary Short-Circuit		
R (Ω)	**L (µH)**	**C (pF)**	**R (Ω)**	**L (µH)**	**C (pF)**
92.43	467.94	39.17	101.39	431.33	38.45

For the case with corona discharge, the values of resistance, inductance and capacitance obtained by short-circuiting the primary winding as shown in Table 4.2 were used in determining the resonant frequency of the igniter. During the determination of the resonant frequency, the resistance, inductance and capacitance of the high voltage probe were added to the electrical parameters of the igniter.

4.4 Electrical Parameters of High Voltage Probe

The high voltage probe was used for measuring the igniter voltage. The measurement was done using impedance analyzer to investigate if the high voltage probe added a resistance, inductance and capacitance to the system. The results of the measurement are shown in Table 4.4.

Table 4.4: Electrical Parameters of High Voltage Probe

R (Ω)	L (μH)	C (pF)
56.11Ω	158.79	12.61

The impedance added by the high voltage probe to the series RLC circuit was hypothesized to be a series resistance, inductance and a parallel capacitance added to the igniter's capacitance as shown in Figure 4.1.

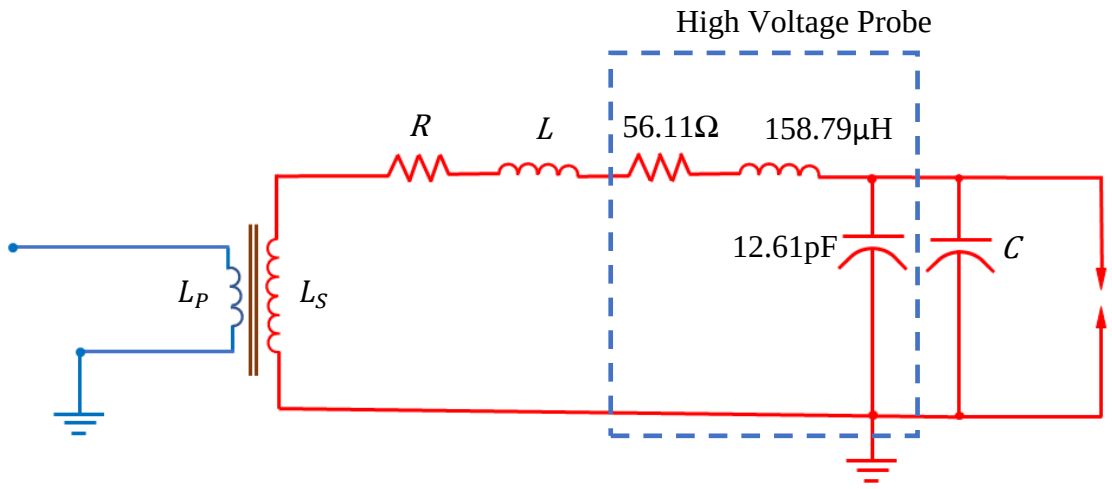

Figure 4.1: Circuit Representation of High Voltage Probe

The values of resistance, inductance and capacitance of the voltage probe determined above were added to the resistance, inductance and capacitance of the igniter to determine the resonant frequency. The resonant frequency was determined for both igniters used in tests with and without corona discharge using Equation 2.2 of Chapter 2. The resistance and inductance of the igniter were added in series with that of the voltage probe's resistance and inductance whereas the capacitance of the voltage probe was added in parallel as shown in Figure 4.1. For the case with corona discharge, the resonant frequency was determined

to be 751KHz by making use of the measurements listed in Tables 4.2 and 4.4. This value was close to the experimentally obtained resonant frequency of 760KHz. Since there was impedance variation during corona discharge, the resonant frequency was affected. Similarly, the resonant frequency for the case without corona discharge was determined to be 916.79KHz from the electrical component values described in Tables 4.3 and 4.4.

4.5 Effect on Electrical Parameters of Transformer and Igniter with Change in Position of Primary Coil

The effect on electrical parameters such as quality factor, resonating inductance of igniter, and secondary inductance used in transformer action were investigated as well. The primary coil was placed inside the metal shell at distances from the metal shell surface as represented in Figure 2.7. The measurement of electrical component values of transformer and igniter were performed using procedure described in section 2.6.4. Results are shown in Tables 4.5 and 4.6.

4.5.1 Measurement of Secondary Winding Connected to Igniter

Table 4.5: Measurement of Electrical Parameters of Secondary Winding Connected to the Igniter with Change in Position of Primary Coil

Distance From Metal Shell Surface (mm)	Primary Open-Circuit			Primary Short-Circuit		
	R (Ω)	**L (µH)**	**C (pF)**	**R (Ω)**	**L (µH)**	**C (pF)**
0	61.40	336.48	27.1	61.45	325.72	27.3
10	61.74	336.52	27.2	64.85	326.32	27.1
20	63.46	337.95	27.1	65.06	322.75	27.4
30	61.89	342.98	26.9	62.57	333.66	27.0
37	62.23	338.53	25.9	61.99	336.20	25.9

Table 4.6: Parameters of Igniter and Transformer Secondary with Change in Position of Primary Coil

Distance from Metal Shell Surface (mm)	Secondary Inductance (µH)	Quality Factor Q	Resonating Inductance (µH)
0	10.76	56.20	325.72
10	10.21	53.55	326.32
20	15.20	52.76	322.75
30	9.32	56.13	333.66
37	2.33	58.06	336.20

The parameters such as quality factor, secondary inductance and resonating inductance were determined as shown in Table 4.6. The values of quality factor and resonating inductance were determined using Equations 2.1 and 2.2 respectively. The values in the above tabulation are graphically represented in Figure 4.2. It was observed that the resonating inductance and quality factor were least in value at a distance of 20mm from the surface of metal shell. The values of quality factor and resonating inductance were maximum at a distance of 37mm, which was farthest from the metal shell surface.

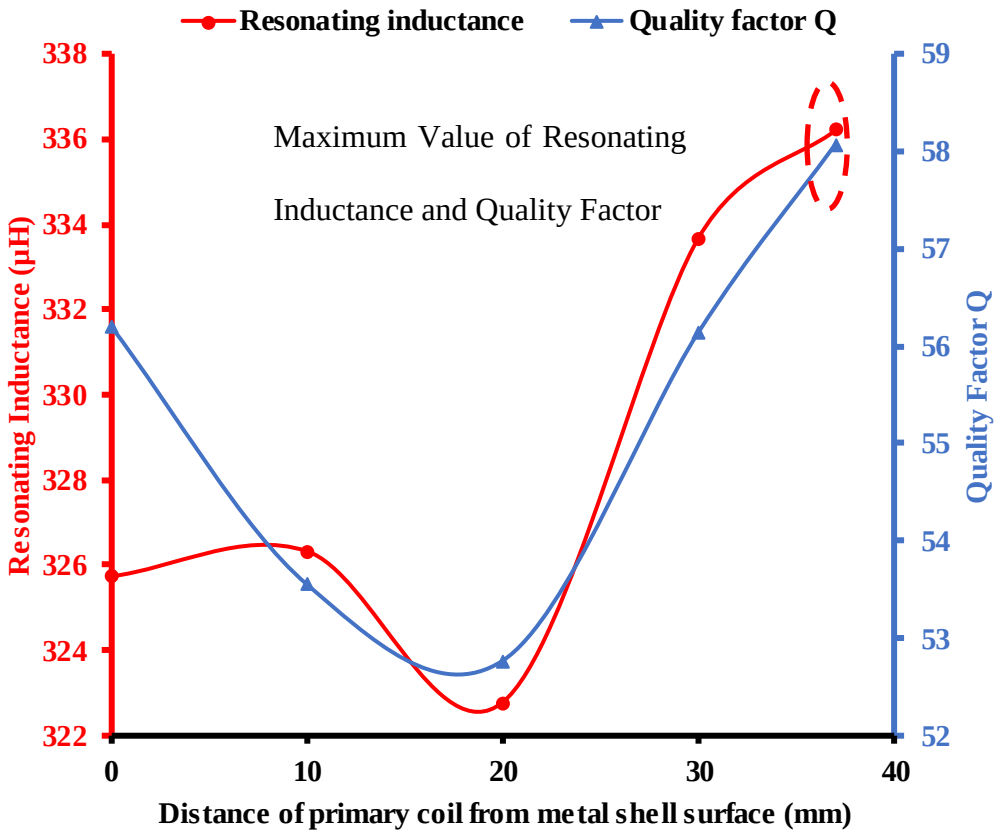

Figure 4.2: Variation of Resonating Inductance and Quality factor

Figure 4.3 shows the variation of secondary inductance with change in position of primary coil from the metal shell surface. It was observed that the secondary inductance attained peak value at a distance of 20mm from the metal shell surface. At a distance of 20mm from the metal-shell surface, the portion of inductance used for transformer action had the highest value compared to other positions. Whereas, at a distance of 37mm which was the farthest position from the metal shell surface, the quality factor and resonating inductance had highest value compared to other positions. This behavior could be attributed to the fact that at certain positions of the primary coil, the flux produced by the primary winding that linked with the secondary was higher compared to that at other positions which caused a

high value of secondary inductance [31]. In this case, at a distance of 20mm from metal shell surface, highest value of secondary inductance was observed. It was also observed that at a distance of 20mm, the leakage inductance was minimum, indicating that the leakage of flux produced by the primary winding that linked with the secondary winding was minimum [31].

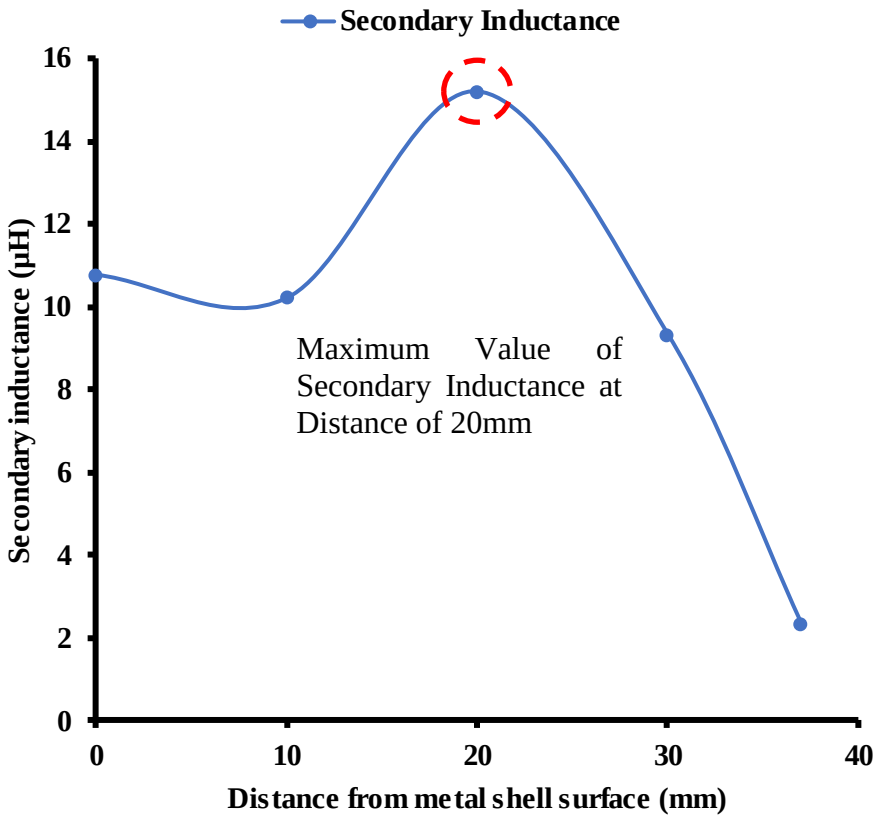

Figure 4.3: Variation of Secondary Inductance

CHAPTER 5: MODELLING OF CORONA IGNITION SYSTEM

5.1 Outline

This chapter describes the modelling of corona ignition system without corona discharge. The simplified circuit and the equations representing the model of corona ignition system are presented. The equations are used in Matlab Simulink environment along with the electrical component values of corona ignition system determined in Chapter 4 to simulate the dynamics of the model. The results obtained from simulations are compared with the measured experimental data for model verification.

5.2 Model of Corona Ignition System

The modelling of the corona ignition system is done using linear state-space modelling [39]. As menitoned in Chapter 3 the circuit of corona ignition system is hypothesized to be a pure RLC circuit connected to a transformer for the case without corona discharge. Since there is no corona discharge, the impedance of the system remains constant and can be represented as a series RLC circuit connected to a transformer. The conditions of the simulation performed are similar to the test described in Chapter 3 for case without corona discharge. The derivation of the model using linear state-space modelling is presented in this section.

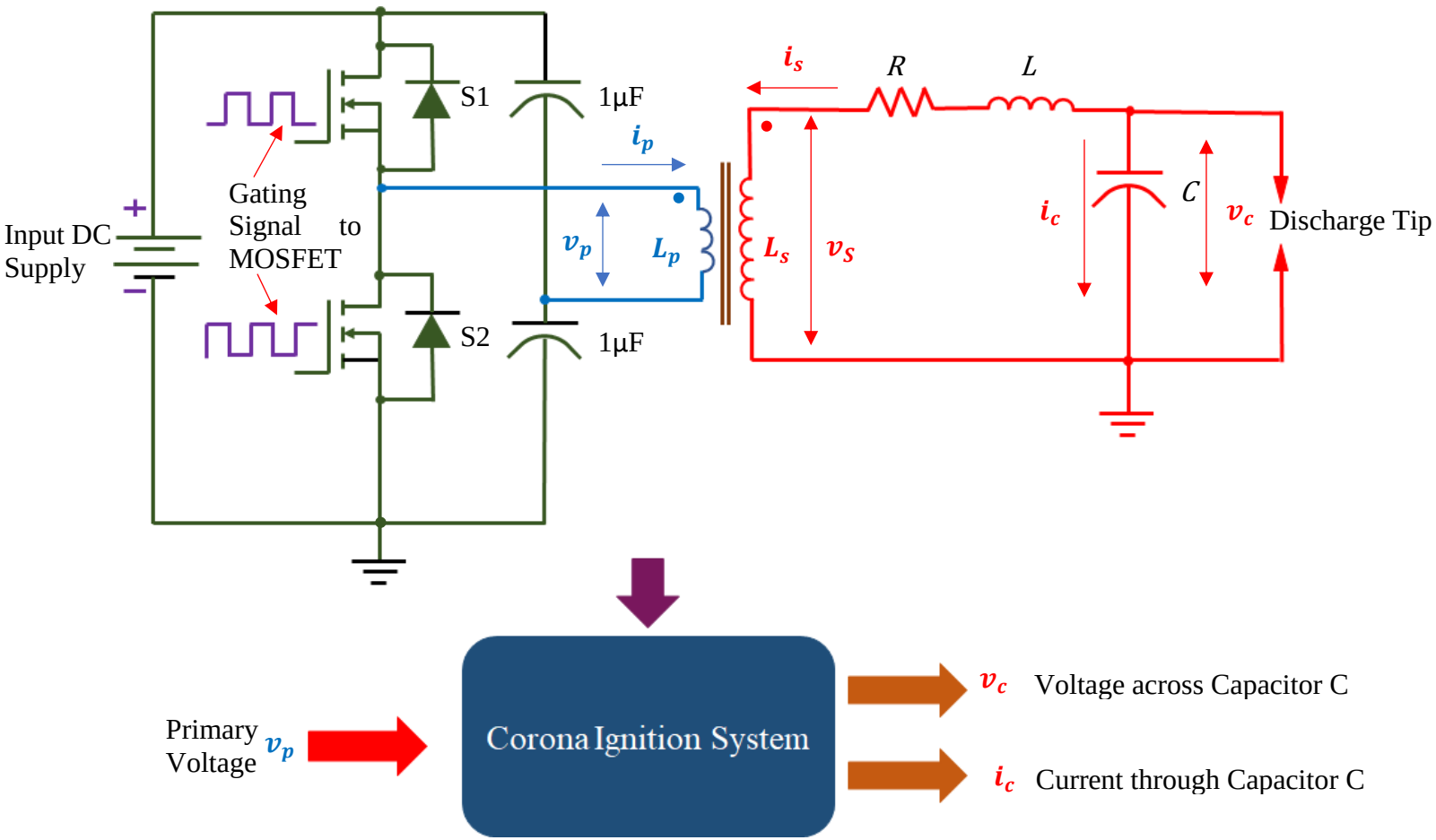

Figure 5.1: Circuit Representation and Model of Corona Ignition System

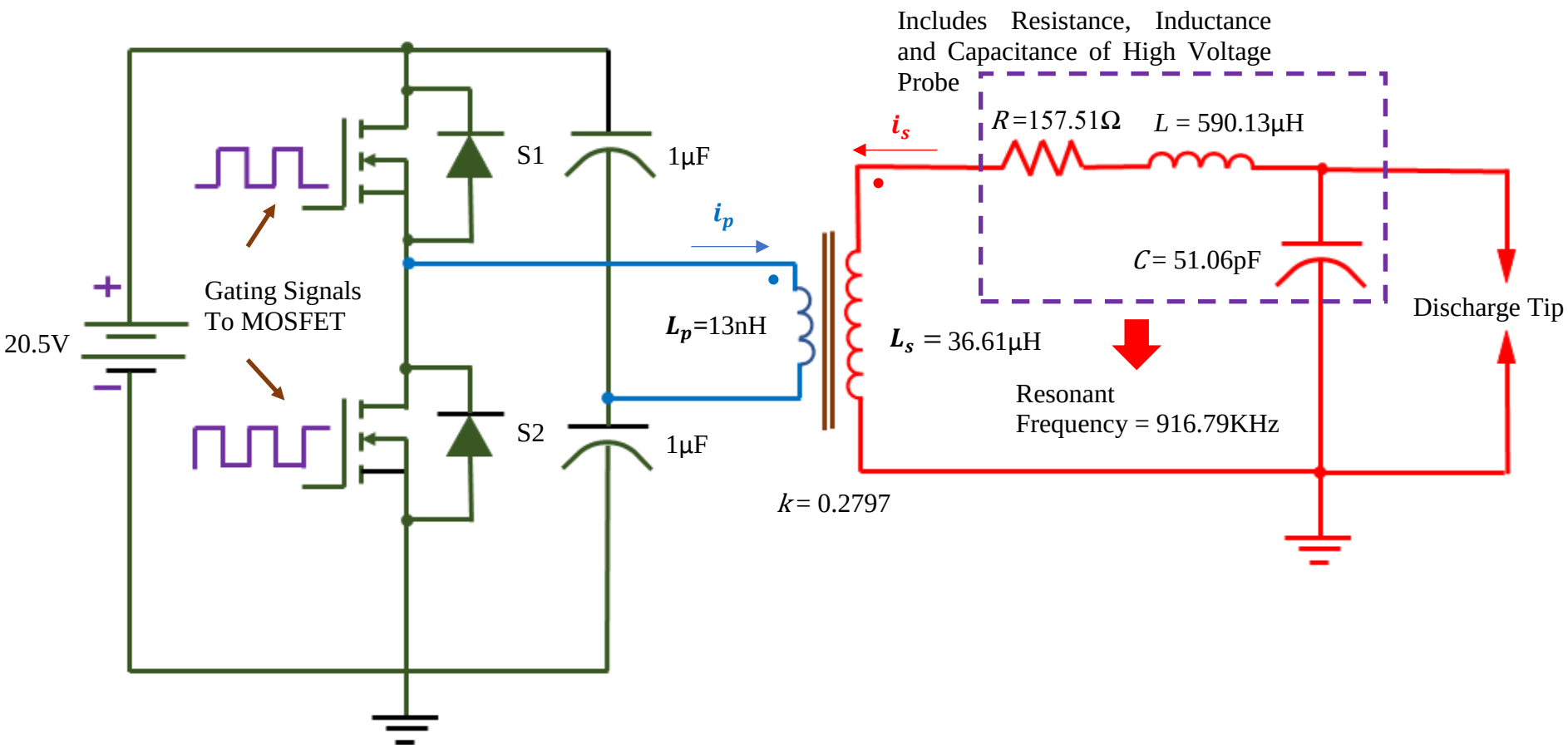

Figure 5.2: Values of Electrical Parameters of System

The equations for the mutual inductor are as follows

$$v_p = L_p \frac{di_p}{dt} + M \frac{di_s}{dt} \tag{5.1}$$

$$v_s = L_s \frac{di_s}{dt} + M \frac{di_p}{dt} \tag{5.2}$$

$$\text{Where, } M = k\sqrt{L_p L_s} \tag{5.3}$$

Re-writing Equation 5.1

$$\frac{1}{L_p}\left(v_p - M \frac{di_s}{dt}\right) = \frac{di_p}{dt} \tag{5.4}$$

Putting Equation 5.4 in 5.2, we get

$$v_s = L_s \frac{di_s}{dt} + \frac{M}{L_p}\left(v_p - M \frac{di_s}{dt}\right) \tag{5.5}$$

Applying KVL for the RLC circuit, we get

$$v_s = i_s R + L \frac{di_s}{dt} + v_c \tag{5.6}$$

But, the current through the capacitor C, $i_c = -i_s$, and hence we re-write Equation 5.6 as,

$$v_s = -i_s R - L \frac{di_s}{dt} + v_c \tag{5.7}$$

Equating 5.5 and 5.7,

$$L_s \frac{di_s}{dt} + \frac{M}{L_p}\left(v_p - M\frac{di_s}{dt}\right) = -i_s R - L\frac{di_s}{dt} + v_c \tag{5.8}$$

Simplifying 5.8,

$$\frac{di_s}{dt}\left(L_s + L - \frac{M^2}{L_p}\right) = -i_s R + v_c - \frac{Mv_p}{L_p} \tag{5.9}$$

Writing equation for the current through the capacitor C,

$$-i_s = C\frac{dv_c}{dt} \tag{5.10}$$

Now, for the state-space representation, we have the states given by the following table:

Table 5.1: States, Inputs and Outputs of the Model of Corona Ignition System

States	Input	Outputs
$\boldsymbol{x_1 = -i_s}$	$u(t) = v_p$	$y_1 = v_c$
$\boldsymbol{x_2 = v_c}$		$y_2 = -i_s$

$$\dot{x} = Ax + Bu \tag{5.11}$$

$$y = Cx + Du$$

Now converting the Equations 5.9 and 5.10 into state-space form using states specified in Table 5.1, we get

$$\begin{bmatrix}\dot{x_1}\\ \dot{x_2}\end{bmatrix} = \begin{bmatrix}\frac{-R}{L_S+L-\frac{M^2}{L_p}} & \frac{-1}{L_S+L-\frac{M^2}{L_p}}\\ 1/C & 0\end{bmatrix}\begin{bmatrix}x_1\\ x_2\end{bmatrix}+\begin{bmatrix}\frac{M}{L_p\left(L_S+L-\frac{M^2}{L_p}\right)}\\ 0\end{bmatrix}[u] \tag{5.12}$$

$$\begin{bmatrix}y_1\\ y_2\end{bmatrix} = \begin{bmatrix}0 & 1\\ 1 & 0\end{bmatrix}\begin{bmatrix}x_1\\ x_2\end{bmatrix}+\begin{bmatrix}0\\ 0\end{bmatrix}[u]$$

Table 5.2 represents the parameters of the system which are used in the state-space model of corona ignition system. The resistance, inductance and capacitance of the igniter include the resistance, inductance and capacitance of the voltage probe. The parameters which are measured as described in Chapter 4 are used in the model of corona ignition system each of which have their own physical meaning [17]. The experimental gating signal which is measured while performing the test is amplified to a value of 10.25V to represent the output voltage of the half-bridge inverter, and is fed as input to the linear state-space model of the system in Matlab Simulink. The results of simulation are presented in the following section. Since the coaxial cables of the voltage and current measurement probes produce a certain time delay for the measured voltage and current signals as described in Chapter 2, these time delays are taken into account in the model. The delays produced by the voltage and current measurement probes are 23.09ns and 7.69ns respectively.

Table 5.2: Electrical Component Values used in the Corona Ignition System Model

Parameter	Value
Primary Inductance (nH)	13
Secondary Inductance (μH)	36.61
Coefficient of Coupling	0.2797
Mutual Inductance (μH)	0.1929
Igniter Resistance (Ω)	157.51
Igniter Inductance (Secondary Leakage) (μH)	590.13
Igniter Capacitance (pF)	51.06

5.3 Comparison Between Model and Measurement

The model was simulated at conditions same as the experiment as described in Table 5.3. The measured voltage, current, and gating signals were used in the comparison with simulated model. The frequency sweep was done at frequencies namely 889.8KHz, 900.3KHz, 909.8KHz, 940.3KHz, 980.4KHz, 1000KHz.

Table 5.3: Conditions of Experiment and Simulation

Parameter	Value
Gating Signal Duration	0.5ms or 500μs
Input DC supply	20.5 Volts
Input Frequency	Varied
Duty cycle	50%
Sampling Frequency	62.5MHz

5.3.1 Investigation of Frequency Domain Behavior

The amplitude behavior of the model was investigated by determining the peak voltage, current, and instantaneous power at each of the swept frequencies. The steady-state values were used for determining the value of peak igniter voltage, current and instantaneous power. The graph indicating the variation of peak voltage, current and instantaneous power for various frequencies is shown in Figure 5.3.

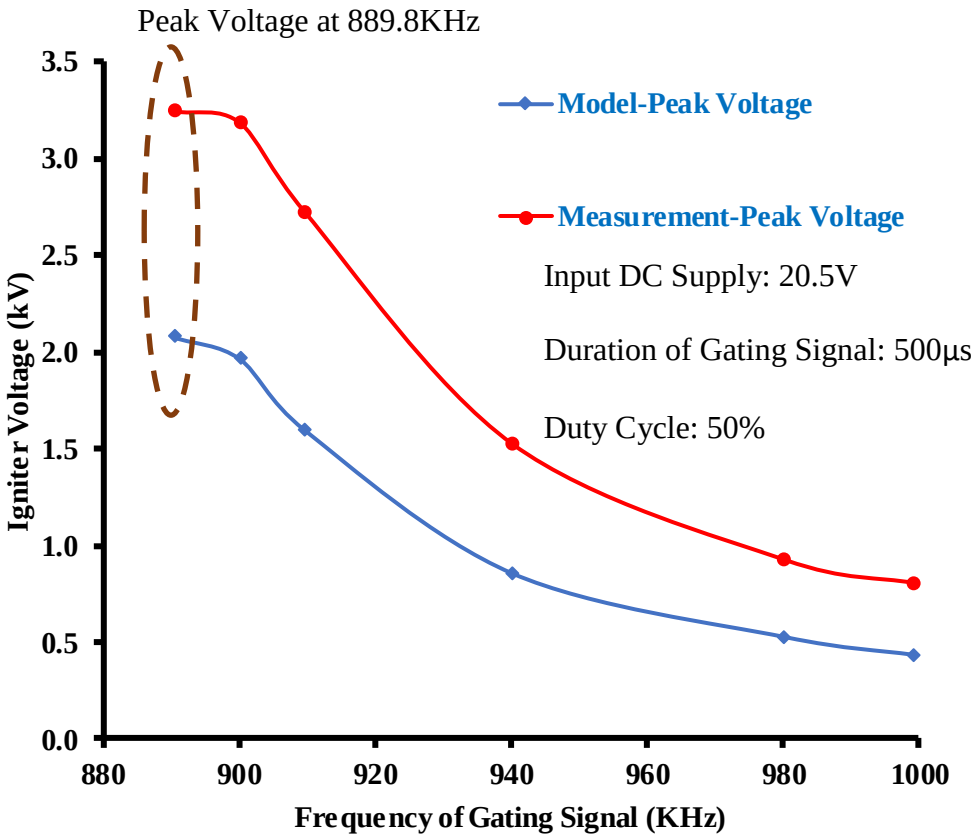

Figure 5.3: Variation of Peak Igniter Voltage for Model and Measurement vs. Frequency of Gating Signal

From Figure 5.3, it was observed that the model captured the trend of peak igniter voltage of the circuit. However, the amplitudes of the measurement and model were different. In both cases, maximum voltage was observed at 889.8KHz.

From Figure 5.4, the maximum value of current was observed at a frequency of 889.8KHZ. This was similar to Figure 5.3 where the maximum voltage compared to other frequencies was observed. The trend shown in Figure 5.3 was similar to the experimental data whereas the magnitude was different for all frequencies.

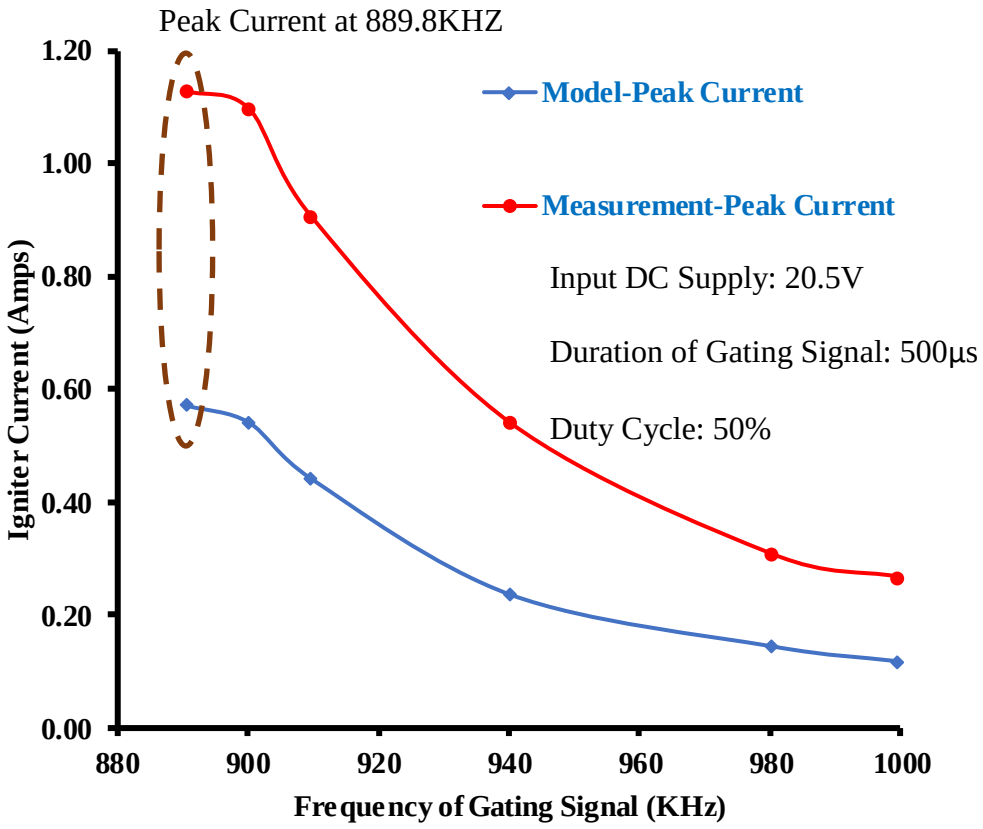

Figure 5.4: Variation of Peak Current for Model and Measurement vs. Frequency of Gating Signal

It was observed that the peak instantaneous power of the model and measurement followed the same trend (Figure 5.5). The maximum value of instantaneous power was observed at a frequency of 889.8KHz similar to Figures 5.3 and 5.4. This was different from the calculated undamped resonant frequency of 916.79KHz. in Chapter 4.

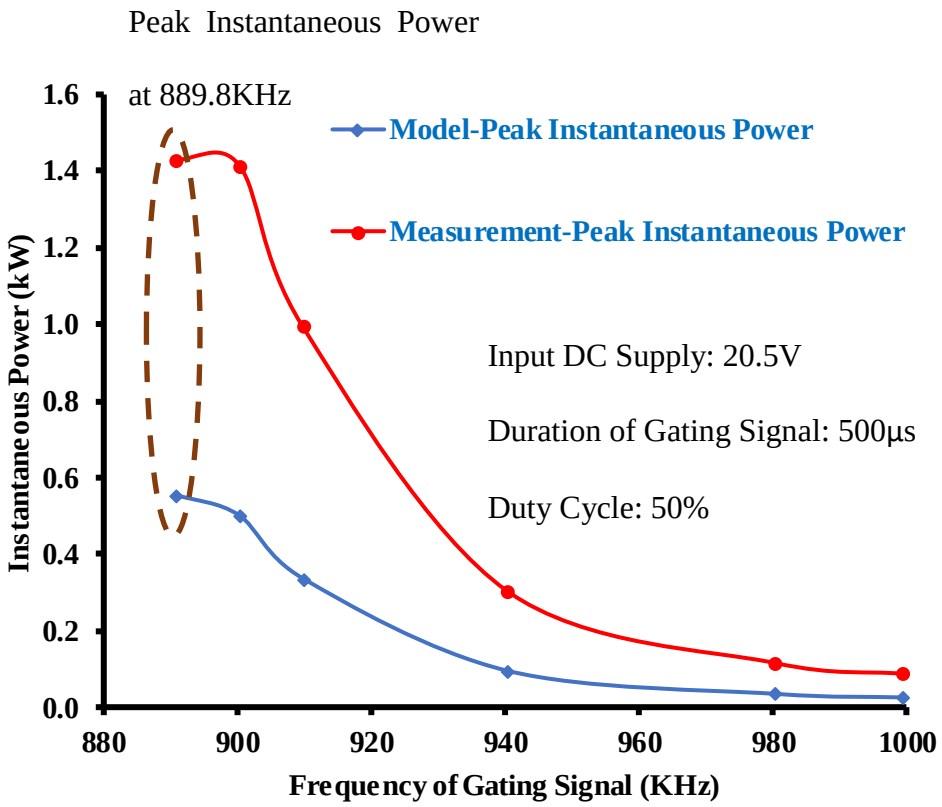

Figure 5.5: Variation of Peak Instantaneous Power for Model and Measurement vs. Frequency of Gating Signal

The frequency domain behavior was investigated by observing the variations of frequencies of voltage and current signals with frequency of input gating signal. The comparison between measured and modeled results are shown in Figure 5.6.

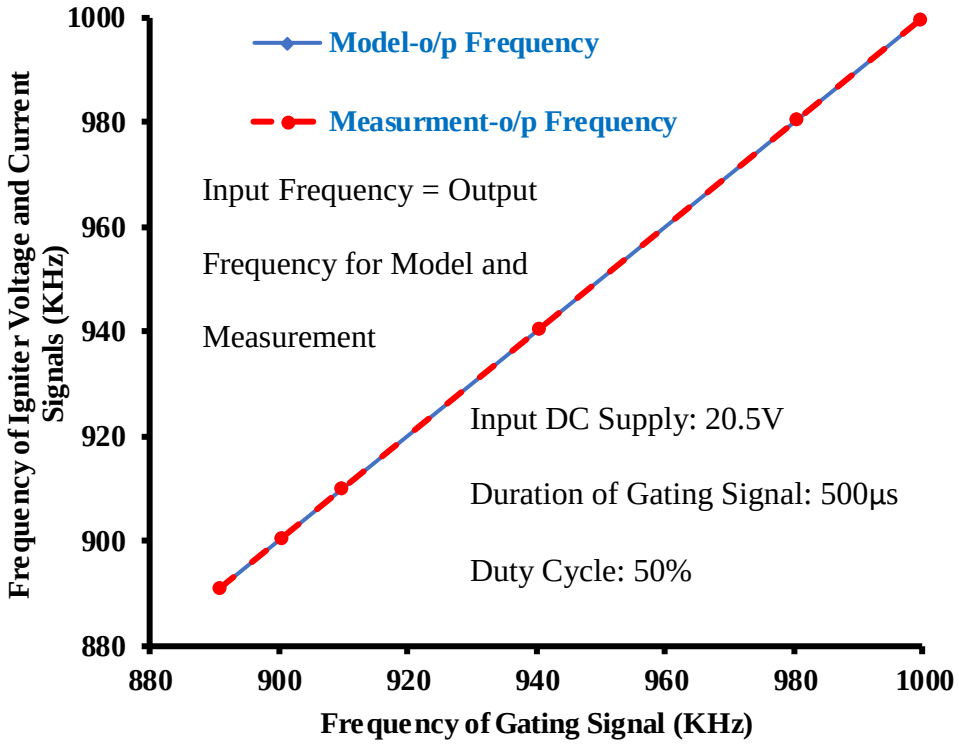

Figure 5.6: Input Frequency vs. Output Frequency for Model and Measurement

It was observed that the frequency of the measured and modeled voltage and current signals were the same as the frequency of the input gating signal. Hence, input frequency was same as the output frequency. The model captured the trend of the measurement as well.

The phase difference between the modeled and measured igniter voltage and applied gating signal vs frequency was studied. As shown in Figure 5.7, the model was able to capture the decreasing trend of phase difference between the measured igniter voltage and the gating signal with change in frequency. However, it was observed that the measured igniter voltage was leading the gating signal whereas the modeled igniter voltage was lagging the applied gating signal.

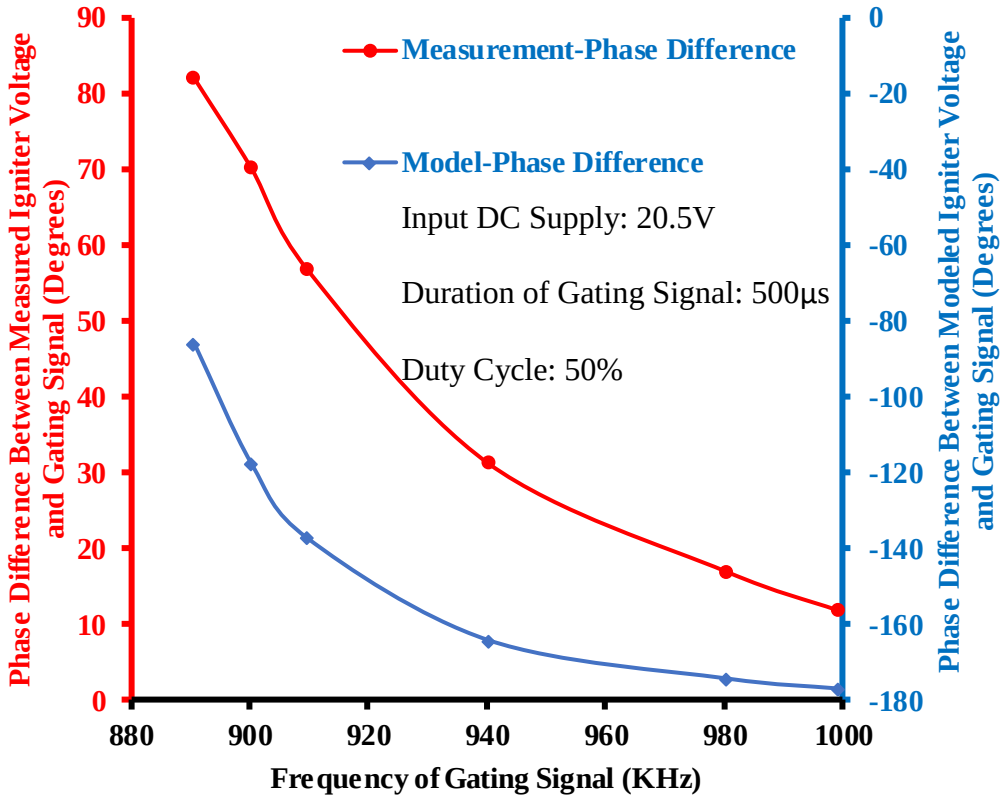

Figure 5.7: Phase Difference between Igniter Voltage and Gating Signals vs. Frequency for Model and Measurement

It was observed that the phase difference between modeled voltage and current signals captured the trend of the phase difference between the measured voltage and current signals except at a frequency of 940.3KHz. As illustrated in Figure 5.8, the phase difference between the voltage and current signals was a negative value indicating capacitive behavior for both the model and measurement.

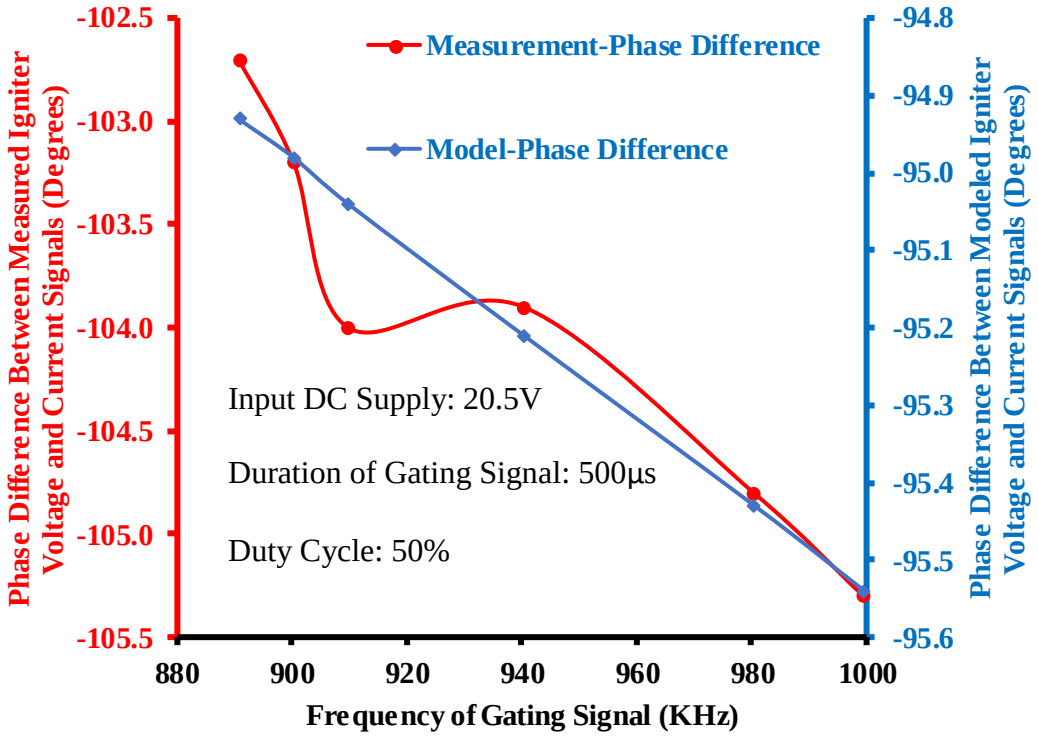

Figure 5.8: Variation of Phase Difference Between Igniter Voltage and Current Signals vs. Frequency

5.3.2 Investigation of Time Domain Behavior

The time domain behavior of the model was compared with that of the measurement. The envelope of igniter voltage and current obtained from the measurement were compared with the model for a gating signal frequency of 889.8KHZ. From Figures 5.9 and 5.10, it was observed that the model was able to capture the trend of the magnitude behavior of the system in the time domain for the voltage and current respectively. The magnitudes of igniter voltage and current for the model and measurement were however different values. It was also observed that, for all frequencies at which the frequency sweep was conducted, the model was able to capture the trend of the measured experimental data.

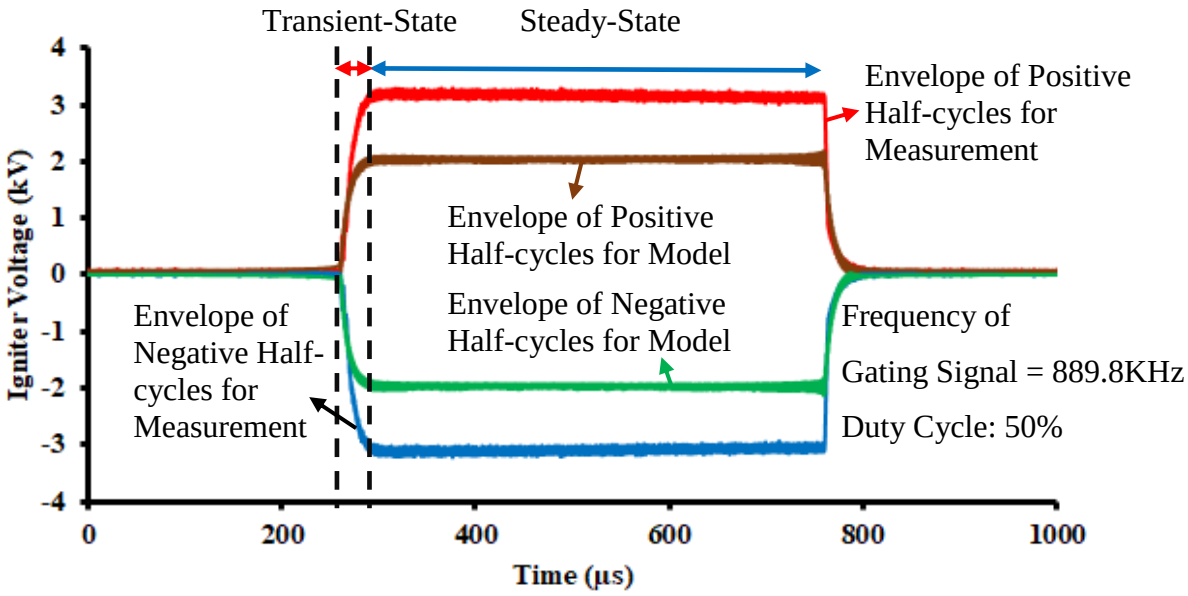

Figure 5.9: Envelope of Igniter Voltage for Measurement and Model

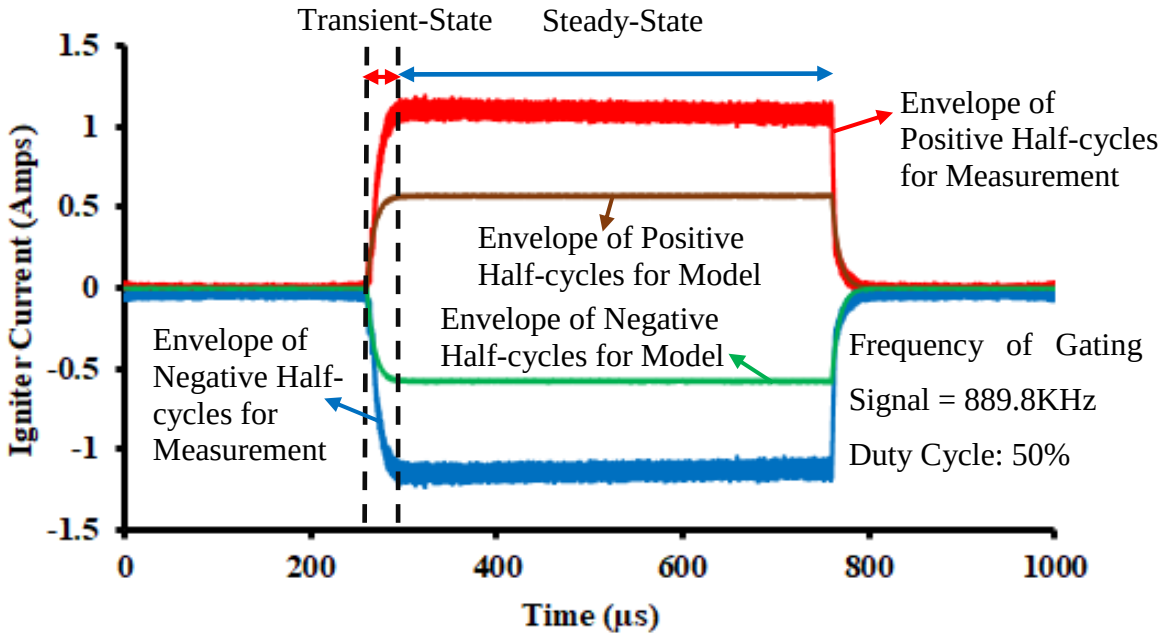

Figure 5.10: Envelope of Igniter Current for Model and Measurement

From Figures 5.11 and 5.12, show the measured and modeled igniter voltage signals that were 180 degrees out of phase with each other. From Figure 5.11, it was found that the measured igniter voltage signal begins 180 degrees out of phase compared to the voltage obtained from the model upon application of gating signal. The 180 degree phase shift was observed between the model and measurement in the steady-state as shown in Figure 5.12. Upon comparison of the modeled and measured igniter current signals, similar phase shift of about 180 degrees was observed as well. Such a phase shift between the modeled and measured igniter voltage and current signals was observed at all swept frequencies.

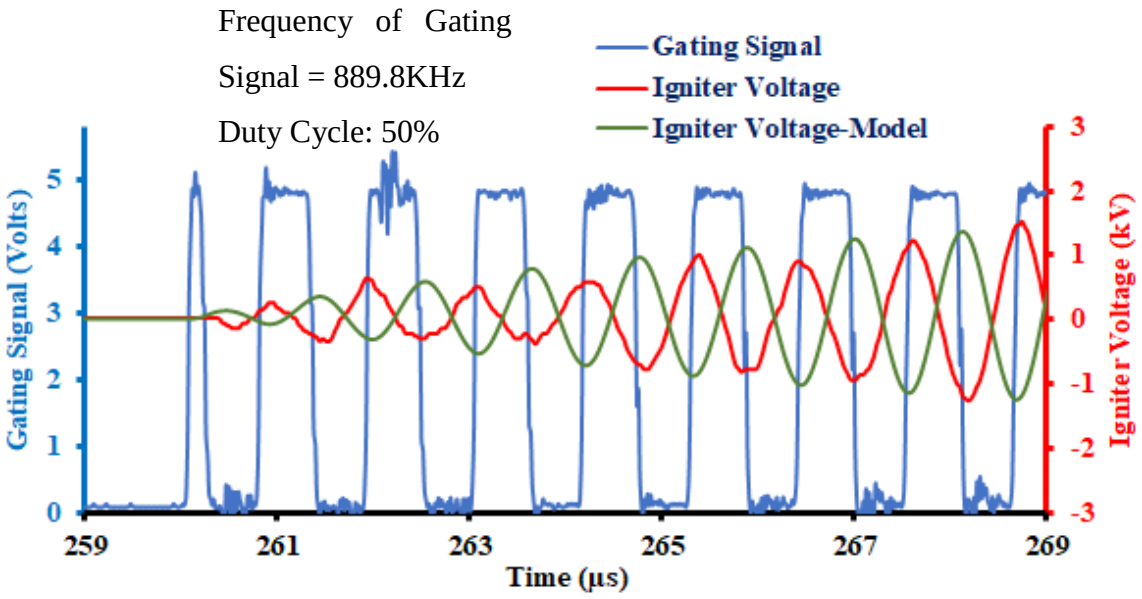

Figure 5.11: Modeled and Measured Igniter Voltage with Gating Signal

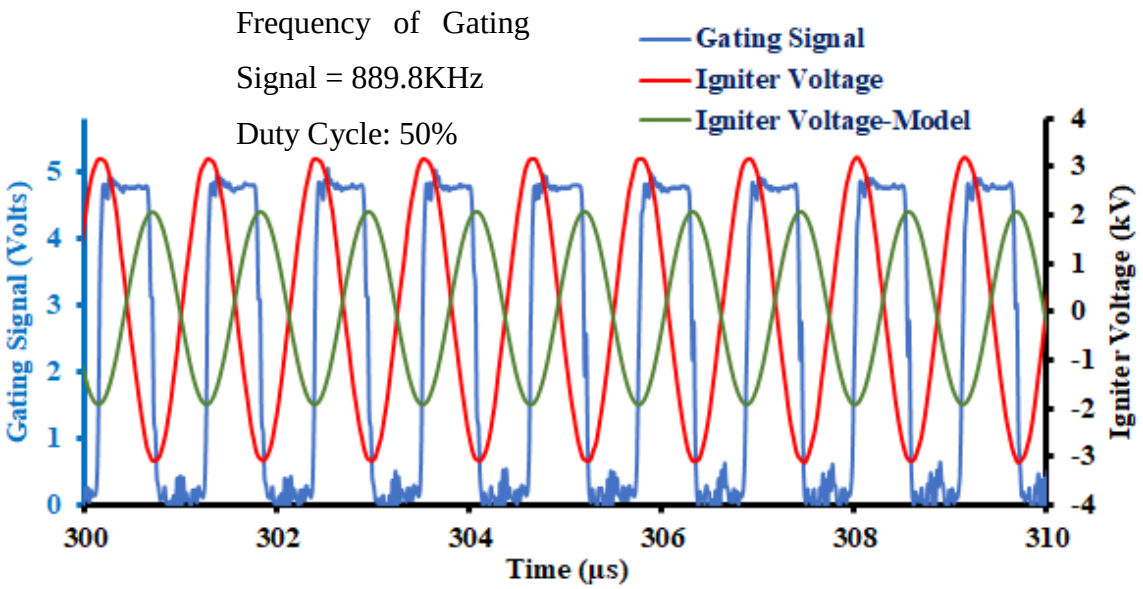

Figure 5.12: Modeled and Measured Igniter Voltage in Steady-State

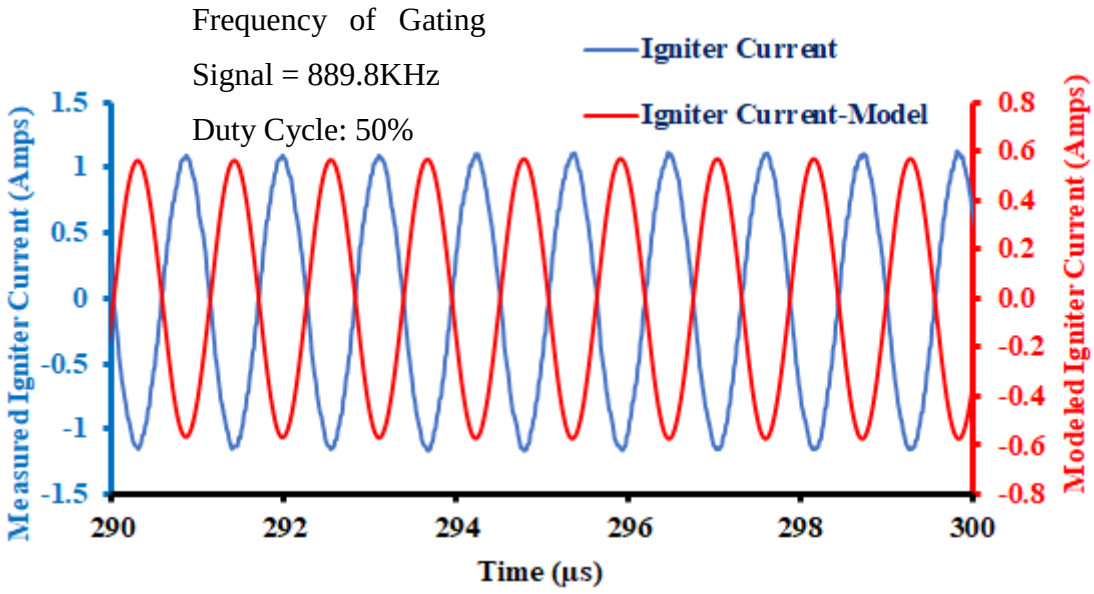

Figure 5.13: Modeled and Measured Igniter Current in Steady-State

Hence, it was demonstrated by comparison with experimental results that the model captured the trend of the magnitude behavior and exhibited capacitive behavior similar to the measured experimental data. It was also observed that the model could not capture the phase behavior of the experimental data since the voltage and current signals obtained from the model were 180 degrees out of phase in comparison to the experimentally obtained voltage and current.

CHAPTER 6: CONCLUSION AND FUTURE WORK

This chapter outlines the summary of results and the conclusions drawn from the results. The recommendations for future scope of work is presented.

6.1 Conclusion and Summary of Results

The behavior of a corona ignition system with and without corona discharge was studied, and an impedance analyzer was used to determine the various electrical component values of a corona ignition system. These measured parameters were then used in the physics based model of corona ignition system to simulate its behavior without corona discharge which was derived using linear state-space modelling. The model verification was performed by simulating the dynamics of the model using Matlab Simulink tool and compared with the results obtained from the experimental measurements. The electrical behavior of the half-bridge inverter used to drive the corona ignition system was also studied through simulation using Matlab Simulink tool.

6.1.1 Half-Bridge Inverter Simulation Results

- It was observed that the Half-Bridge inverter's output voltage contained odd harmonic components which were multiples of the fundamental frequency. This observation was validated by performing frequency domain analysis on the simulation result in the Appendix A.

6.1.2 Test performed with Corona Discharge

- The resonant frequency of the system during corona discharge was observed to be 760KHz since the peak igniter voltage, current, and instantaneous power were obtained at that frequency.

- It was observed that during corona discharge, the impedance of the system varied, which caused a change in phase difference between voltage and current signals. The frequency domain analysis of the signals however showed that the frequency of gating signals applied at half-bridge was equal to the frequency of measured voltage and current signals.
- The time domain analysis of the measured voltage and current signals indicated capacitive behavior because the current was leading the voltage.

6.1.3 Test performed without Corona Discharge

- It was observed that the peak igniter voltage, current, and instantaneous power were observed at a frequency of 889.8KHz.
- The test performed without corona discharge showed that the impedance of the system remained fairly constant due to the fact that once the igniter voltage and current signals reached the steady-state, their amplitude did not fluctuate.
- The system was hypothesized to be a transformer connected to a series RLC circuit. Since, the impedance of the system didn't change without corona discharge, the phase difference between igniter voltage and current signals was a constant value. It was observed that the system exhibited capacitive behavior for all the swept frequencies.
- Frequency domain analysis performed also indicated that the frequency of gating signal applied to the MOSFET's of the half-bridge was equal to the frequency of measured igniter voltage and current signals.

The time domain analysis in both tests with and without corona discharge also showed that the measured voltage signal was delayed and did not appear immediately as the

gating signal was applied. But as time progressed, the voltage signal began to lead the gating signal as shown in Figures 3.16 and 3.17.

6.1.4 Measurement of Electrical Component Values of System

- Measurement was performed using the impedance analyzer to determine the electrical component values of corona ignition system such as primary and secondary inductances of the transformer, and the leakage inductance of the secondary winding of the transformer used for resonation. The resistance and capacitance of the igniter were also determined. The electrical component values of the system were measured so that the values of measured parameters could be used in the physics based model of the corona ignition system without corona discharge.
- The electrical component values of the high voltage probe were measured since it added a certain impedance to the system which affected the system's resonant frequency. The resistance, inductance, and capacitance of the high voltage probe were measured using the impedance analyzer so that the measured values could be included in the first principle's model.
- One of the igniter structures studied had a hollow metal shell, inside which the primary coil could be inserted. The effect of change in position of the primary coil inside the metal-shell on factors such as quality factor, resonating inductance, and secondary inductance of the transformer was determined. It was observed that the quality factor and resonating inductance had the least value at distance of 20mm from metal shell surface whereas the secondary inductance had maximum value at this position. This was because at a distance of 20mm from the metal shell surface,

maximum flux produced by the primary coil linked to the secondary coil with very low leakage of flux causing highest value of secondary inductance compared to at other positions. The leakage inductance at this position was minimum because of least leakage of flux compared to that at other positions inside the hollow metal shell.

6.1.5 Model of Corona Ignition System

- The modelling of corona ignition system was performed using linear state-space modelling, and the measured electrical parameters obtained from impedance measurements were used in the physics based model of corona ignition system. The simulation of the linear state-space model was performed using Matlab Simulink tool. The simulation results were compared with the measurements obtained from test without corona discharge.
- The comparison between results obtained from the model and measurement indicated that the model followed the trend of magnitude behavior of the system. The model obtained peak igniter voltage, current, and instantaneous power at exactly the same frequency as the measurement. The magnitudes of maximum voltage, current, and instantaneous power were however different from the measurement. The envelopes of igniter voltage and current signals obtained from the model during transient and steady-state were also similar to the experimental measurement though magnitudes were different.

6.2 Recommendations and Future Work

- A method needs to be devised that can determine which component of the impedance is specifically varying during corona discharge. Whether the

impedance change is caused by a change of resistance, inductance or capacitance needs to be found, to better understand the system behavior during corona discharge.

- The physics involved in the system during corona discharge needs to be studied to put forward a first principles model of the corona ignition system for the case with corona discharge which can describe its dynamics.
- An effective method of power transfer needs to be investigated so that most of the power supplied at the input is available at the igniter tip. If such high power is made available at the igniter tip, then corona ignition can be successful in potentially igniting highly lean air-fuel mixtures.
- A model which can effectively capture the magnitude and phase behavior of the system for the case without corona discharge needs to be investigated. The non-linearity in the phase behavior which occurs in the transient state must also be studied.

APPENDIX A: HALF-BRIDGE INVERTER SIMULATION RESULTS

The simulation of half-bridge inverter is performed using Matlab Simulink R2016b to understand its electrical behavior. The half-bridge inverter converts a DC voltage at the input into AC voltage at the output. The simulation conditions of the half-bridge inverter are presented in Table A.1.

Table A.1: Simulation Conditions of Half-Bridge Inverter

Parameter	Value
Input DC Supply	77.6V
Duty Cycle	50%
Frequency of Gating Signal	760KHz
Sampling Frequency	62.5MHz

The inputs to the half-bridge inverter were gating signals to switch the MOSFETs complementary to one another along with input D.C. bias. A NOT gate was used to supply complementary gating signals from a function generator to each of the two MOSFETs. A resistor (10μΩ) was connected in series with the D.C. supply. This was due to the fact that the voltage across the capacitor could not be changed instantaneously and the 10μΩ resistance represented the internal resistance of the D.C. supply across which the voltage would drop [40]. The screenshot of the Simulink model of the half-bridge inverter is shown below.

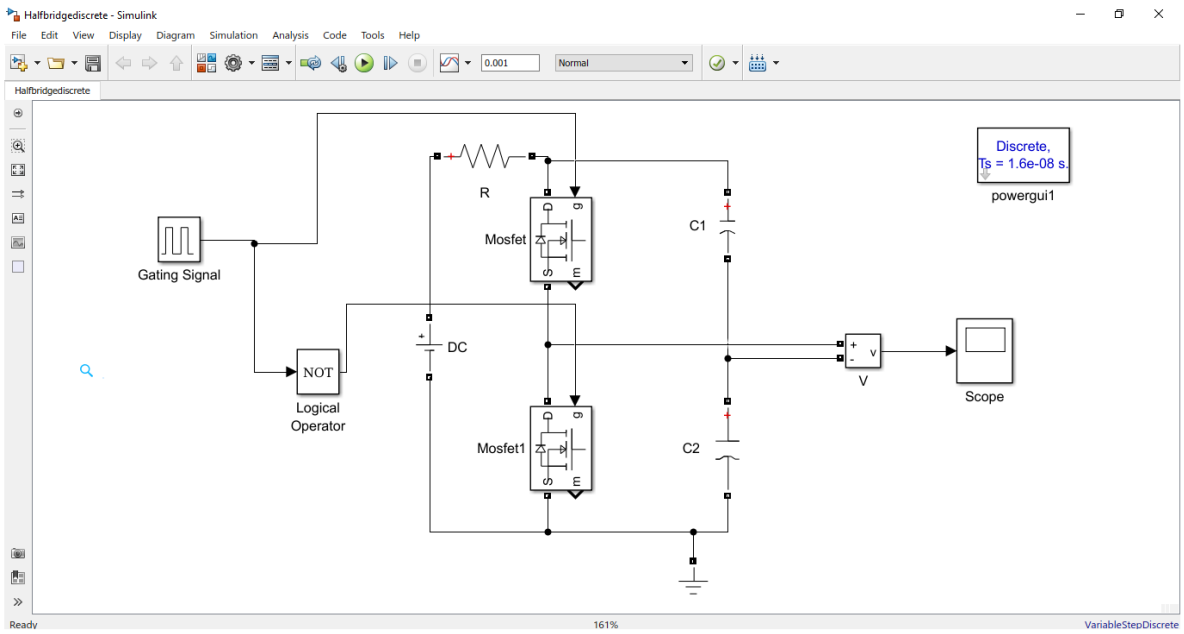

Figure A.1: Simulink Simulation of Half-Bridge Inverter

The simulated load voltage of the half-bridge inverter is shown in Figure A.2. The simulation is performed by discrete sampling of data in Matlab Simulink at a sampling frequency of 62.5MHz. The conditions of the simulation are mentioned in Table A.1. As described in section 2.4, the load voltage of the half-bridge inverter consists of odd harmonic components which are multiples of the fundamental frequency [41]. The fundamental frequency here is the frequency of the gating signal being applied to switch the MOSFETs of the half-bridge inverter. It is observed that the amplitude of the load voltage is approximately equal to half of the input DC supply.

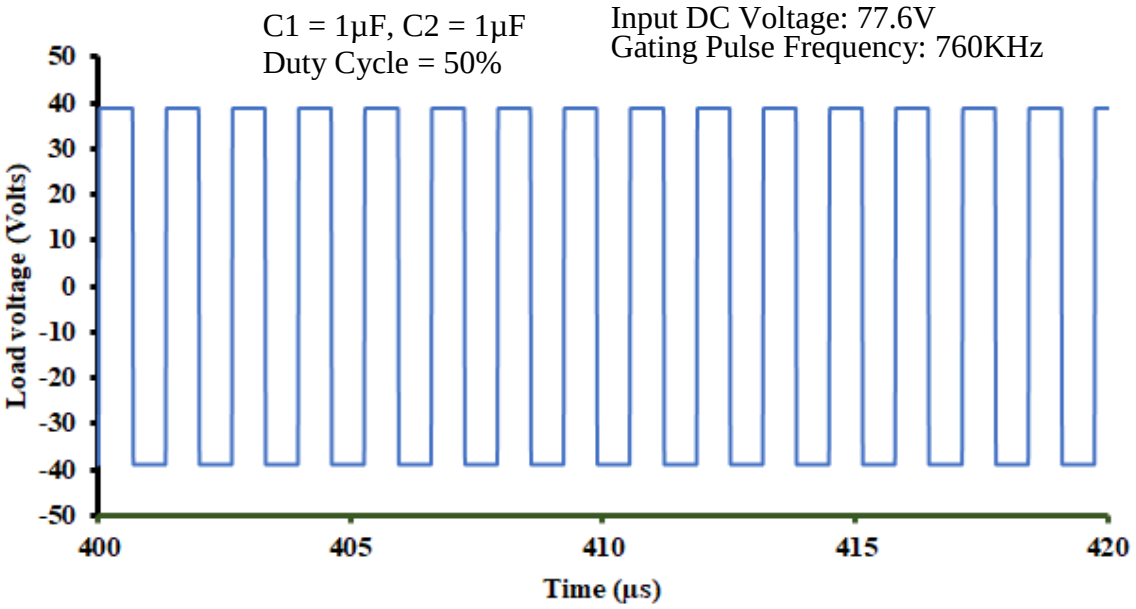

Figure A.2: Load Voltage vs Time

The frequency domain analysis is carried out to validate the concept that the load voltage of the half-bridge had odd harmonics which are multiples of the fundamental frequency. The graph showing the variation of load voltage in frequency domain is shown in Figure A.3. From Figure A.3, it is observed that the load voltage of the half-bridge inverter contains odd harmonic components which are multiples of the fundamental frequency [41].

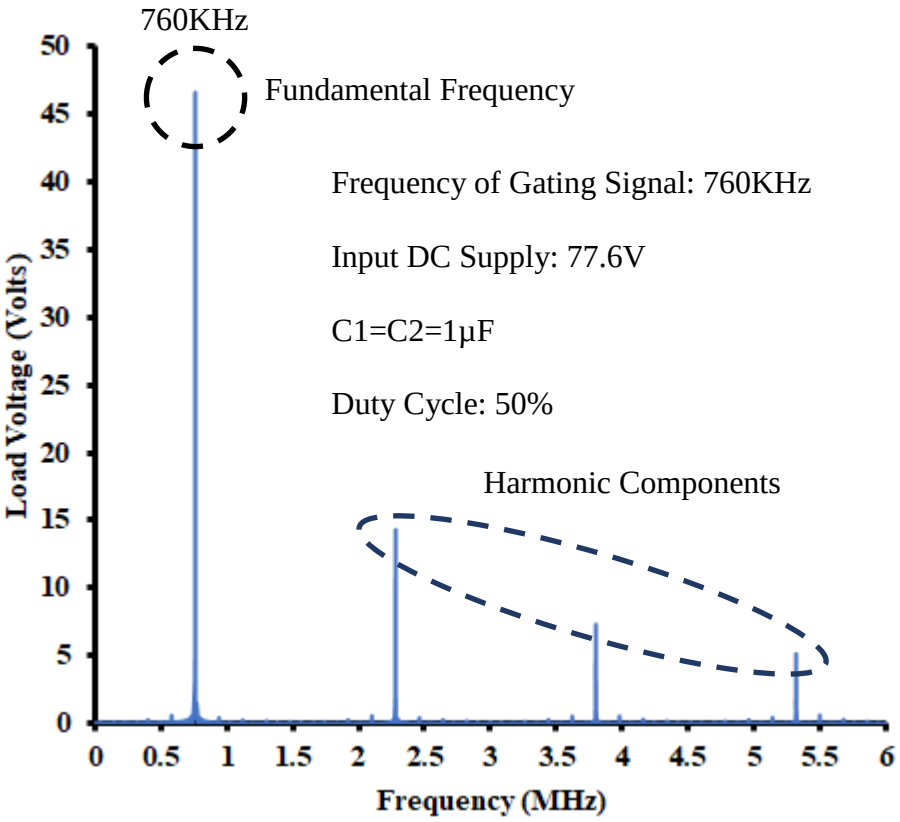

Figure A.3: Load Voltage vs Frequency

REFERENCES

[1] ICCT, “Estimated cost of Emission Reduction Technologies for Light-Duty Vehicles,”2012. [Online]. Available: https://www.theicct.org/sites/default/files /publications/ICCT_LDVcostsreport_2012.pdf. [Accessed: 02-Dec-2017].

[2] US Department of Energy, “Vehicle fuel efficiency (CAFÉ) requirements by year.” [Online]. Available: https://www.afdc.energy.gov/data/10562. [Accessed: 26-Sep-2017].

[3] J. Goldwitz, and J. Heywood, "Combustion Optimization in a Hydrogen-Enhanced Lean-Burn SI Engine," SAE Technical Paper 2005-01-0251, 2005.

[4] M. Battistoni, C. Poggiani, and C. Grimaldi, "Experimental Investigation of a Port Fuel Injected Spark Ignition Engine Fuelled with Variable Mixtures of Hydrogen and Methane," SAE Technical Paper 2013-01-0226, 2013.

[5] B. Porter, H. Blaxill, and N. Jariri, "A Study of Potential Fuel Economy Technologies to Achieve CAFE 2025 Regulations using Fleet Simulation Modeling Software," *SAE Int. J. Alt. Power*. 4(2):352-362, 2015.

[6] National Highway Traffic Safety Administration, “Corporate Average Fuel Economy.” [Online]. https://www.nhtsa.gov/laws-regulations/corporate-average-fuel-economy#corporate-average-fuel-economy-phase-1. [Accessed: 01-Jan-2018].

[7] EIA, “Retail Price of Gasoline in USA.” [Online]. Available: https://www.eia.gov/dnav/pet/hist/LeafHandler.ashx?n=pet&s=emm_epmr_pte_nus_dpg&f=a. [Accessed: 26-Sep-2017].

[8] M. Zheng, “Fundamentals of Clean Engine Technology,” Lecture Notes, University of Windsor, Windsor, Canada, 2016.

[9] J. B. Heywood, *Internal Combustion Engine Fundamentals*. New York, USA: McGraw-Hill, 1988.

[10] A. Mariani, F. Foucher, and B. Moreau, "The Effects of a Radio Frequency Ignition System on the Efficiency and the Exhaust Emissions of a Spark-Ignition Engine," SAE Technical Paper 2013-24-0053, 2013.

[11] M.S. Naidu, V. Kamaraju, *High Voltage Engineering*. New York, USA: McGraw-Hill, 1995.

[12] Federal Mogul Powertrain, "ACIS- Advanced Corona Ignition system." [Online]. Available:http://www.federalmogul.com/enUS/OE/markets/Pages/ProductDetails.aspx?ApplicationId=47&CategoryId=2&ProductId=224. [Accessed: 20-Aug-2017].

[13] V. Heise, P. Farah, H. Husted, and E. Wolf, "High Frequency Ignition System for Gasoline Direct Injection Engines," SAE Technical Paper 2011-01-1223, 2011.

[14] E. Sher, J. Ben-Ya'ish, A. Pokryvailo, and Y. Spector,"A Corona Spark Plug System for Spark-Ignition Engines,"SAE Technical Paper 920810, 1992.

[15] Mathworks, "creating accurate plant models." [Online]. Available: https://www.mathworks.com/solutions/control-systems/creating-accurate-plantmodels.html. [Accessed: 20-Aug-2017].

[16] A. Cimarello, C. Grimaldi, F. Mariani, M. Battistoni, "Analysis of RF Corona Ignition in Lean Operating conditions using an optical access engine", SAE Technical paper, 2017-01-0673, 2017.

[17] S. Yu, Q. Tan, M. Ives, M. Liu et al., "Parametric Analysis of Ignition Circuit Components on Spark Discharge Characteristics," SAE Technical Paper 2016-01-1011, 2016.

[18] J.R. Homer, R. Nagamune, “Physics-Based 3-D Control-Oriented Modelling of Floating Wind Turbines,” *IEEE Transactions on Control Systems Technology*, vol. 26, no. 1, pp. 14 - 26, 2018.

[19] N. Miri, M. Mohammadzaheri, L. Chen, S. Grainger et al, "Physics-based modelling of a piezoelectric actuator using genetic algorithm”, *Proc. IEEE Symposium on Industrial Electronics and Applications,* Kuching, Malaysia, 2013.

[20] J. Burrows, K. Mixell, “Analytical and Experimental Optimization of the Advanced Corona Ignition System,” Proceedings of the 3rd International Conference on Ignition Systems for Gasoline Engines, Berlin, Germany, 2016.

[21] North Star High Voltage, “High Voltage Probes.” [Online]. Available: http://www.highvoltageprobes.com/high-voltage-probes. [Accessed: Aug-2017].

[22] Pearson Electronics, “FAQs.” [Online]. Available: http://www.Pearson electronics .com/products/wideband-current-monitors. [Accessed: 1-Sep-2017].

[23] M. Zheng, S. Yu, M. Wang, inventors; M. Zheng, assignee, Active Control Resonant Ignition System, Unites States Patent US 9484719. Jan 14, 2016.

[24] D.C. Kulshreshtha, *Basic Electrical Engineering*. New Delhi, India: McGraw-Hill, 2009.

[25] J.L. Harrison, “A New Resonance Transformer,” *IEEE Transactions on Electron Devices,* vol. 26, Issue: 10, pp. 1545-1549, Oct. 1979.

[26] C.L. Arora, P.S. Hemne, *Physics for Degree Students*. New Delhi, India: S.Chand, 2013.

[27] F. Labrique, *Power Electronic converters*. Berlin, Germany: Springer, 1993.

[28] J.S. Chitode, *Power Electronics*. Pune, India: Technical Publications, 2008.

[29] A. DiPaola, S. DiPaola, *Introduction to low voltage systems*. New York, USA: DELMAR CENGAGE Learning, 2006.

[30] Keysight Technologies, “E4990A Impedance analyzer help.” [Online]. Available: http://ena.support.keysight.com/e4990a/manuals/webhelp/eng/. [Accessed: 20-March-2017].

[31] Voltech Instruments Inc, “Measuring leakage inductance.” [Online]. Available: http://www.voltech.com/Articles/104-105%20Leakage%20Inductance/104-105 .pdf. [Accessed: 10-Jul-2017].

[32] Exality Corporation, “Measuring transformer Coupling factor k.” [Online]. Available: http://exality.com/files/Measuring%20Transformer %20Coupling%20 F actor%20k.pdf. [Accessed: 20-March-2017].

[33] D.M. Katz, *Physics for scientists and engineers*. Massachusetts, USA: CENGAGE Learning, 2017.

[34] K.J. Coakley, J.D. Splett, M.D. Janezic, and R.F. Kaiser, “Estimation of Q factors and Resonant Frequencies,” *IEEE Transactions on Microwave Theory and Techniques*, vol. 51, no. 3, pp. 862 - 868, 2003.

[35] V. Lvovich, P. Vanysek, D. Hansen, M. Orazem, *Impedance technique: Diagnostics and Sensing Applications*. New Jersey, USA: The Electrochemical Society, 2010.

[36] W.G. Min, S.H. Lee, H.S. Kim, and S. Y. Hahn, “Removal of DC offset in Current and Voltage Signals Using a Novel Fourier Filter Algorithm,” *IEEE Transactions on Power Delivery*, vol. 15, no. 1, pp. 73 - 79, 2000.

[37] J. Arrillaga and B. Giessner, “Phase leading input current compensation for CRM boost PFC converter, ” presented at the Energy Conversion Congress and Exposition (ECCE), Milwaukee, WI, USA, Sept. 2016.

[38] G.J.J. Winands, A.J.M. Pemen, E.J.M. van Heesch et al, "Matching a Pulsed Power Modulator to a Corona Plasma Reactor", *Proc. 34th IEEE International Conference on Plasma Science,* Albuquerque, 2007.

[39] T.M. Marin, "State-Space Formulation for Circuit Analysis," *IEEE Transactions on Education*, vol. 53, no. 3, pp. 497 - 503, 2010.

[40] Mathworks, "Why do I receive an error when a source block is in a loop with only capacitors or inductors in SimPowerSystems." [Online]. Available: https://www . mathworks.com/matlabcentral/answers/103160-why-do-i-receive-an-error-when-i-connect -a-source-block-in-a-loop-with-only-capacitors-or-inductors. [Accessed: 5-Feb-2017].

[41] J. S. Chitode, U.A. Bakshi, *Power Devices and Machines*. Pune, India: Technical Publications, 2009.

VITA AUCTORIS

NAME:	Akshay Ravi
PLACE OF BIRTH:	Madurai, Tamil Nadu, India
YEAR OF BIRTH:	1993
EDUCATION:	Bachelor of Engineering in Electrical and Electronics Engineering Meenakshi Sundararajan Engineering College, Anna University, India May 2015
	Master of Applied Sciences in Electrical and Computer Engineering University of Windsor, ON, Canada March 2018